UNIVERSITY OF CALGARY

Phase Behaviour of Mixtures of Heavy Oil and n-Butane

by

Yulman Agustin Perez Claro

A THESIS

SUBMITTED TO THE FACULTY OF GRADUATE STUDIES

IN PARTIAL FULFILMENT OF THE REQUIREMENTS FOR THE

DEGREE OF MASTER OF SCIENCE

GRADUATE PROGRAM IN CHEMICAL AND PETROLEUM ENGINEERING

CALGARY, ALBERTA

MAY, 2019

Abstract

Solvent-based methods are a potential alternative to thermal methods for the recovery of heavy oils because they are less water and energy intensive. *n*-Butane is a solvent of interest for these processes because it has a saturation pressure that is close to the operating (reservoir) pressure of many heavy oil reservoirs. Operating at a pressure near the saturation pressure maximizes the solubility of the solvent in the oil while avoiding the formation of a second liquid phase. To design these processes, it is first necessary to predict the phase behaviour but there are few data available in the literature upon which to base a prediction.

The phase behaviour of heavy oil and *n*-butane mixtures was examined at temperatures up to 230°C and pressures up to 10 MPa. Both vapour-liquid and liquid-liquid regions were observed. The amount of the heavy pitch phase was measured at temperatures from 20 to 180°C and pressures up to 10 MPa. The liquid phase composition (in terms of C5-asphaltene, maltenes, and *n*-butane) were measured at 130°C and 10 MPa. A ternary diagram was constructed for the liquid-liquid region and equilibrium ratios (*K*) were determined and used to confirm the consistency of the data. The phase behaviour data for mixtures of *n*-butane and bitumen were consistent with the trends in the phase boundaries and masses versus carbon number observed with propane (Mancilla-Polanco *et al*., 2018) and *n*-pentane diluted bitumen (Johnston *et al*., 2017b).

The Peng-Robinson Equation of State was used to match the data by adjusting the binary interaction parameters with two approaches: 1) temperature dependent parameters (TDvdW model); 2) composition dependent parameters (CDvdW model). The TDvdW model matched both the vapour-liquid and liquid-liquid boundaries to within the uncertainty of the measurement but significantly under-predicted the heavy phase masses. The CDvdW model matched not only the phase boundaries but also the phase masses and compositions generally to within the experimental error. The model deviations increased above the critical temperature of *n*-butane.

Keywords: Phase Behaviour, Heavy oil, *n*-butane, Equation of State.

Acknowledgements

I would like to express my admiration and gratitude towards Dr. Harvey Yarranton for his excellent guidance and support during my research. It was an honor being able to work under his supervision. His passion for science and his commitment with his research group are exceptional. Simultaneously, I would like to acknowledge his team, Mr. Florian Schoeggl and Ms. Elaine Baydak. I am particularly grateful for the assistance given by Mr. Schoeggl, our PVT lab manager. Thank you for sharing your great experience and good memories from the aircraft industry. They are very valuable and I will keep them with me throughout my life. I am also grateful for Ms. Baydak, our AER manager, for all the technical and administrative support.

I am very grateful for the financial support from the sponsors of the Natural Science and Engineering Research Council of Canada (NSERC) Industrial Research Chairs in Heavy Oil Properties and Processing, including NSERC, Canadian Natural Resources Limited (CNRL), CNOOC Nexen, Ecopetrol, Schlumberger, Suncor Energy, and Virtual Materials Group for funding this research project.

I would need to write a whole other thesis to be able to describe all of the good memories and acknowledge the amazing people whom I had the opportunity to meet during my time here in Calgary, Canada. I will be straightforward and polite in this section; if I could I would include all of you. I would like to say thank you to the people I used to play soccer with. It was a great time. We learned that when we played like a team, we partied like an even better team. I would like to say thank you to the past and current members of our research group. You made this journey an incredible experience. I would also like to thank those closest to our group. Time will pass, but memories will stay forever.

Thanks for everything.

Dedication

To my family:

My father, my mother, and my two brothers.

Table of Contents

List of Tables

List of Figures

List of Symbols, Abbreviations and Nomenclature

Symbols

a	Attractive parameter in EoS, Eq. 2.1
a_A, b_A	Adjustable constant, Eq. 4.10
A^{chain}	Helmholtz energy contribution from covalent bonds in SAFT, Eq. 2.5
A^{res}	Residual Helmholtz energy, Eq. 2.5
A^{assoc}	Helmholtz energy contribution from association, Eq. 2.5
A^{seg}	Helmholtz energy contribution from segment in SAFT, Eq. 2.5
A_0^{hs}	Helmholtz energy contribution from hard spheres in SAFT, Eq. 2.6
A_0^{disp}	Helmholtz energy contribution from dispersion forces in SAFT, Eq. 2.6
b	Repulsive parameter in EoS, Eq. 2.1
B	Adjustable constant in modified Henry's law model, Eq. A.2
a_A, b_A	Adjustable constant, Eq. 4.10
c	Volume translation term, Eq. 2.2
C	Adjustable constant in the modified Henry's law model, Eq. A.2
g	Radial distribution function in SAFT EoS, Eq. 2.7
H	Henry's constant, Eq. A.1
H/F	Heavy phase split ratio
k_{ij}	Binary interaction parameter
$k_{ij}^0, k_{ij}^1, and\ k_{ij}^2$	Interaction parameters in temperature dependent correlation of k_{ij}, Eq. 4.9
K	Equilibrium constant, Eq. 2.11
m	Mass
n	Adjustable parameter in the Gao correlation, Eq. 4.11
P	Pressure
P_c	Critical pressure
P_{sat}	Saturation pressure
P_v	Vapour pressure
R	Universal gas constant, 8.314 J/mol*K
T	Temperature
T_R	Reduced temperature
T_c	Critical temperature
v	Molar volume
w	Mass fraction
x	Mole Fraction

Superscripts

F	Feed component
H	Heavy phase
L	Light phase

Subscripts

asph	Asphaltene component
bit	Bitumen component
malt	Maltene component
$C3$	Propane component
$C4$	n-Butane component
$C5$	n-Pentane component
i	Component i
j	Component j
m	Mixture
$solv$	Solvent component

Greek symbols

α	Alpha function in EoS
$\beta^{A_i B_j}$	Association volume parameter in CPA EoS
δ	Solubility parameter
$\varepsilon^{A_i B_j}$	Association energy parameter in CPA EoS
$\Delta^{A_i B_i}$	Association strength between two sites, Eq. 2.8
ω	Acentric factor
χ_{A_i}, χ_{B_j}	Mole fraction of molecule i or j not bonded at A or B-sites with other active sites, Eq. 2.8
γ	Activity coefficient
ρ	Molar density

Abbreviations

AAD	Average Absolute Deviation
APR	Advanced Peng Robinson EoS
AVR	Athabasca Vacuum Residue
BPR	Back Pressure Regulator
CDvdW	Composition Dependent Binary Interaction Parameter using van der Waals mixing rules
CEoS	Cubic Equation of State
CPA	Cubic Plus Association EoS
EoS	Equation of State
ES-SAGD	Expanding Solvent SAGD
GC	Gas Chromatography
HPM	High Pressure Microscope
LL	Liquid-Liquid Equilibrium
MRS	Modified Regular Solution
NBP	Normal Boiling Point
NRTL	Non-Random Liquid Theory
OF	Objective Function
PC-SAFT	Perturbed Chain Statistical Associating Fluid Theory

PR	Peng Robinson EoS
PVT	Pressure Volume Temperature
P-X	Pressure-Composition
SAFT	Statistical Association Fluid Theory
SAGD	Steam Assisted Gravity Drainage
SARA	Saturates-Aromatics-Resins-Asphaltenes
SimDist	Simulated Distillation
SRK	Soave-Redlich-Kwong EoS
SvdW	Symmetric van der Waals mixing rules
TBP	True Boiling Point
TDvdW	Temperature Dependent Binary Interaction Parameter using van der Waals mixing rules
VL	Vapour-Liquid Equilibrium
VLL	Vapour-Liquid-Liquid Equilibrium
VLLL	Vapour-Liquid-Liquid-Liquid Equilibrium

Chapter 1: Introduction

There are 1.85 trillion barrels of heavy oil in place in Canada of which 177 billion barrels are currently considered recoverable (Alberta Energy Regulator, 2018; BP, 2018). The recoverable reserves are relatively low because heavy oils have a viscosity between 1,000 to 1,000,000 mPa.s (Gray, 1994), which makes them challenging to produce. Most commercially successful *in situ* recovery processes for heavy oil are steam or steam-based methods. Steam is used to heat the oil to reduce its viscosity so that the oil can flow and be produced (Butler, 1981). However, thermal methods are energy and water intensive, are relatively expensive, and have a high greenhouse gas fingerprint (Ali, 2015).

An alternative means of decreasing the viscosity of heavy oil is to inject a solvent alone or with steam. Alone, the solvent dilutes the heavy oil and reduces its viscosity. With steam, the heavy oil viscosity is reduced by both heat and dilution. Both solvent based (no steam) and solvent-assisted (with steam) processes have been tested in field pilots (Miller *et al*., 2003; Chang *et al*., 2013; Bayestehparvin *et al*., 2018). The solvents considered include butane, condensate, mixtures of propane with methane or diesel, naphtha, and natural gas liquids. The pilots with solvent alone were not successful but solvent-assisted pilots showed improvements in oil recovery and reduced the steam requirements. The residence time of the solvent in the reservoir and recovery of the injected solvent are the main issues limiting the economics of these processes relative to thermal processes. The full potential of these processes has not yet been realized because the interaction of the heavy oil and solvent in the reservoir and the physics of the recovery process are still poorly understood (Bayestehparvin *et al*., 2018).

Many proposed solvent-based recovery processes are designed to operate near the saturation pressure to maximize the solubility of the solvent in the oil while avoiding the formation of a second liquid phase. *n*-Butane is a solvent of interest for heavy oil recovery processes because it has a saturation pressure at typical operating temperatures that is close to the reservoir pressure of many heavy oil reservoirs. *n*-Butane is also a relatively low cost solvent.

The injection of an *n*-alkane, such as *n*-butane, into heavy oil can lead to complex phase behaviour including the formation of vapour-liquid, liquid-liquid and vapour-liquid-liquid regions. The second liquid phase may appear as a mobile liquid or a dispersed glassy asphaltene-rich phase depending on the conditions (Johnston *et al*., 2017b; Mancilla-Polanco *et al*., 2018). These asphaltene-rich phases can potentially damage the reservoir and deposit in the wellbore and surface facilities. Therefore, a detailed evaluation of phase behaviour is required for reservoir simulation and process design. While phase behaviour data are available for mixtures of heavy oil with propane and *n*-pentane (Zou *et al*., 2007; Badamchi-Zadeh *et al*., 2009a; Dini *et al*., 2016; Johnston *et al*., 2017b; Mancilla-Polanco *et al*., 2018), there are few data for mixtures of heavy oil and *n*-butane.

Ideally, experimental phase behaviour data should be collected at different operating conditions. However, this approach is expensive, time consuming, and can only capture part of the phase behaviour. Therefore, phase behaviour modeling is also necessary. Most commercial simulators use a cubic equation of state (CEoS) to model complex hydrocarbon phase behaviour. CEoS can match the boundaries of vapour-liquid, liquid-liquid, and vapour-liquid-liquid regions but generally fail to predict phase compositions and masses (including asphaltene yields) accurately (Johnston *et al*., 2017b). Recently, composition dependent binary interaction parameters were implemented in the Peng Robinson CEoS to model the phase behaviour for a Western Canadian bitumen diluted with *n*-pentane (Johnston *et al*., 2017a) and propane (Mancilla-Polanco *et al*., 2018). One drawback of this method is that binary interaction parameters must be tuned for each solvent. To date, there are not enough phase behaviour data available for mixtures of heavy oil and *n*-butane to tune the model.

1.1 Objectives

This thesis focuses on mixtures of *n*-butane and bitumen with the following overall objectives:

1. Collect phase behaviour data for mixtures of *n*-butane and bitumen at different temperatures, pressures and feed solvent contents, including phase boundary and phase masses. Analyze the heavy (L_2) phase morphology, and the composition of both the light (L_1) and heavy (L_2) phase.

2. Test the ability of a CEoS with temperature and composition dependent binary interaction parameters to match the data.

The specific objectives are to:

1. Determine the saturation pressure (VL_1 boundary) for n-butane diluted bitumen systems at 50, 90, 130, 180 and 230°C.
2. Measure the onset (L_1L_2 boundary) for mixtures of n-butane and bitumen at 50, 90, 130, and 180°C, and at 5 and 10 MPa.
3. Construct phase boundary diagrams at 50, 90, 130, 180 and 230°C.
4. Study the morphology of the heavy pitch (L_2) phase in the (L_1L_2) region through micrograph images taken with a high pressure microscope (HPM) apparatus.
5. Construct C5-asphaltene and pitch* (solvent-free bitumen in the heavy phase) yield diagrams at different temperatures and pressures for n-butane diluted bitumen.
6. Compare the results with mixtures of bitumen with different carbon number n-alkanes.
7. Test the ability of the APR EoS to predict the phase behaviour of n-butane diluted bitumen including the modeling of phase boundaries, phase splitting, phase masses, and phase compositions.

The investigation was performed on a Western Canadian bitumen at temperatures from 20 to 230°C and pressures up to 10 MPa. The Peng Robinson (APR) EoS with composition dependent binary interaction parameters was selected to model the data. The APR EoS is the Peng Robinson EoS implemented in VMGSim^{TM} with volume translation (VMG, 2011). The Peng Robinson cubic EoS is commonly used in oil industry applications such reservoir simulations (CMG, 2016; Eclipse, 2016) and the APR version has satisfactory modeled phase boundaries for mixtures of heavy oil and solvents in previous studies (Castellanos *et al*., 2011; Agrawal *et al*., 2012; Johnston *et al*., 2017a; Mancilla-Polanco *et al*., 2018).

1.2 Thesis Structure

This project is organized into six chapters as described below.

Chapter Two provides a brief review of crude oil chemistry. The characterization techniques used to represent the crude oil chemistry for phase behaviour modeling are discussed. Previous phase

behaviour measurements for mixtures of heavy oils and solvents are presented. The methods used to model this phase behaviour are reviewed.

Chapter Three outlines the experimental methods used in this thesis starting with the materials used including the distillation assay and properties of the bitumen sample. The experimental methods used to collect phase boundaries, phase masses, and phase composition for mixtures of bitumen and n-butane are described.

Chapter Four provides the modeling methodology used in this thesis to predict the phase behaviour of n-butane diluted heavy oil using the Advanced Peng-Robinson equation of state (APR-EoS). The characterization of the crude oil into a set of pseudo-components with assigned properties is discussed. The implementation and tuning of the APR-EoS is presented.

Chapter Five presents the experimental phase behaviour data and modeling results for mixtures of n-butane and WC-B-B5 bitumen. Pressure-composition (P-X) phase diagrams, including saturation pressures and onsets are presented at different temperatures. The morphology of the pitch phase in the liquid-liquid phase region is examined. The C5-asphaltene and pitch* yields are reported. The experimental results are also compared against previously collected data for propane (Mancilla-Polanco et al., 2018) and n-pentane (Johnston et al., 2017b) diluted bitumen. Finally, the APR EoS with composition dependent binary interaction parameter is tuned to match the data.

Chapter Six highlights the major experimental and modeling contributions from the thesis. Recommendations are also provided for future studies.

Chapter 2: Literature Review

This chapter begins with a brief review of the chemistry of crude oils. The characterization techniques used to represent the crude oil chemistry for phase behaviour modeling are presented. The chapter concludes with a summary of the measured phase behaviour for diluted heavy oils and the methods used to model this phase behaviour.

2.1 Chemistry of Crude Oil

Petroleum is a naturally occurring mixture of hydrocarbons and other compounds containing variable amounts of sulfur, nitrogen, oxygen and trace amounts of metallic constituents including iron, nickel and vanadium (Speight, 2007; Riazi, 2005). This definition includes petroleum in the form of gas (natural gas), liquid (crude oil), semi-solid (bitumen), or solid (asphaltite). Crude oils that contain dissolved gases are called live oils. Those which have lost all dissolved gases are referred to as dead oils or simply crude oil. Crude oils are further classified according to their dead oil specific gravity and viscosity according to the UNITAR classification, Table 2.1.

Table 2.1 UNITAR classification of oils by physical properties at 15.6°C (Gray, 1994).

Classification	Viscosity mPa·s	Density kg/m³	API Gravity
Light Oil	$<10^2$	<934	>20°
Heavy Oil	10^2 - 10^5	934 - 1000	20° - 10°
Bitumen	$>10^5$	>1000	<10°

Crude oils are mixtures of millions of different chemical species (McKenna *et al*., 2010). These species can be classified into the following four chemical families (Altgelt and Boduszynski, 1994):

- *Paraffins* are saturated hydrocarbons with straight or branched chains (*n*-paraffins or isoparaffins, respectively). The molecular formula for paraffins is C_nH_{2n+2}.

- *Naphthenes* are also called cycloalkanes. The molecular formula for a single cyclic ring is C_nH_{2n}. Most naphthenes in petroleum are cyclic alkanes with paraffinic side chains. Naphthenes can include multiple rings and the rings are defined as fused if they share more than one carbon atom.

- *Aromatics* are unsaturated hydrocarbons containing a least one benzene ring in their molecular structure. The molecular formula for a single aromatic ring is C_nH_n. Aromatic compounds may contain paraffinic side chain and/or naphthenic rings. Like naphthenes, aromatics can include multiple rings and the rings are defined as fused if they share more than one carbon atom.

- *Heterocompounds* are hydrocarbons from the previous groups in which one or more heteroatoms (N, S, O, V, Ni, Fe) form part of the molecular formula. Heteroatoms are commonly found within the higher molecular weight fractions of crude oil.

There is a clear relationship between chemical structure and normal boiling point, as shown in Figure 2.1. For components with the same carbon number, alkanes have the lowest boiling point and aromatics and polyfunctional components have the highest boiling points. The complexity in chemical structure increases dramatically with increasing carbon number (or boiling point). In other words, the number of components in a single boiling cut increases with boiling point or equivalently, the boiling point range within a single carbon number fraction increases with carbon number. As the molecular weight and boiling point increase, other properties such as aromaticity and heteroatom content also increase as shown in Figure 2.1. The properties of a crude oil also follow a smooth continuous trend with boiling point or carbon number (Boduszynski, 1987).
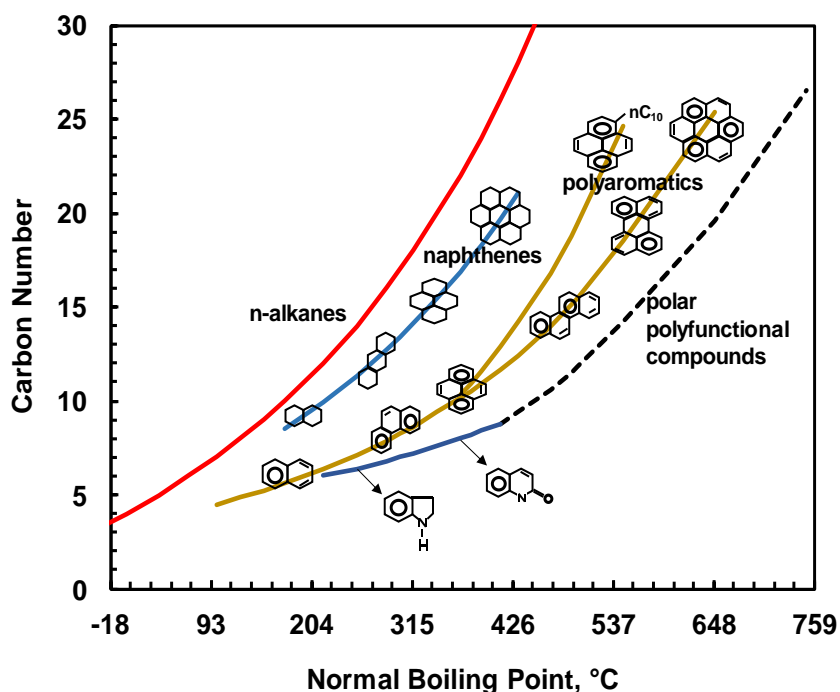
Figure 2.1 The relationship between boiling point, carbon number and chemical structure of crude oil components. Adapted from Altgelt and Boduszynski (1994).

2.2 Oil Characterization

2.2.1 Oil Characterization Assays

Since crude oil has millions of components, it is currently impossible to characterize a crude oil by its constituent molecular species. Instead, crude oils are represented by a set of pseudo-components that accurately represent the distribution of properties of the crude oil. Pseudo-components can be defined from a distillation assay, a GC assay, or SARA analysis (Castellanos-Diaz *et al.*, 2011; Agrawal *et al.*, 2012). Distillation and GC assay data are the preferred methods for equations of state (EoS) based applications. SARA analysis is mostly used for asphaltene precipitation models applied to diluted heavy oils (Tharanivasan *et al*., 2009). Each characterization assay is described below.

Distillation

Distillation separates a crude oil into a number of fractions based on a difference in volatility (Whitson and Brulé, 2000). Each fraction represents a group of chemical species within a well-defined molecular weight range (Boduszynski, 1987; Altgelt and Boduszynski, 1994). The main advantage of distillation assays compared to GC assays is that the normal boiling point is measured directly and other properties such as density can be measured if the distillation cuts are collected. Also, normal boiling points are more representative of the molecular interactions that define the physical properties of a cut (Riazi, 2005). The main disadvantages of distillation assays are that they are time consuming, expensive, and have a limited boiling range.

The distillation techniques proposed for crude oils are summarized elsewhere (Riazi, 2005) and include a variety of atmospheric (ASTM D-86, D-2892) and vacuum distillation methods (ASTM D5236, D-1160). Atmospheric distillation techniques are only suitable for light oils because only up to 5 wt% of a heavy oil or bitumen can be distilled at atmospheric pressure (Castellanos Díaz *et al*., 2014). Conventional vacuum distillation methods, such as spinning band distillation, can distill up to 20 wt% of a heavy oil at pressures down to approximately 130 Pa (Sánchez-Lemus *et al*., 2014).

To extend the distillation range for heavy oils, a deep vacuum distillation apparatus was designed to distill up to 50 wt% of those fluids (Castellanos-Diaz *et al.*, 2011). This device operates at pressures down to 1×10^{-7} Pa and allows the collection of up to six distillation cuts. Properties of collected distillation cuts for seven heavy oils from disparate geographical locations were measured and used to develop extended property correlations for heavy oil fractions (Sánchez-Lemus *et al*., 2016; Ramos-Pallares *et al.*, 2016). It was also demonstrated that the extended boiling points followed a Gaussian extrapolation of conventional vacuum distillation data (Sánchez-Lemus *et al*., 2014). Therefore, a conventional distillation is sufficient to generate an oil characterization.

Gas Chromatography

Gas chromatography (GC) is a separation technique based on the retention time of crude oil components as they interact with a mobile phase and a packed column stationary phase. A standard GC assay provides the mass distribution of single carbon number fractions (ASTM D4626). In simulated distillation (SimDist) assays, the retention time of each component is correlated to the boiling point for each component (ASTM D-2887). The determination of the boiling point distribution of crude oil fractions by GC is rapid, reproducible, and more economical than laboratory-scale physical distillation.

The petrochemical industry often uses GC for crude oil characterization due to the speed of the analysis (Vickers, 2002). The most commonly used methods are ASTM D2887, D5307, D6352, and D7169. ASTM D7169 has extended the applicability of SimDist to heavier fractions of crude oil. However, the extrapolation does not match experimental data for heavy oil fractions (Sánchez-Lemus *et al*., 2014). Other authors have found a similar discrepancy with SimDist data at higher boiling points (Gilgenast *et al.*, 2011). SimDist likely does not apply to aromatic compounds where there is no linearity between retention time and boiling point (Sánchez-Lemus *et al*., 2016).

SARA Analysis

A common method to assay heavy oil is SARA fractionation where the oil is separated into saturates, aromatics, resins, and asphaltenes, as shown in Figure 2.2. The asphaltenes are separated by solubility. The deasphalted oil (termed maltenes) is separated into the other fractions by adsorption. A description of each of the SARA fraction is provided below:

- Saturates consist of paraffins and cycloparaffins with molecular weights typically between 300 g/mol and 600 g/mol and densities between 0.869 and 0.880 g/cm³ (Speight, 2007). They are the least polar fraction of the crude oil.
- Aromatics consist mainly of compounds with one to a few aromatic rings with alkyl-chains or naphthenic rings attached to the aromatic ring. Their molecular weights range from 300 to 800 g/mol and their densities from 0.990 to 0.999 g/cm³ (Speight, 2007).

- Resins are similar to aromatics but have higher polarity and a lower hydrogen/carbon (H/C) ratio. Their molecular weights range from 700 to 1300 g/mol and their densities from 1.044 to 1.049 g/cm³ (Speight, 2007).

- Asphaltenes are the most polar, aromatic, and heaviest fraction of the crude oil. The asphaltenes have a wide variety of structures containing aromatic rings, naphthenic rings, heteroatoms, and paraffinic chains (Speight, 2007). Asphaltenes include self-associating species that formed nanoaggregates of 2-6 monomers with an average diameter of 5 to 9 nm (Yarranton *et al*., 2000; Yarranton *et al*., 2013). The molecular weight of asphaltene monomers is between 500 to 1500 g/mol (Yarranton *et al*., 2007; Mullins, 2007). The average density of asphaltenes is typically between 1050 and 1200 kg/m³ (Barrera *et al*., 2013).

```
                        ┌──────────────┐
                        │  Crude Oil   │
                        └──────┬───────┘
                    n-pentane or n-heptane
              ┌────────────────┴────────────────┐
     ┌────────────────┐              ┌──────────────────┐
     │  Asphaltenes   │              │ Deasphalted Oil  │
     └────────────────┘              └────────┬─────────┘
                                          Clay
                              ┌───────────────┴───────────────┐
                        ┌────────────┐              ┌──────────────┐
                        │   Resins   │              │    Oils      │
                        └────────────┘              └──────┬───────┘
                                                    Silica Gel
                                          ┌───────────────┴──────────────┐
                                    ┌────────────┐              ┌──────────────┐
                                    │ Aromatics  │              │  Saturates   │
                                    └────────────┘              └──────────────┘
```
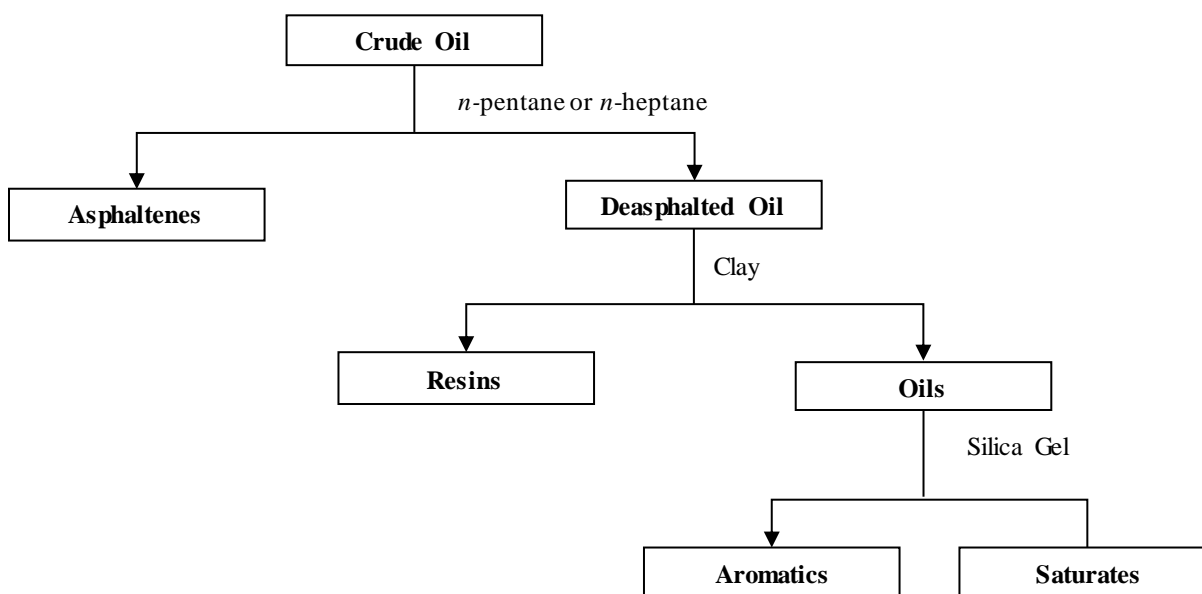
Figure 2.2 SARA fractionation procedure for crude oils. Adapted from Powers *et al*. (2016).

2.2.2 Oil Characterization Based on Distillation Assays

Distillation is the preferred characterization method for phase behaviour calculations with equations of state (Whitson and Brulé, 2000; Pedersen *et al*., 2006). The distillation data can be obtained from a physical distillation or SimDist. Standard GC data can also be used for oil

characterization but this approach has not been applied to heavy oils because there are no boiling point data for heavy fractions upon which to base a correlation from carbon number to boiling point. This thesis focuses on characterization based on distillation assays.

Figure 2.3 shows a typical normal boiling point (NBP) distribution curve from a spinning band distillation. As recommended by Castellanos-Diaz *et al.* (2011), a Gaussian distribution is used to extrapolate the boiling curve over the maltenes (deasphalted oil). The Gaussian extrapolation presumes a normal distribution of boiling points as is typical for crude oils (Altgelt and Boduszynski, 1994). The *n*-pentane insoluble asphaltenes (C5-asphaltenes) are characterized separately because they are considered to be associated species. Their characterization is based on a Gamma function molecular weight distribution. The boiling point distribution curve is then divided into boiling point cuts, each of which represents a pseudo-component with the average properties of that cut. The properties for each pseudo-components are calculated from empirical correlations such as the Lee-Kesler (Kesler, 1976), Katz-Firoozabadi (Katz and Firoozabadi., 1978), Twu (Twu, 1984) and Soreide (Soreide, 1989) correlations. The correlations are constrained or tuned to match experimental data such as the average molecular weight and the crude oil density. This characterization approach has been evaluated and validated by several authors from the same group (Castellanos-Diaz *et al.*, 2011; Sánchez-Lemus *et al.*, 2016; Agrawal *et al.*, 2012; Johnston *et al.*, 2017b; Mancilla-Polanco *et al.*, 2018). A more detailed description of the characterization is provided in Chapter 4.
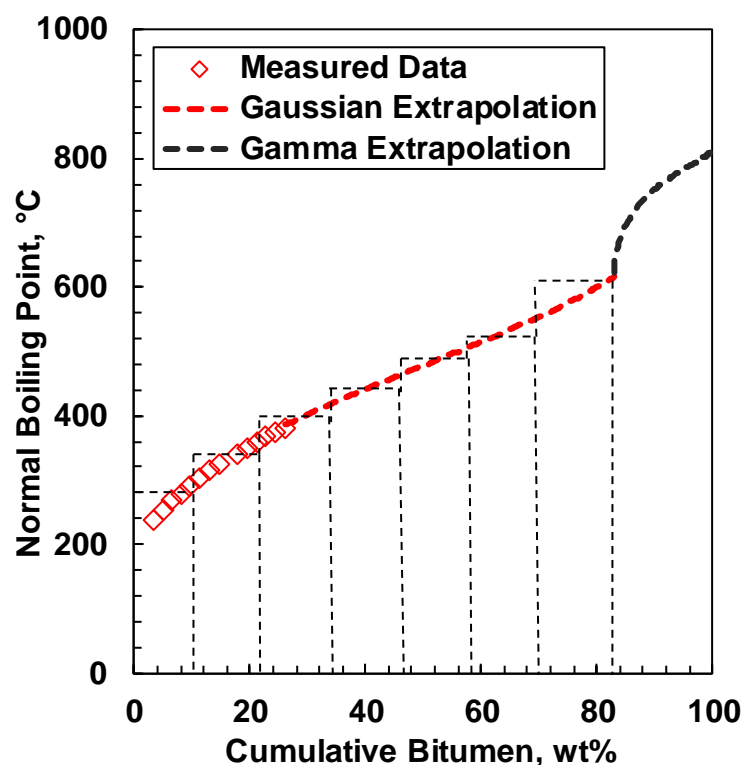
Figure 2.3 Normal boiling point distribution for a Western Canadian Bitumen with maltene pseudo-components indicated with light dashes. Data from Castellanos-Diaz *et al*. (2014).

2.3 Bitumen/Solvent Phase Behaviour

This section presents a summary of the measured phase diagrams of solvent diluted bitumen. The morphology of the asphaltene-rich phases formed from these mixtures is also discussed.

Phase Diagrams

Diluted bitumen systems exhibit multiphase behaviour including vapour-liquid (VL), liquid-liquid (LL), vapour-liquid-liquid (VLL), and in some cases vapour-liquid-liquid-liquid (VLLL) regions. The phase behaviour depends on temperature, pressure, solvent type and content. In this thesis, when two liquid phases are present, they are denoted as follows: L_1 = the primary phase (bitumen and solvent) and L_2 = the secondary phase that appears as solvent is added (solvent-rich or asphaltene-rich). When three liquid phases are present, they are denoted as: L_1 = bitumen-rich, L_2 = solvent-rich, and L_3 = asphaltene-rich.

First consider data for mixtures of an *n*-alkane and bitumen. Mehrotra and Svrcek (1988) found a VL_1 boundary for mixtures of methane and Cold Lake bitumen at temperatures from 26.8 to 103.4°C, pressure up to 10 MPa, and solvent contents up to 1.6 wt%. They also found that the solubility of methane in Cold Lake bitumen increased linearly with an increase in pressure and decreased slightly with an increase in temperature.

The same authors reported both VL_1 and VL_1L_2 regions for mixtures of ethane and Cold Lake bitumen at temperatures from 24.2 to 101.6°C, pressures up to 10 MPa, and solvent contents up to 13 wt%. The L_1 phase was a heavy solvent-rich bitumen phase and the L_2 phase was a light ethane-rich phase. Their data are shown on pressure-composition (P-X) diagrams in Figure 2.4.
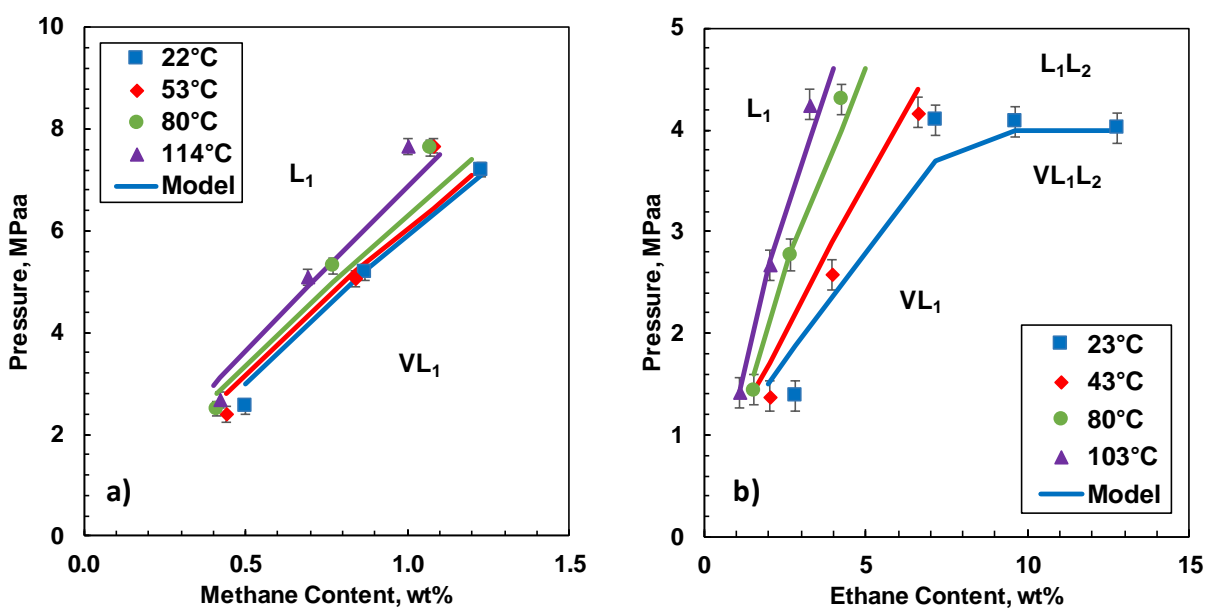
Figure 2.4 Pressure-composition (P-X) phase diagram for mixtures of bitumen with: a) methane; b) ethane. Data (symbols) from Mehrotra and Svrcek (1988) and modeling (lines) from Agrawal *et al*. (2012).

Badamchi-Zadeh *et al*. (2009) observed VL_1 and L_1L_2 regions in mixtures of propane and Athabasca bitumen at temperatures from 10 to 50°C, pressure up to 1.5 MPa, and solvent content up to 25.4 wt%. Dini *et al*. (2016) investigated mixtures of propane and Peace River bitumen at

temperatures from 30 to 120°C, pressure from 1 to 6 MPa and solvent content up to 85.7 wt%. They defined the phase diagrams as Type III according to the van Konynenburg-Scott nomenclature (Van Konynenburg and Scott, 1980). This diagram is characterized by a VL_1L_2 region extending from a freezing point up to a temperature exceeding the critical point of the solvent. Mancilla-Polanco *et al*. (2018) reported the phase behaviour for mixtures of propane and a Western Canadian bitumen including phase compositions at temperatures from 20 to 180°C, pressures up to 10 MPa, and solvent contents up to 90 wt%. Two liquid phases were observed: a solvent-rich bitumen phase (L_1) and an asphaltene-rich phase (L_2) as shown in Figure 2.5. At 90°C with a propane content of 50 wt%, a VL_1L_2 region was detected. However, at 135°C and the same solvent content, the L_1 was phase was supercritical and no vapour phase was observed.
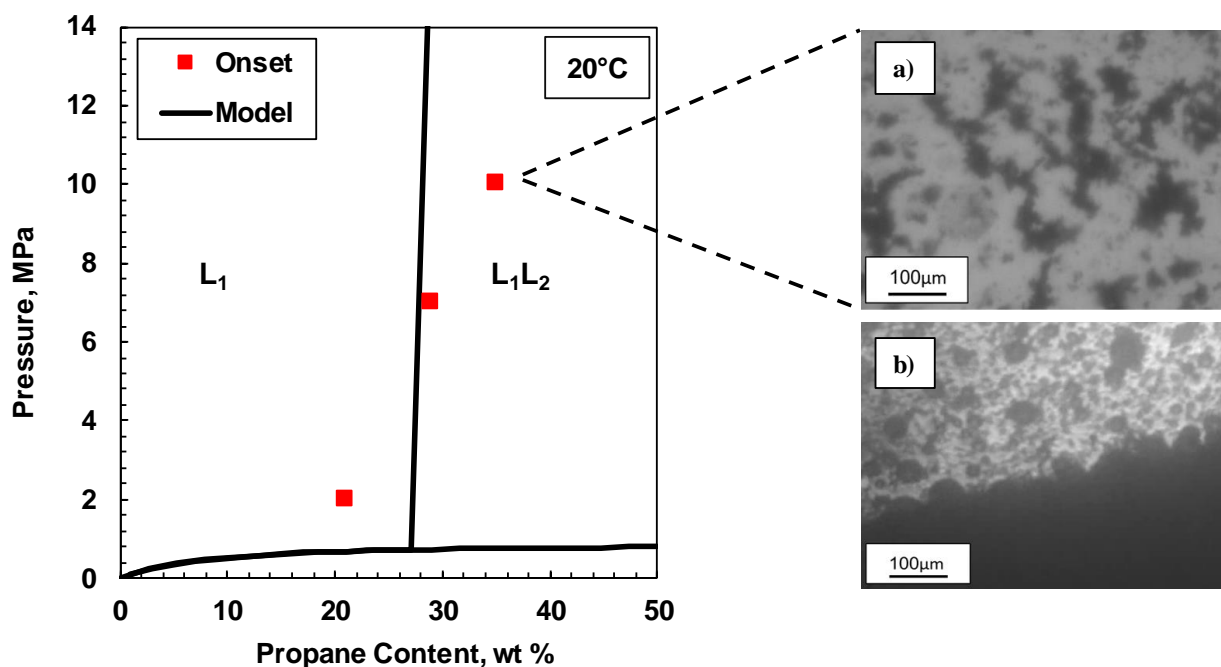
Figure 2.5 Pressure-composition diagram for mixtures of propane and a Western Canadian bitumen at 20°C. Micrograph image of the asphaltenes phase morphology at: a) 20°C and 10 MPa; b) 50°C and 2 MPa. Data and images from Mancilla-Polanco *et al*. (2018).

Yazdani and Maini (2007) investigated mixtures of *n*-butane and Frog-Lake heavy oil at room temperature and *n*-butane contents from 15 to 32 wt% and constructed a (P-X) diagram at room temperature. They observed only a VL_1 region. Gao and Li (2017) studied the phase behaviour for

mixtures of *n*-butane/Athabasca-bitumen/water at temperatures up to 160°C and pressures up to 10 MPa. They detected four phases (WVL_1L_2) at 160°C, 8.26 MPa, an *n*-butane content of 54.65 wt%, and a water content of 28.37 wt%. The liquid phases were a water phase (W), a solvent-rich bitumen phase (L_1), and an asphaltene-rich phase (L_2).

Zou *et al.* (2007) studied the phase behaviour for mixtures of *n*-pentane and Athabasca vacuum residue (AVR) at temperatures from 22 to 340°C, pressure up to 14.4 MPa. They observed three and four phase equilibria including VL_1L_3 and $VL_1L_2L_3$ regions where L_1 is a bitumen-rich phase, L_2 is a solvent-rich phase, and L_3 is likely an asphaltenes-rich phase. The four phase region was found at 160°C, 1.85 MPa, and a solvent content of 45 wt%.

Johnston *et al*. (2017b) studied the phase behaviour of mixtures of *n*-pentane and Peace River bitumen at temperatures up to 230°C, pressures up to 14 MPa, and solvent contents up to 90 wt%. They found both VL_1 and L_1L_2 phase boundaries at temperatures from 23 to 230°C. The two liquid phases were a solvent-rich bitumen phase (L_1) and an asphaltene-rich phase (L_2), as shown in Figure 2.6. The second liquid phase appeared at solvent content around 50 wt% at most temperatures and pressures.
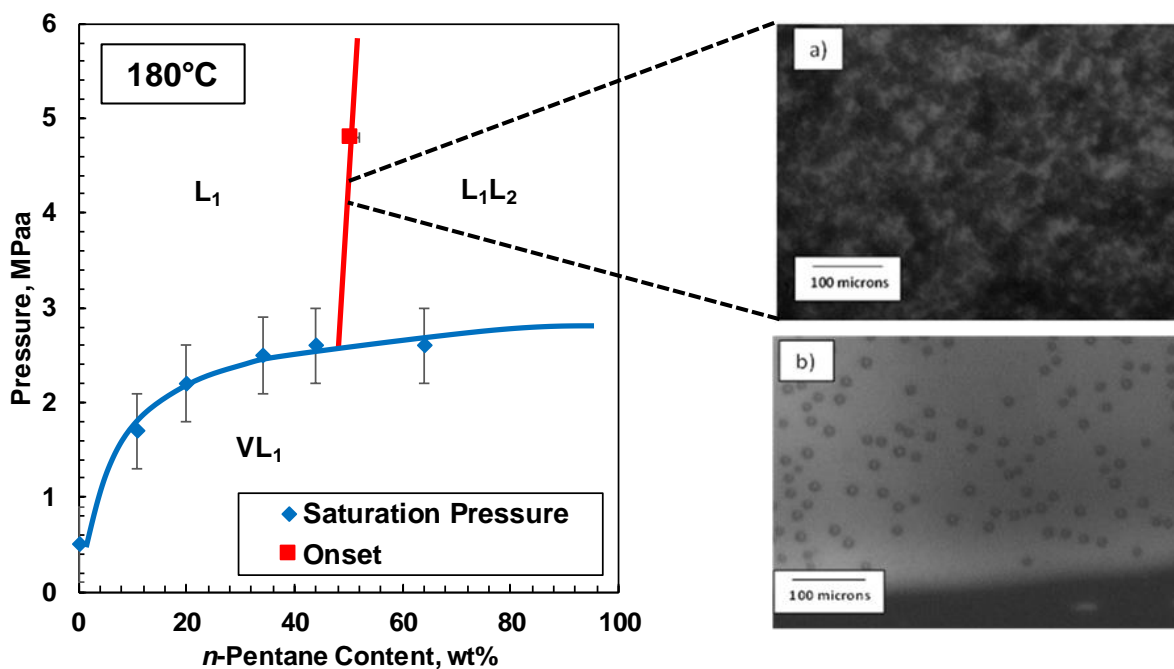
Figure 2.6 Pressure-composition phase diagram for mixtures of *n*-pentane and bitumen at 180°C. Micrograph image of the asphaltene phase morphology at: a) 23°C (glass-like particles); b) 165°C (liquid droplets). Data and images from Johnston *et al*. (2017b).

The mixtures of *n*-alkane and bitumen show the following trends with increasing *n*-alkane carbon number: 1) the saturation pressure decreases; 2) the onset of the second liquid phase (L_1L_2 boundary) shifts to higher *n*-alkane content; 3) the second liquid phase shifts from a light *n*-alkane-rich phase to a heavy asphaltene-rich phase. In other words, for mixtures of ethane and bitumen, light components are rejected. For mixtures of *n*-pentane and higher carbon number *n*-alkanes, heavy components (mainly asphaltenes) are rejected. In mixtures with propane and likely *n*-butane, a significant fraction of the bitumen partitions to each phase. Methane has too low solubility in bitumen to initiate a second phase.

There are also some data for solvents other than *n*-alkanes. Badamchi-Zadeh *et al*. (2009a) studied the phase behaviour of CO_2 with Athabasca bitumen at a fixed temperature of 25°C, pressures of 3.96 and 6.02 MPa, and a solvent content of 18 wt%. They found that above 11 wt% CO_2 content, the saturation pressure did not change as the CO_2 content increased, indicating the presence of an

additional liquid phase. Similarly, Mehrotra and Svrcek (1988) evaluated the phase behaviour for CO_2 with Cold Lake bitumen at temperatures from 15 to 98°C, pressure up to 12 MPa, and solvent contents up to 14 wt%. They also noted the formation of a second phase at approximately 12 wt% in the CO_2 content at lower temperatures. The phase diagram is qualitatively similar to that of ethane and bitumen.

Mehrotra and Svrcek (1988) evaluated the solubility effect for mixtures of nitrogen and Cold Lake bitumen at temperatures of 31.0, 56.8 and 97.8°C, pressures up to 10 MPa, and solvent contents up to 0.8 wt%. They found that the solubility of nitrogen in bitumen was small. There was little change in the nitrogen solubility with temperature and an increase in solubility with increasing pressure. The phase diagram is qualitatively similar to that of methane and bitumen.

Heavy Phase Yield and Composition

The amount and composition of the heavy phase is an important factor in process applications such as deasphalting and oil sands froth treatment, and in flow assurance issues such as deposition and fouling. Most studies focus on asphaltene precipitation because asphaltenes are a key factor in deposition and fouling. Typically, onsets and/or yields are reported. An onset is the condition (temperature, pressure, or solvent content) at which asphaltenes first precipitate. In this discussion, onset refers to the solvent (*e.g*. pentane) content where the solvent is in fact a precipitant. Yield is the mass of asphaltenes (or crude oil) in the heavy phase divided by the mass of crude oil in the feed. The lower the solubility of the asphaltenes, the higher the onset (more solvent required to precipitate asphaltenes) and the higher the yield, as shown in Figure 2.7.

Asphaltene solubility is relative insensitive to temperature. In *n*-pentane and higher carbon number *n*-alkanes, asphaltene solubility tends to increase slightly as the temperature increases up to 100°C (Andersen and Stenby, 1996; Akbarzadeh *et al*., 2005; Panuganti *et al*., 2012; Johnston *et al.,* 2017b). Above 100°C, asphaltene solubility appears to decrease (Andersen *et al.,* 1998; Johnston *et al.,* 2017b). The reversal in the trend can be explained based on the activity coefficient of the asphaltenes which depends on the difference between both the molar volume and the solubility parameter of the asphaltene and the medium (Akbarzadeh *et al*., 2005; Powers *et al.*, 2016). An

increase in temperature has two effects: 1) higher relative molar volume ratio between asphaltenes and the solution which increases asphaltene solubility; 2) lower solubility parameter of the oil (Sirota, 2005) which decreases the asphaltenes solubility. The molar volume changes dominate at temperatures below 100°C but the solubility parameter changes tend to dominate at elevated temperatures. Mancilla-Polanco *et al.* (2018) found that asphaltene solubility in propane was insensitive to temperature at the conditions investigated (50 to 130°C). It appears that the changes in molar volume and solubility parameter cancel each other out with propane.
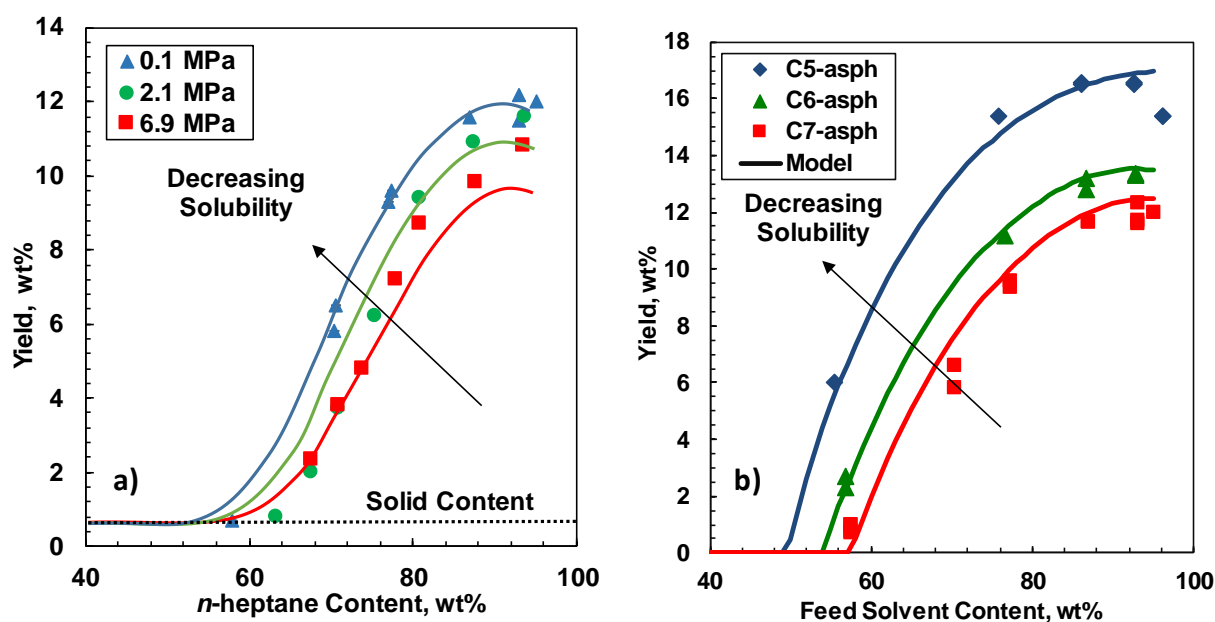
Figure 2.7 Asphaltene yield curves at room temperature for Athabasca bitumen: a) diluted with *n*-heptane at different pressures; b) diluted with different *n*-alkanes at atmospheric pressure. Data from Akbarzadeh *et al.* (2005).

In general, more asphaltenes precipitate as pressure decreases in live crude oils and heavy oils with solvents (Akbarzadeh *et al.*, 2005; Johnston *et al.*, 2017b; Panuganti *et al.*, 2012; Tharanivasan *et al.*, 2010; Pedersen *et al.*, 2006). In other words, crude oils and solvents become poorer solubilizers for asphaltenes as the pressure drops and the fluid density decreases. Mancilla-Polanco *et al.* (2018) observed the same trend in propane diluted bitumen.

For mixtures of *n*-alkanes and bitumen, the amount of heavy phase decrease (solubility increases) as the carbon number of the *n*-alkane solvent increases (Andersen and Birdi, 1991; Akbarzadeh *et al*., 2005; Wiehe *et al*., 2005). Akbarzadeh *et al*. (2005) studied the asphaltene precipitation with Wester Canadian bitumen at room temperature, atmospheric pressure with *n*-pentane, *n*-hexane and *n*-heptane over the whole range of feed composition. The yield, defined as the amount of asphaltenes over the bitumen in feed for the three solvents is shown in Figure 2.7. Note that the solvent content at which asphaltene starts to precipitate (onset) increases as the carbon number of the *n*-alkane solvent increases.

The heavy phase includes some of the other oil constituents and some of the solvent. However, there are relatively little data on crude oil yields and phase compositions. Johnston *et al.* (2017b) measured *n*-pentane content in the heavy phase to be from 20 to 30 wt% for mixtures of *n*-pentane and Western Canadian bitumen at 180°C. Polanco-Mancilla *et al.* (2018) measured propane content in the heavy phase to be from 1 to 27 wt% for mixtures of propane and a Western Canadian bitumen at temperatures from 50 to 130°C. The high propane content was observed at temperatures below 100°C where the asphaltene-rich phase appears as glassy particles and may be due to entrainment of the continuous phase within the settled particles.

Asphaltene-Rich Phase Morphology

The asphaltene-rich phase can appear as glassy particles, a liquid, or in a transitional state between the two. The morphology of the asphaltene phase depends on the temperature, pressure, type of solvent, and solvent content (Sirota, 2005; Johnston *et al*., 2017b; Mancilla-Polanco *et al.*, 2018).

Isolated asphaltenes exhibit a glass transition. Zhang *et al*. (2004) studied the glass transition temperature of isolated asphaltenes using differential scanning calorimetry. They analyzed the behaviour of four asphaltenes (*n*-heptane insolubles) obtained from different vacuum residue sources: Iranian Light, Khafji, Kuwait, and Maya crude oils. The lower end of the glass transition temperature range for all four asphaltenes was found to be between 120 and 130°C. The asphaltenes attained completely liquid behaviour at temperatures between 220 and 240°C. Similarly, Gray *et al*. (2004) evaluated the melting behaviour of five different heptane-insoluble

asphaltenes: Athabasca asphaltenes from Canada, Arabian Heavy and Light from Saudi Arabia, Gudao from China, and Maya from Mexico. They found that a liquid melt formed at temperatures between 214 and 311°C and reported a melting point ranging between 224 and 245°C except for the Maya which was significantly higher at 294°C.

Asphaltenes in solutions of solvents such as *n*-heptane and toluene at ambient temperatures, the asphaltenes-rich phase appears as glassy particles (Rastegari *et al*., 2004). In mixtures of a crude oil and *n*-pentane or a higher carbon number solvent at temperatures below approximately 100°C, the asphaltene-rich phase also appears as glassy particles. However, at higher temperatures the asphaltene-rich phase reaches a glass transition and becomes a liquid by approximately 130°C, as shown in Figure 2.6 (Agrawal *et al*., 2012; Johnston *et al*., 2017b). Others have also found a glass transition at temperatures ranging from 75-150°C for asphaltenes precipitated from a Cold Lake bitumen with *n*-pentane (Nielsen *et al*., 1994; Mehrotra *et al*., 1989).

Mancilla-Polanco *et al*. (2018) examined the asphaltene-rich phases in mixtures of propane and bitumen. At 20°C, the asphaltene-rich phase appeared as glassy particles near the onset of precipitation but in a transition state above the onset as the maltene content of the asphaltene-rich phase increased. At 50°C, irregular transition state particles that merged on the high pressure microscope glass surface even appeared near at the onset. Above, 90°C, the phase appeared as droplets that coalesced into a continuous liquid phase, as shown in Figure 2.5. Hence, the glass transition shifts to lower temperatures as the maltene content of the asphaltene-rich phase increases. The phase morphology did not appear to be sensitive to pressure likely because the phase composition did not change significantly with pressure.

2.4 Models for Bitumen/Solvent Phase Behaviour

Both equations of state and activity coefficient approaches (mainly regular solution theory) have been used to model the phase behaviour of mixtures of bitumen and solvent. Typically, equations of state are used to determine phase boundaries and sometimes to model asphaltene precipitation. Equations of state are applicable for the whole phase diagram but tend to lose accuracy in the liquid-liquid region. Activity coefficient approaches are used to model asphaltene precipitation.

Activity coefficient models are only suitable for liquid phases far from the critical point. Both approaches are briefly discussed below.

2.4.1 Cubic Equations of State

Cubic Equation of States (CEoS) have been used extensively in chemical and petroleum engineering to predict the phase behaviour of mixtures of different components. There are several forms of CEoS but only the Peng-Robinson (PR) EoS is presented here as an example because it is the form most commonly used in petroleum applications. The general form of the PR EoS is given by:

$$P = \frac{RT}{v - b} - \frac{a\alpha(T_r, \omega)}{v(v + b) + b(v - b)} \tag{2.1}$$

where a and b are EoS parameters referred to as the attractive parameter and the co-volume parameter, respectively. For pure substances, the two parameters are determined from the component critical properties.

CEoS do not provide accurate liquid phase density estimations. Peneloux *et al*. (1982) introduced a volume translation parameter, c, to improve the density calculation and it was extended to the PR EoS by Jhaveri and Youngren (1988) to obtain the following expression:

$$P = \frac{RT}{v - b} - \frac{a\alpha(T_r, \omega)}{(v + c)(v + b + 2c) + (b + c)(v - b)} \tag{2.2}$$

The volume translation term improves the estimation of molar volumes and phase densities without altering the phase equilibrium calculations. Mathias *et al*. (1989) developed and defined a new volume translation term to further improve the liquid phase density estimations in the vicinity of the critical point.

For multicomponent mixtures, mixing rules are employed to estimate EoS parameters a and b. The classical van der Waals mixing rules are given by:

$$a_m = \sum_i \sum_j x_i x_j \sqrt{a_i a_j}(1 - k_{ij}) \tag{2.3}$$

$$b_m = \sum_i x_i b_i \qquad (2.4)$$

where a_m and b_m are the corresponding EoS parameters for mixtures. x_i and x_j are the mole fraction of component i and j, respectively, and k_{ij} is the binary interaction parameter. Binary interaction parameters are commonly determined minimizing the difference between the modeled and the experimental data. Therefore, they are not treated as physical term but as a fitting parameter. Van der Waals mixing rules are considered to be symmetric because there is only one interaction parameter for each binary pair ($k_{ij} = k_{ji}$). Symmetric mixing rules are unable to adequately represent the phase behaviour of mixtures of species whose polarities differ significantly (Castellanos-Diaz *et al*., 2011; Agrawal *et al*., 2012).

Cubic Equations of State Applied to Bitumen/Solvent Systems

Mehrotra and Svrcek (1988) used the Peng-Robinson (PR) EoS to calculate the solubility for five pure gases (nitrogen, carbon monoxide, methane, carbon dioxide and ethane) in Athabasca bitumen. The Athabasca bitumen was characterized as a mixture of three pseudo-components. The binary interaction parameter was optimized to match the solubility data.

Jamaluddin *et al*. (1991) used a modified three parameters Martin EoS to predict the solubility of CO_2 in heavy oils and bitumen. The crude oil was considered as a single pseudo-component. A constant interaction parameter and a constant adjusted critical compressibility were recommended to match the experimental data. They found that the Martin EoS is as accurate as the PR EoS; however, the Martin EoS predicted the density more accurately.

Saber *et al*. (2012) used the PR EoS to model the phase boundaries for mixtures of an Athabasca vacuum residue (AVR) and *n*-alkane solvents from *n*-pentane to dodecane at temperatures from 150 to 350°C and pressures up to 25 MPa. The AVR was treated as a mixture of 20 pseudo-components. A group contribution method was used to estimate the critical properties and acentric factors of each pseudo-component. The binary interaction parameters between residue pseudo-components and each *n*-alkane were tuned to a limited number of saturation pressures (VL$_1$ boundary) and onset (L$_1$L$_2$ boundary) data points. The model was used to generate pressure-

composition diagrams and was in qualitative agreement with the measured values. The authors concluded that the PR EoS with a group contribution based characterization can be a potential heavy oil modeling tool for the simulation of paraffinic deasphalting, separation, and refining processes for ill-defined hydrocarbon mixtures. However; more data points are required to rigorously test this approach.

Agrawal *et al*. (2012) investigated the applicability of the PR EoS to the phase behaviour of mixtures of bitumen with *n*-pentane, ethane, methane, and carbon dioxide. The asphaltenes were represented as already associated nano-aggregates and self-association was not further considered. They introduced a temperature dependent correlation for the binary interaction parameters. The model matched saturation pressures and onsets to within the experimental error; however, it under-predicted the amount of the heavy phase.

Johnston *et al*. (2017a) evaluated several set of asymmetric mixing rules on the phase behaviour of mixtures of *n*-pentane and bitumen at temperatures from 20 to 280°C and pressures up to 10 MPa. The mixing rules included asymmetric van der Waals, Sandoval/Wilczek-Vera/Vera, and Huron–Vidal mixing rules with an NRTL (non-random liquid theory) activity coefficient model. Asymmetric van der Waals mixing rules have two distinct interaction parameter values for each binary pair ($k_{ij} \neq k_{ji}$). The asymmetric mixing rules improved the model but could not match both saturation pressures and asphaltene yields within the accuracy of the measurements.

Johnston *et al*. (2017a) also evaluated composition dependent mixing rules. Binary interaction parameters can vary with composition, specifically for highly polar and asymmetric systems (Adachi and Sugie, 1986; Panagiotopoulos and Reid, 1986). For example, Panagiotopoulos and Reid (1986) developed a two-parameter mixing rule with k_{ij} as a linear function of composition. They obtained a significant improvement in the representation of binary and ternary phase equilibrium data for highly polar and asymmetric mixtures. Johnston *et al*. (2017a) developed a symmetric compositional dependent binary interaction parameter correlation for solvent/asphaltene interactions as a function of temperature and feed composition and was able to match asphaltene yields and saturation pressures within the accuracy of the measurements.

Mancilla-Polanco *et al.* (2018) extended the Johnston *et al.* (2017) approach to mixtures of propane and a Western Canadian bitumen at temperatures from 50 to 130°C and pressures up to 10 MPa. They proposed a compositionally dependent mixing rule to represent the binary interaction parameter as a function of the normal boiling point of each pseudo-component and the propane feed composition. The tuned model accurately fitted both the saturation boundaries, yields, and the mass fraction of pentane insoluble asphaltenes in the heavy phase.

2.4.2 PC-SAFT Equation of State

The statistical associating fluid theory (SAFT) equation of state estimates the Helmholtz energy of a system as a departure from the ideal gas value (Chapman, 1989). The departure function, also known as the residual Helmholtz energy, accounts for contributions arising from short-range and long-range molecular interactions, formation of chemical bonds, and molecular association. Each one of these contributions can be estimated from the first order perturbation theory of Wertheim (1986) according to the procedure proposed by Chapman (1989).

The residual Helmholtz energy consists of three intermolecular force contribution terms, Figure 2.8. The first term, A^{seg}, which accounts for the contribution of the dispersion forces between segments. The second term, A^{chain}, provides the contribution of the presence of covalent chain-forming bonds between segments. The third term, A^{assoc}, accounts for association between molecules.

$$A^{res} = A^{seg} + A^{chain} + A^{assoc} \qquad (2.5)$$
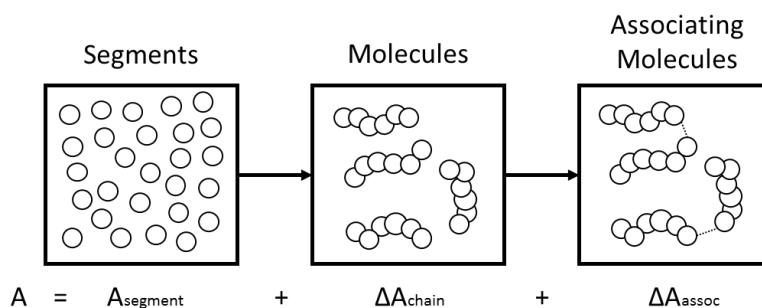
Figure 2.8 Residual Helmholtz energy contribution for SAFT (Chapman, 1989).

Gross and Sadowsky (2001) developed the perturbed chain (PC) form of the SAFT EoS by extending the perturbation theory of Barker and Henderson (Barker and Henderson, 1967) in order to account for the effect of chain length on the segment dispersion energy. This model applies to phase behaviour that can be qualitatively described through London dispersion interactions; that is, there is no association. PC-SAFT uses a hard sphere reference fluid described by the Mansoori-Carnahan-Starling-Leland Equation of State (Mansoori *et al.*, 1971). The PC-SAFT EoS as implemented by Gonzalez *et al.* (2005) is given by,

$$\frac{A^{res}}{RT} = \frac{A^{seg}}{RT} + \frac{A^{chain}}{RT} = m\left(\frac{A_0^{hs}}{RT} + \frac{A_0^{disp}}{RT}\right) + \frac{A^{chain}}{RT} \tag{2.6}$$

where A_0^{hs}, and A_0^{disp} are respectively the hard sphere and dispersion contributions to the model and *m* is the number of segments per molecule. Two parameters in addition to *m* are required for each non-associating component or pseudo-component: the diameter of each molecular segment (σ) and the segment dispersion energy (ε/k). Correlations for these parameters are available in the literature (Gross and Sadowski, 2001; Ting *et al.*, 2003). This form of SAFT is suitable for the phase behaviour of mixtures involving high molecular weight fluids (polymer solutions or associated asphaltenes).

PC-SAFT Applied to Bitumen/Solvent Systems

The SAFT EoS has been successfully applied to model the vapour-liquid equilibria, density, and asphaltenes precipitation onset for crude oils (Ting *et al.*, 2007). The asphaltenes are represented as already associated nano-aggregates and self-association is not further considered. For example, Gonzalez *et al.* (2005) used the PC-SAFT EoS to match the onset of asphaltene precipitation and vapour-liquid equilibria from a model live oil (a mixture of asphaltenes, toluene, and a dissolved gas) and from a recombined oil (reservoir oil with a mixture of CH_4, C_2H_6, N_2, CO_2, and light *n*-alkanes). They simulated reservoir pressure depletion and gas injection (CO_2, N_2, CH_4, and C_2H_6) processes. Gonzalez *et al.* (2007) also demonstrated that PC-SAFT-based EoS with four pseudo-components can match not only the onset of asphaltene precipitation and the bubble point but also the amount and the composition of the asphaltene-rich phase from live oils.

Tavakkoli *et al*. (2014) presented a methodology for the PC-SAFT EoS to model the phase stability of asphaltenes in crude oil dilutes with *n*-alkanes. They demonstrated that binary interaction parameters play a key role controlling the onset of precipitation as well as the shape of the asphaltenes precipitation curve. They also studied the effect of asphaltenes polydispersity in modeling the amount of precipitation from *n*-alkane diluted crude oils.

Fouad *et al*. (2018) developed a methodology to predict light oil phase behaviour without the need of asphaltenes onset data. They recommended focusing future efforts on extending the methodology to a wide range of crude oil, such as heavy oil and bitumen in order to develop a fully predictive model (Fouad *et al*., 2018).

2.4.3 Cubic Plus Association Equation of State

The cubic plus association (CPA) EoS was first used to describe the phase behaviour of associating fluids by the combined application of a cubic equation of state along with a theoretical background of the perturbation theory, which would account for the association part between species forming hydrogen bonds (Kontogeorgis *et al*., 1996). The CPA EoS can be expressed in term of pressure as a sum of a cubic EoS and the contribution of an association term as given by Michelsen and Hendriks (2001). The following expression represents the CPA model using the Soave-Redlich-Kwong (SRK) EoS (Kontogeorgis *et al*., 2006).

$$P = \frac{RT}{V_m - b} - \frac{a}{V_m(V_m + b)} - \frac{1}{2}\frac{RT}{V_m}\left(1 + \rho\frac{\partial lng}{\partial \rho}\right)\sum_i x_i \sum_{A_i}\left(1 - X_{A_i}\right) \tag{2.7}$$

where P is the pressure, R is the universal gas constant, T is the temperature, V_m is the molar volume, a and b are the CEoS parameters, ρ is molar density, g is the radial distribution density function, x_i is the mole fraction of component i, subscript A denotes a type of site on the molecules in component i, and X_{Ai} is the fraction of site A in component i that is not bonded to other sites.

For the association term in Equation 2.7, each component must be classified into an association type with a specified number of association sites per molecule. The association sites must be defined as either positive representing proton donors, or negative representing proton accepters. By default, only sites with an opposite sign can associate with each other. The fraction of

unoccupied sites, X_{Ai}, is then related to the association strength $\Delta^{A_iB_j}$ between two sites (site A and B) on two different molecules (i and j) as follows:

$$X_{A_i} = \frac{1}{1 + \rho \sum_j x_j \sum_{B_j} X_{B_j} \Delta^{A_iB_j}} \tag{2.8}$$

When $i \neq j$, the interaction is termed cross-association and when $i=j$, the interaction represents self-association. The self-association strength $\Delta^{A_iB_i}$ can be expressed as follows:

$$\Delta^{A_iB_i} = g \left[exp \left(\frac{\varepsilon^{A_iB_i}}{RT} \right) - 1 \right] b_{ii} \beta^{A_iB_i} \tag{2.9}$$

where $\varepsilon^{A_iB_i}$ is the association energy and $\beta^{A_iB_i}$ is the association volume. The self-association and cross-association energies can be adjusted manually or calculated from the self-association terms using the Elliot mixing rule given by:

$$\Delta^{A_iB_j} = \sqrt{\Delta^{A_iB_i}\Delta^{A_jB_j}} \tag{2.10}$$

The association energy and volume are the two defining parameters for the association term in the CPA-EoS; that is, all of the interaction terms can be determined from the $\varepsilon^{A_iB_i}$ and $\beta^{A_iB_i}$ of the components and pseudo-components. Hence, once the number and type of association sites for the associating components has been defined, the CPA-EoS requires a total of 5 parameters for each component: T_c, P_c, and ω for the CEoS terms, and; $\varepsilon^{A_iB_i}$ and $\beta^{A_iB_i}$ for the association term. As with a CEoS, binary interaction parameters must also be defined for each pair of components or pseudo-components.

CPA Applied to Bitumen/Solvent Systems

Li and Firoozabadi (2010) modeled asphaltene precipitation from solutions of an *n*-alkane and toluene. They adjusted only one parameter, the cross-association energy between asphaltenes and aromatics/resins (or toluene) molecules. Similarly, Arya *et al.* (2017) used the CPA EoS to model the asphaltene precipitation onset and asphaltene yield from degassed crude oil upon the addition of an *n*-paraffin. They compared the results with PC-SAFT EoS and concluded that CPA EoS gave more reliable results. Asphaltene yields calculated with PC-SAFT EoS did not decrease with the carbon number of the *n*-paraffin.

Recently, Zhang *et al*. (2019) studied the phase behaviour modeling for *n*-alkane diluted bitumen. They defined the self-associating pseudo-components as *n*-pentane insoluble (CPA C5) or as propane insoluble (CPA C3) content. Both approaches matched the phase boundary data for mixtures of *n*-pentane and higher *n*-alkane carbon number to within experimental error. The CPA C3 approach also matched yields and phase compositions within experimental error except near the critical temperature of the solvent. The CPA C5 approach could not match the yield data for propane diluted bitumen but was less computationally intense.

2.4.4 Regular Solution Theory

Regular solution theory is an activity coefficient model for liquid-liquid equilibrium where the composition of each liquid phase is calculated from the equilibrium ratios (*K*) for each component as follows:

$$K_i = \frac{x_i^H}{x_i^L} = \frac{\gamma_i^L}{\gamma_i^H} \tag{2.11}$$

where *x* and *γ* are the mole fraction and activity coefficient, respectively, subscripts *i* and *m* denote the component (or pseudo-component) and mixture, respectively, and superscripts *L* and *H* refer to the light and heavy phase, respectively. In a regular solution, the activity coefficient for the light phase is given by:

$$\gamma_i^L = exp\left[\frac{v_i^L}{RT}(\delta_i^L - \delta_m^L)^2\right] \tag{2.12}$$

where *v* is the molar volume, *δ* is the solubility parameter, *R* is the universal gas constant, and *T* is temperature. The activity coefficient for the heavy phase is calculated similarly.

For systems with significant size differences between molecules, the model has been modified to include an entropic contribution. The activity coefficient of components are calculated according to the Prausnitz-Hildebrand equation (Christian, 1971) which includes an entropic term from the Flory-Huggins lattice theory (Flory, 1953) and an enthalpic term from the Hildebrand-Scatchard (Christian, 1971) regular solution theory.

Regular Solution Theory Applied to Bitumen/Solvent Systems

Regular solution theory has been applied to asphaltene precipitation from depressurized live oils and solvent diluted heavy oils (Hirschberg *et al*., 1984; Wang and Buckley, 2001; Alboudwarej, *et al*., 2003; Tharanivasan *et al*., 2010). Of these, the Modified Regular Solution (MRS) model has been extensively used for the modeling of asphaltene precipitation from *n*-paraffin diluted heavy oils (Yarranton and Masliyah, 1996; Alboudwarej *et al*., 2003; Akbarzadeh *et al*., 2005) and is presented here. This model assumes that at solvent content above the onset of asphaltene precipitation, the system splits into two liquid phases: a light phase (L) rich in solvent, saturates and aromatics and, a heavy phase (H) rich in asphaltenes and resins. The oil is characterized into SARA fraction based pseudo-components. In this version of the model, only asphaltenes and resins are allowed to precipitate and the equilibrium of the asphaltenes and resins is then given by:

$$K_i = \frac{\gamma_i^L}{\gamma_i^H} = exp\left(ln\frac{v_i^L v_m^H}{v_i^H v_m^L} - \frac{v_i^L}{v_m^L} + \frac{v_i^H}{v_m^H} + \frac{v_i^L}{RT}(\delta_i - \delta_m^L)^2 - \frac{v_i^H}{RT}(\delta_i - \delta_m^H)^2 \right) \qquad (2.13)$$

The equilibrium ratios of the saturates, aromatics, and solvent are set to zero. Finally, the mass of asphaltene and resins precipitated are calculated using a flash calculation routine. The inputs for this model are the molar volumes and solubility parameters of each component and the composition of the mixture.

Alboudwarej *et al*. (2003) applied the Modified Regular Solution (MRS) model to asphaltene precipitation from Athabasca bitumen diluted with *n*-pentane, *n*-hexane, and *n*-heptane. The asphaltene fraction was represented as a set of pseudo-components defined from a gamma distribution of molecular weights. The solubility parameter of asphaltene pseudo-components were adjusted to match onset and yield and, a correlation for their calculation was proposed as a function of asphaltene pseudo-component specific gravity. The solubility parameters and molar volume for saturate and aromatic fractions were experimentally determined. Akbarzadeh *et al* (2005) proposed correlations for the calculation of solubility parameter of saturates and aromatics as a function of temperature. The MRS model was successfully tested on modeling asphaltene precipitation from seven different crude oils from disparate geographical locations diluted with *n*-alkanes ranging from C5 to C8 at temperatures up to 100°C. Recently, Powers *et al.* (2016) modified the correlations for asphaltene solubility parameters to apply to both native and reacted

asphaltenes. Similarly, Yarranton *et al*. (2018) updated the solubility parameter and density correlations for saturates, aromatics and resins. A major disadvantage of this model is that the composition and amount of the heavy phase cannot be calculated because only asphaltenes and resins are allowed to partition to the heavy phase.

2.5 Summary

Heavy oils are mixtures of millions of components including alkanes, napthenes, aromatics, and heterocompounds. When mixed with paraffinic solvents, they can exhibit complex phase behaviour including up to four hydrocarbon phases (vapour-liquid-liquid-liquid). In most cases, up to two liquid phases are formed. The second liquid phase ranges from a solvent-rich phase in heavy oil diluted with ethane to an asphaltene-rich phase in *n*-pentane and higher carbon number *n*-alkanes. The asphaltene-rich phase can appear as glassy particles or as a liquid depending on the conditions.

Recently, there have been significant advances in modelling the full range of heavy oil/solvent phase behaviour. The PR-EoS with composition dependent binary interaction parameters was tuned to model the phase boundaries, yields, and phase compositions for mixtures of heavy oil and propane and *n*-pentane. Similar results were obtained with CPA without the use of composition dependent parameters. The SAFT EoS approach has also succeeding in modeling a wide range of crude oil phase behaviour.

Chapter 3: Experimental Methods

The types of experiments performed in this thesis are presented in Figure 3.1. The vapour-liquid (VL_1) boundary was determined in a blind cell apparatus using the constant composition expansion method. The liquid-liquid (L_1L_2) boundary was determined using solvent titration in a high pressure microscope (HPM). The onset point was defined as the solvent content at which the second liquid phase appeared. The morphology of the second heavy phase was examined visually. Phase compositions in terms of solvent, maltenes, and n-pentane-insoluble asphaltenes (C5-asphaltenes), were measured in both a blind cell and a PVT cell apparatus. The C5-asphaltene and pitch* yields from the heavy phase were also measured in both a blind cell and a PVT cell apparatus. Yield is defined here as the mass of the specified material in the heavy phase divided by the mass of bitumen in the feed. Following the terminology of deasphalting processes, the heavy phase is referred to as "pitch". "Pitch*" refers to the solvent-free pitch; that is, the bitumen in the heavy phase. The procedures are described in more detail below. Distillation assay data and bitumen properties are also reported.
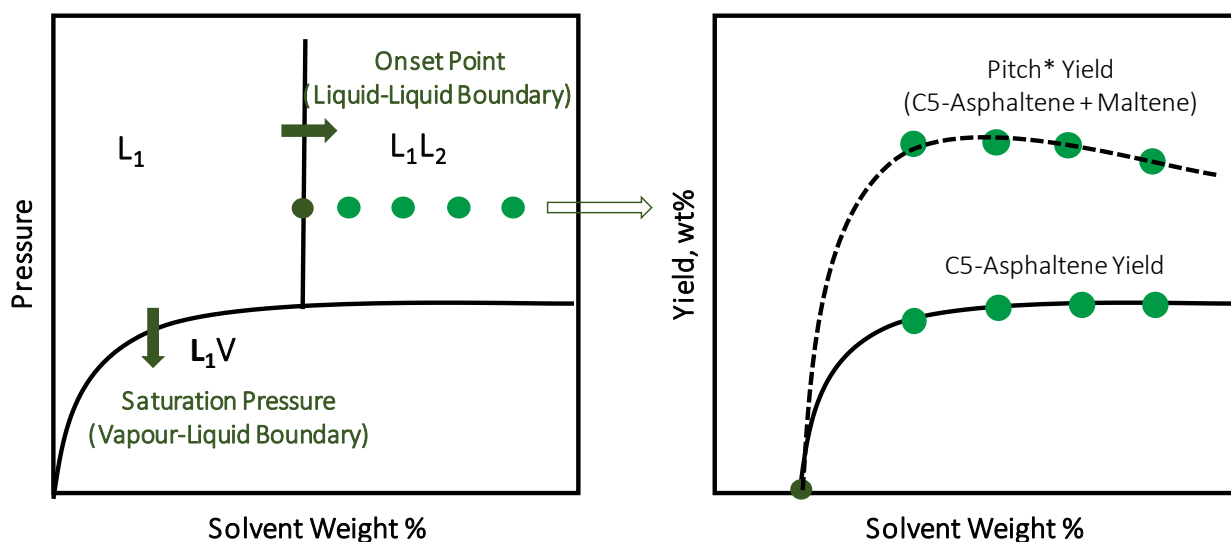
Figure 3.1 Phase diagrams showing the experiments used to map the phase behaviour for n-butane diluted bitumen.

3.1 Materials

The bitumen sample used in this study, WC-B-B5 is a well-head sample from a SAGD process from a Western Canadian reservoir provided by Shell. The sample had been dewatered prior to delivery and the water content was less than 1 wt%. Selected properties and a SARA assay of the water-free bitumen are provided in Table 3.1. SARA data was collected by Elaine Baydak following an experimental procedure describe elsewhere (Yarranton *et al*., 2018). A spinning band distillation assay is provided in Table 3.2. The spinning band distillation was performed using a modified ASTM D1160 procedure described elsewhere (Sánchez-Lemus *et al*., 2014). Technical grade (99+% pure) *n*-butane, *n*-pentane, toluene were purchased from Praxair and VWR International, LLC.

Table 3.1 Selected properties and SARA assay of WC-B-B5 bitumen.

Property	WC-B-B5
Specific Gravity	1.020
Viscosity at 50°C, 1 atm, cP	7,600
Distillables, wt%	19.52
Saturates, wt%	7.68
Aromatics, wt%	29.80
Resins, wt%	18.90
C5-asphaltenes, wt%	23.5
TI, wt%	0.60

Table 3.2 Spinning band distillation assay of WC-B-B5 bitumen.

Volume Distilled vol%	Normal Boiling Point, °C
1.7	192.5
3.4	223.1
5.1	241.3
6.7	258.6
8.4	270.9
10.1	278.8
11.8	295.5
13.5	304.4
15.2	307.5
16.9	318.3
18.5	328
20.2	344.7

3.2 Vapour-Liquid Boundary

Apparatus

The vapour-liquid boundaries (saturation pressures) were measured for mixtures of *n*-butane and WC-B-B5 bitumen at *n*-butane contents up to 48 wt% and temperatures ranging from 50 to 230°C. The saturation pressures were measured using the blind cell apparatus shown in Figure 3.2. The apparatus consists of five 100 cm³ blind cells (stainless steel cylinders) with floating pistons. The maximum pressure rating for each blind cell is 70 MPa. The blind cells are housed in an air bath which controls the temperature within ±0.1°C and can operate at temperature from 20 to 300°C. The volume of each blind cell, and hence the pressure of the sample fluid, is controlled by a variable volume positive displacement pump used to inject or remove hydraulic oil.
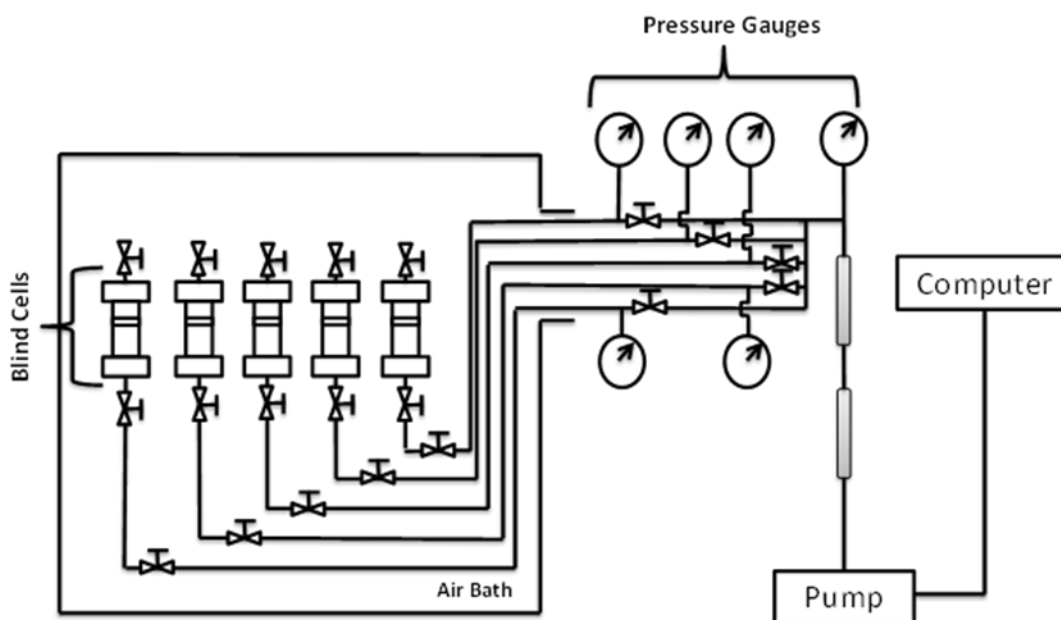
Figure 3.2 Schematic of the blind cell apparatus configured for saturation pressure measurements.

Procedure

To perform the experiment, bitumen was placed into each blind cell at atmospheric conditions and then the blind cells were placed under vacuum to remove any air present within the sample. *n*-Butane was then injected at a pressure above the saturation point in order to move the fluid as a liquid. The mass of each fluid was determined gravimetrically with a precision of ±0.01 g. The blind cells were pressurized to well over the saturation pressure and placed on the roller mixer for three days.

After mixing, the saturation pressure was determined with the step-wise isothermal expansion method based on the methodology described by Agrawal *et al*. (2012). The sample fluid was first compressed to a pressure well above its expected bubble point and the air bath was set at the experimental temperature. Then, the pressure was decreased with a stepwise volume expansion. At each pressure step, the mixture was considered to have reached equilibrium when the pressure, temperature, and the volume were all constant for a minimum of two hours. Equilibration time ranged from 12 to 24 hours. The volume was measured by the computer-controlled pump with a

precision of ±0.1 cm³. The saturation pressure was then determined from the change in slope of the pressure-volume isotherm, as shown in Figure 3.3. The uncertainty in the saturation pressure was determined from the deviations from a modified Henry Law model (Badamchi-Zadeh *et al.*, 2009b) fit to the data (see Appendix A). On average, the uncertainty in the saturation pressure measurements was ± 0.14 MPa based on a 90% confidence interval.
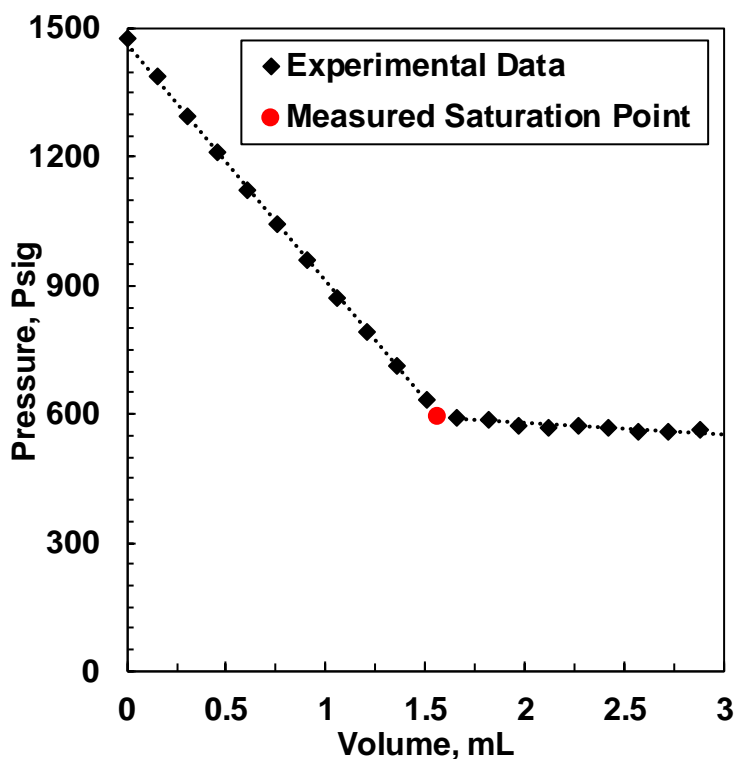
Figure 3.3 Pressure-volume isotherm of 20 wt% *n*-butane in bitumen at 180°C.

3.3 Liquid-Liquid Boundary

Apparatus

The liquid-liquid boundary (heavy phase onset) is defined as the solvent content at which the second phase (L_2) appears. The onsets were measured for mixtures of *n*-butane and WC-B-B5 bitumen at temperatures ranging from 50 to 180°C and pressures up 10 MPa using a high pressure microscope (HPM) coupled with a PVT cell, Figure 3.4. The HPM system consists of a cell with two sapphire windows, a light source, and a high focal length camera connected to a computer in

order to capture digital images and videos. The gap between the windows is adjustable (100-400 μm) and was set to 100 μm. The HPM system is placed in-line between two high pressure cylinders with floating pistons and magnetic stirrers, both of which are connected to a computer-controlled pump and a back pressure regulator. The pump and regulator are used to push fluid back and forth from one mixing cylinder, through the gap between windows in the HPM, to the second cylinder. The HPM is rated for temperatures up to 200°C and pressures up to 70 MPa.
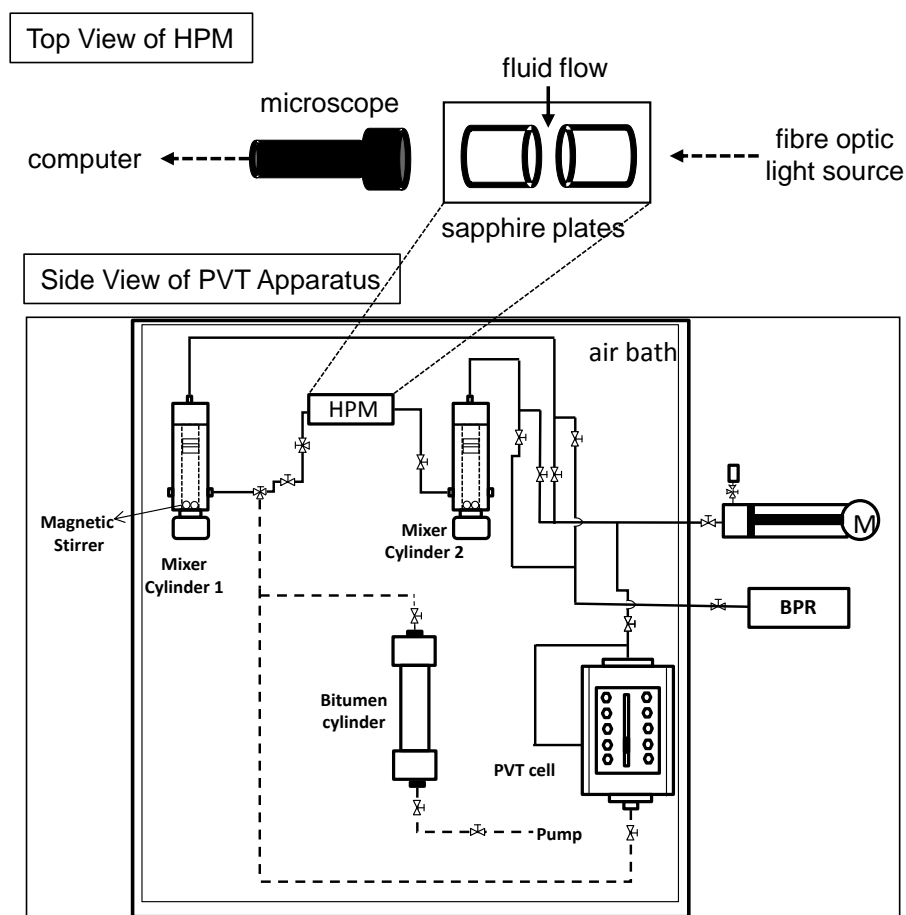
Figure 3.4 Schematic of the HPM apparatus (Agrawal *et al*., 2012).

The dead volume of the apparatus is required to accurately determine the injected fluid volumes that enter the mixing cylinders. Here, the dead volume is the volume of the transfer lines that connect the HPM cell to both mixing cylinders and it was measured by Agrawal (2012). To

measure the dead volume, the floating pistons of both mixer cylinders were displaced to the bottom of the cylinders. A constant pressure was applied on the hydraulic oil side of the piston using a back pressure regulator (BPR). Toluene was injected on the sample side using a computer-controlled pump at a pressure lower than that recorded by the BPR. The volume of injection was determined from the pump displacement once the pressure stabilized and was determined to be 7.7 ±0.2 cm³.

Procedure

The heavy phase onset point was measured by titrating the bitumen with diluent (in this case *n*-butane), using the methodology from Agrawal *et al.* (2012). Prior to any measurement, the HPM assembly was cleaned with toluene and vacuumed out. The floating pistons of both mixing cylinders were displaced to the bottom of each cylinder. The specified pressure was applied on the hydraulic oil side of the piston using a back pressure regulator (BPR). The initial pump reading, the mass of the hydraulic oil container, the temperature, and the pressure were recorded.

A specified amount of dewatered bitumen was injected into the sample side of the HPM mixing cylinders while maintaining a constant pressure. The pump reading, mass of the hydraulic oil container, temperature, and pressure were again recorded. The volume of the bitumen injected was determined in two ways: 1) from the difference between the initial and the final pump readings; 2) from the volume of displaced hydraulic oil after adding the dead volume. The pump displacement was taken as the accurate measurement and the hydraulic oil displacement was used only for validation. The hydraulic oil displacement was within 3% in average of the volume from the pump readings. The mass of the bitumen injected was calculated from its density at the operating pressure and temperature.

The solvent, in this case *n*-butane, was first injected at a pressure above the saturation pressure (liquid state) in a cleaned and vacuumed PVT cell. The *n*-butane was then injected step-wise at a flow rate of 10 cm³/h from the PVT cell to the mixing cylinder that contained the bitumen. This relatively low flow rate was selected to avoid high local solvent concentrations which would cause premature asphaltene precipitation. The magnetic stirrers in the mixer cylinders were turned on

only for injections and mixing. After each injection step, the volume of injected solvent was determined from the cathetometer readings and verified with pump displacements. The contents of the mixing cylinder were displaced slowly to the other mixing cylinder in order to displace the *n*-butane remaining in the transfer line. Then, the fluid was moved back and forth between the two cylinders until a uniform mixture was formed as indicated by constant pump pressure readings at constant flow rate. During this process, the fluid was also monitored using the HPM cell for indications of the appearance of a second phase. If a second phase did not appear, *n*-butane was again injected from the PVT cell and the process was repeated until a second phase was observed.

The *n*-butane content at the onset of the heavy phase (L_1L_2 boundary) was taken to be the intermediate content between the highest content at which no phase was observed and the lowest content at which the second phase was detected, Figure 3.5. Note that a small number of particles are visible below the onset, Figure 3.5a. These are toluene insoluble particles inherent in the bitumen. The onset of the heavy pitch phase is detected by a significant increase in number of visible particles, Figure 3.5b. The uncertainty in the onset measurement is half the increment of the titration (typically 2 to 3 wt%) plus 0.5 wt%.
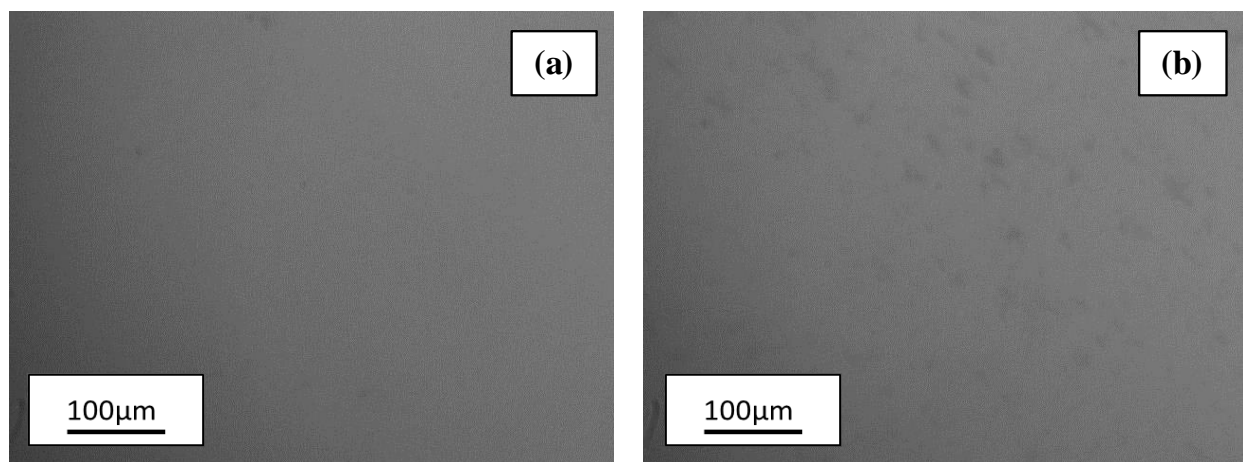
Figure 3.5 HPM micrographs of *n*-butane diluted WC-B-B5 bitumen at 130°C and 5 MPa at: a) 37.2 wt% *n*-butane; b) 40.2 wt% *n*-butane. The onset was reported as 38.7 ± 2.0 wt%.

3.4 Phase Compositions from Blind Cells

Apparatus

The blind cell apparatus described in Section 3.2.1 was modified with the addition of sample cylinders to each blind cell as shown in Figure 3.6. The sample cylinders are identical in design to the blind cells. The composition of each phase, defined as mass content of *n*-butane, maltenes, and, C5-asphaltenes was determined gravimetrically from samples taken from the light (*n*-butane-rich) and heavy (asphaltene-rich) phases. The compositions were determined at temperatures from 20 to 180°C and pressures up to 10 MPa.
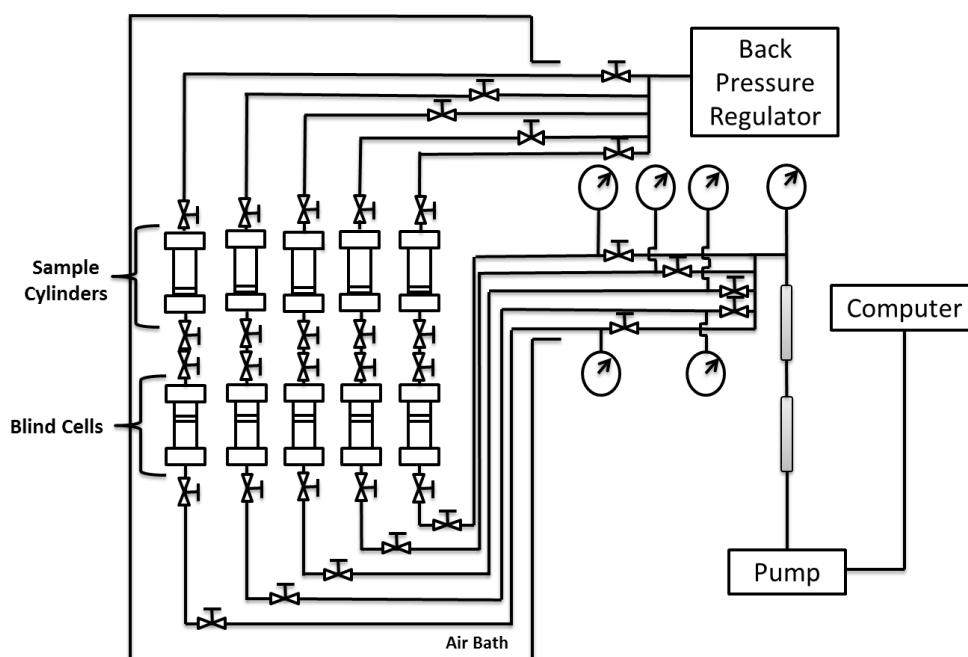
Figure 3.6 Schematic of the blind cell apparatus configured for yield measurements.

Procedure

Known masses of WC-B-B5 bitumen and *n*-butane were injected into the blind cells at ambient conditions. For ambient temperature experiments, the samples were mixed at 21°C on a roller for 3 days to ensure complete mixing. For higher temperature experiments, the blind cells were placed in oven and brought to the target temperature and pressure. The samples were mixed by inverting

each blind cell once daily for five days. The blind cells were then oriented so that the heavy pitch phase settled on the floating piston and left to equilibrate for a minimum of three days.

Light and heavy phase samples were collected as shown in Figure 3.7. One limitation of the blind cell apparatus is that it is not possible to determine the position of the interface between the light and heavy phase. Therefore, only some of the light phase was withdrawn and then an intermediate "buffer" sample was withdrawn of sufficient volume to collect the remainder of the light phase plus some of the heavy phase. The volume was determined based on the expected heavy phase volume. The heavy phase volume was assumed to be intermediate between heavy phase volumes from propane/bitumen and *n*-pentane/bitumen mixtures (Mancilla-Polanco *et al*., 2018; Johnston *et al*., 2017b) less a 20% margin of error (*i.e.* add 20% to intermediate sample volume). It was confirmed that the intermediate sample reached the heavy phase because pitch was found in the connecting tube between the blind cell and sample cylinder after the intermediate sample was removed. Finally, all of the remaining heavy phase was withdrawn.
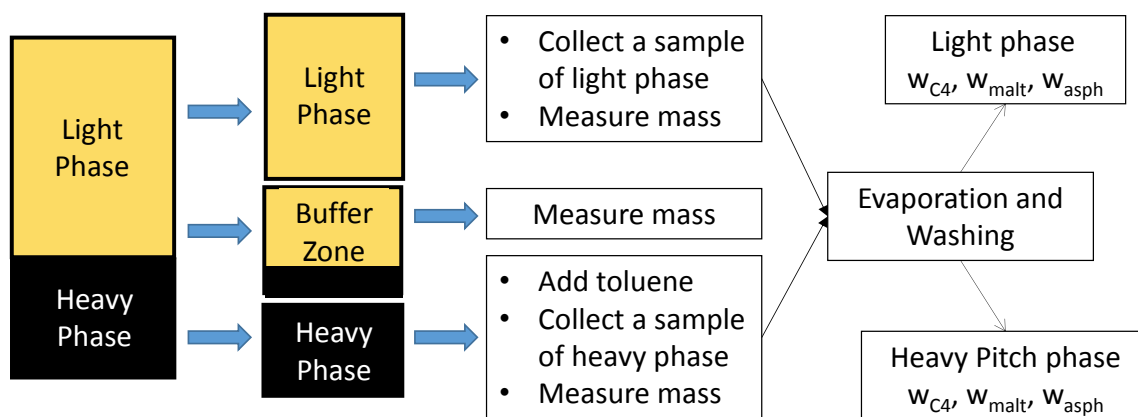
Figure 3.7 Sketch of the sample collection methodology to measure phase composition and yields in the blind cell apparatus.

The light phase sample was displaced at experimental pressure and temperature into a sample cylinder. The sample cylinders used for collecting the sample of light phase were identical to the blind cells used for the feed mixtures. The sample cylinders were assembled with a piston at the top position to minimize the dead volume and vacuumed out at ambient conditions. The dead

volumes from the blinds cell to the sample cylinder ranged from 0.5 to 1.0 cm³. The pump was used to displace a target volume from the feed blind cell to the sample cylinder and compressed N_2 was used to maintain pressure in the sample cylinder at experimental conditions.

Before collecting the intermediate sample, thermal insulation was wrapped around the feed cylinder and it was left to re-equilibrate for three days. This procedure was implemented to avoid creating a temperature gradient during sample collection that could cause convective mixing. After the intermediate sample was removed, a known mass of toluene was injected from a sample vessel into the feed cylinder to assure that the heavy phase remained in liquid state when it was cooled. The mixture (toluene + heavy phase) was displaced back into the same sample cylinder using the same procedure as for the light phase.

Subsamples of the light and heavy phase were taken to determine the phase compositions. To collect the light phase subsample, some of the light phase was slowly discharged at pressure from the light phase sample cylinder through a stainless steel line to a test tube allowing the butane to vaporize at the exit of the steel line. The liquid in the test tube (maltenes + C5-asphaltenes) was allowed to dry at 21°C and atmospheric pressure for approximately 5 days. The total mass of the subsample was determined from the change in mass of the light phase sample cylinder. The mass of evaporated n-butane was the total mass of the subsample less the mass of the residual liquid in the test tube. A second subsample was collected following the same procedure.

The residual liquid was diluted with n-pentane at 40 cm³ per gram of residue to separate the asphaltenes from the maltenes. The mixture was sonicated and agitated for 1 hour until it was completely dispersed. It was left to settle for 24 hours and then centrifuged for 5 minutes at 4000 rpm and the supernatant was decanted. The remaining residue (C5-asphaltenes with some residual maltenes) was washed with 20 cm³ n-pentane, sonicated for 60 minutes, and centrifuged for 5 minutes. The supernatant was decanted and the C5-asphaltenes left to dry in a vacuum oven until the mass was constant. The mass of maltenes is the difference between the mass of the liquid in the test tube C5-asphaltenes is the mass of the C5-asphaltenes. The composition of the light phase sample was determined from the masses of n-butane, maltenes, and C5-asphaltenes of the

subsample. The uncertainty and repeatability of the phase compositions were 0.3 and ±0.2 wt%, respectively. The repeatability for the light phase compositions was calculated based on the average absolute deviation (AAD) at 50°C and 10 MPa.

A heavy phase subsample was collected in the same way as the light phase subsample except that the liquid subsample was dried at 80°C under vacuum until the mass was stable and at least equal to the toluene mass had been evaporated. The composition of the heavy phase was determined as described above except that the evaporated solvent included both *n*-butane and toluene. The toluene mass was calculated from the known toluene content of the toluene diluted heavy phase removed from the blind cell. The mass of *n*-butane is the difference between the total mass of evaporated material and the toluene mass. The phase compositions were calculated from the component masses from the subsamples. The uncertainty of the phase compositions was ±1.7 wt%.

Phase Mass and Yield Calculation

The phase mass was calculated from the component material balances. A material balance for a single component is given by:

$$w_i^F - w_i^L - \frac{H}{F}(w_i^H - w_i^L) = 0 \tag{3.1}$$

where *H/F* is the mass ratio of the heavy phase to the feed, w_i is the mass fraction of component *i*, and superscripts *F, L*, and *H* denote the feed, light phase, and heavy phase, respectively. The three component material balances (*n*-butane, maltenes, and C5-asphaltenes) were solved simultaneously by adjusting H/F to minimize the following objective function (OF):

$$OF = \sum_{i-1}^{3} \left| w_i^F - w_i^L - \frac{H}{F}(w_i^H - w_i^L) \right| \tag{3.2}$$

Once the H/F ratio was determined, the phase mass was calculated from the ratio and the known feed mass. The C5-asphaltene and pitch* yields (mass of component in heavy phase divided by mass of bitumen in feed) were then calculated as follows:

$$Y_A = \frac{w_A^H}{1 - w_S^F}\frac{H}{F} \tag{3.3}$$

$$Y_{P*} = \frac{1 - w_S^H}{1 - w_S^F}\frac{H}{F}$$

(3.4)

where Y is yield and subscripts A, $P*$, and S denote C5-asphaltenes, Pitch*, and solvent (n-butane), respectively. On average, the uncertainty of the C5-asphaltene and pitch* yields were 0.6 and ±4.1 wt%, respectively. The repeatability for both the C5-asphaltene and pitch* yields were calculated based on the average absolute deviation (AAD) at 50°C and 10 MPa with values of 0.5 and ±2.1 wt%, respectively.

3.5 Phase Compositions from PVT Cell

Apparatus

Phase compositions were determined in the PVT cell at 130°C, 10 MPa and n-butane contents up to 90 wt%. The phase composition measurements were performed using a DB Robinson Jefri PVT cell placed in a temperature controlled air bath, Figure 3.8. The maximum pressure rating for the PVT cell is 70 MPa and it can operate at temperatures up to 200°C. The temperature is controlled within ±0.1°C. The maximum capacity of the PVT cell is 100 cm^3. The PVT cell is equipped with a floating piston but the magnetic mixer was removed to minimize the dead volume and ensure a clean separation of the light phase from the heavy phase. The floating piston separates the hydraulic fluid from the bitumen/solvent mixture. The volume of the sample fluid inside the cell is determined from fluid level measurements using a calibrated cathetometer. The cathetometer is precise to ±10^{-6} m^3. The volume of the fluid sample is controlled by a computer-controlled positive displacement pump, which allows the injection and removal of hydraulic oil. The dead volume of the PVT cell was measured as described for the HPM in Section 3.3.1 and was determined to be 0.8 ±0.2 cm³.
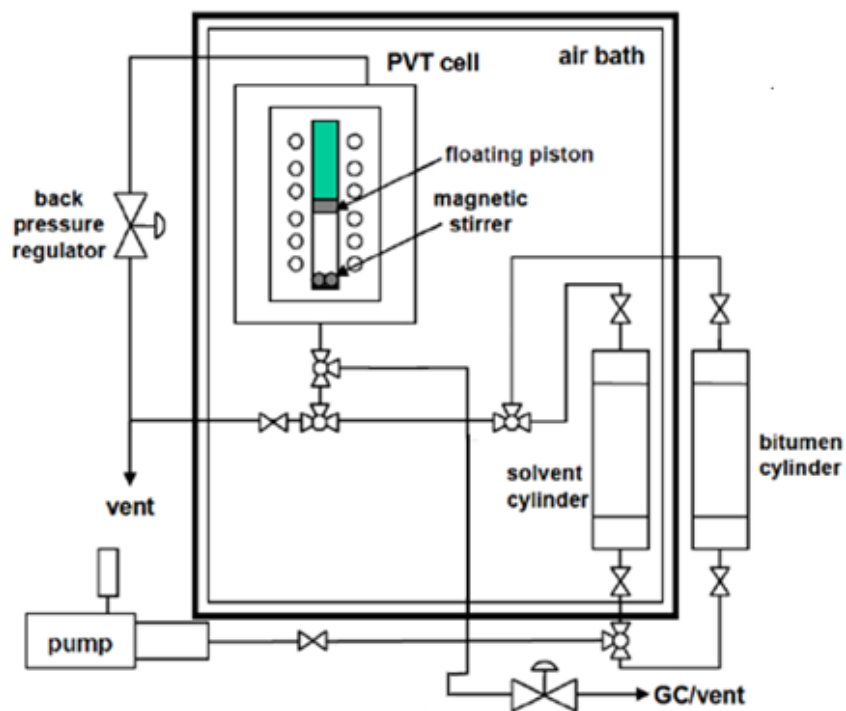
Figure 3.8. Schematic of PVT cell apparatus.

Procedure

Prior to any measurements, the PVT cell was cleaned with toluene and vacuumed to remove any air in the system. A feed composition was selected so that the overall mixture would split into two phases (the light phase and the heavy phase) at the target temperature and pressure. Bitumen was transferred from a cylinder to the PVT cell at 50°C and 10 MPa. A temperature of 50°C was selected to reduce the bitumen viscosity sufficiently to inject the bitumen. The transfer procedures were similar to those described for the HPM in Section 3.3.

The PVT cell apparatus was then heated to experimental temperature and the pressure was maintained at the target experimental condition using the hydraulic pump. The required amount of *n*-butane was injected at the same conditions. The bitumen and *n*-butane injection volumes were measured in two ways, one from the PVT cell using the cathetometer and the other from volume of the fluid displaced using the pump. The mass of the fluid was calculated based on the averaged

injected volume (cathetometer and pump measurements) and the injected fluid density. The feed composition was determined from the masses of the injected bitumen and *n*-butane. The bitumen and the *n*-butane were mixed by inverting the PVT cell several times daily for 3 days until equilibrium was reached.

The advantage of the PVT cell over the blind cells is that the interface between the light and heavy phase can be observed visually when the light phase is non-opaque (typically at or above 80 wt% solvent). In this case, phase volumes were recorded and the entire mass of each phase was collected as shown in Figure 3.9. Since the phase masses and compositions were measured, it was possible to check the mass balance. The disadvantage of the PVT cell is that only one mixture can be tested at the same time compared with five mixtures in the blind cell apparatus.
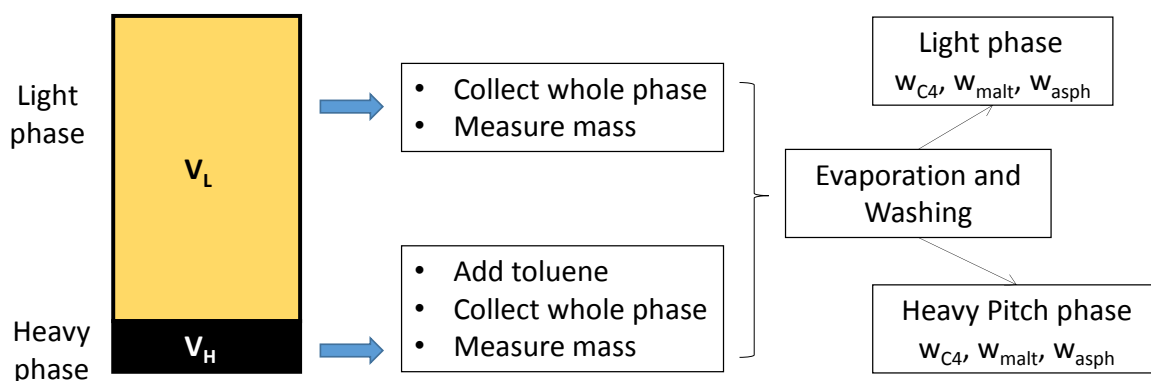
Figure 3.9 Sketch of the sample collection methodology to measure phase composition and yields in the PVT cell.

Once equilibrium was reached, the PVT cell was rotated to allow the heavy pitch phase to settle on the piston. The interface between the heavy and light phases was clearly visible and the volume of the heavy phase was measured using the cathetometer. The light phase was collected at pressure by displacing the light solvent-rich phase into a sample cylinder with a known mass. Then the exact volume of the light phase was displaced into the sample cylinder. An exact mass of toluene was injected into the remaining heavy phase from a sample cylinder into the PVT cell to assure the heavy pitch phase remained in liquid state when it was cooled. The mixture (toluene + heavy

pitch phase) was displaced back into the same sample cylinder using the same collection procedure as for the light phase, Figure 3.9.

After releasing the nitrogen pressure, the mass of each phase collected in the sample cylinders were measured directly using a Sartorius FB6 34 EDE-H scale with a precision of ±0.01 g. The light and heavy phase sample cylinders were re-pressurized above their saturation pressure. Two samples of the light phase and heavy phase were transferred to test tubes as described for the blind cell apparatus in Section 3.4. The mass fraction of n-butane, maltenes, and C5-asphaltenes in each sample was determined as described in Section 3.4. The uncertainties of light phase compositions, n-butane content in heavy phase, and C5-asphaltene and maltene content in the heavy phase were ±0.3 wt%, ±1.0 wt%, and ±4.1 wt%, respectively.

Mass Balance and Yield Calculation

In this case, the phase masses and H/F ratio were measured directly and the material balance was used to check the data. The error in the overall and component material balances were calculated as shown in Equation 3.1. The yields were calculated from Equations 3.3 and 3.4 using the measured *H/F* ratio. The uncertainty of the C5-asphaltene and pitch* yields were ±1.6 and ±1.9 wt%, respectively.

Chapter 4: Phase Behaviour Modeling

This chapter discusses the modeling methodology used in this thesis to predict the phase behaviour of n-butane diluted heavy oil using the Advanced Peng-Robinson equation of state (APR-EoS). The modeling methodology is similar to that developed by Johnston *et al*. (2017a) for n-pentane diluted bitumen and applied by Mancilla-Polanco *et al*. (2018) to model propane diluted heavy oil phase behaviour. The crude oil is represented as a set of pseudo-components defined from distillation assay data. Pseudo-component physical and critical properties are calculated from well-established correlations. These properties are then used as input in the APR-EoS in VMGSim^{TM} (VMG, 2011). The APR-Eos is tuned to match the data by adjusting binary interaction parameters.

4.1 Heavy Oil Characterization

A schematic of the oil characterization methodology is provided in Figure 4.1. The maltene and C5-asphaltene fractions were characterized separately, as recommended by Castellanos-Diaz *et al*. (2011). The separate characterization is required because the asphaltenes self-associate and their properties do not follow the same trends as those of the maltenes versus the cumulative mass distilled (Ramos-Pallares *et al.*, 2016). The maltenes were divided into pseudo-components based on their boiling point distribution. The asphaltenes were treated as a single pseudo-component for phase behaviour modeling purposes, as recommended by Johnston *et al*. (2017a) and Mancilla-Polanco *et al*. (2018).
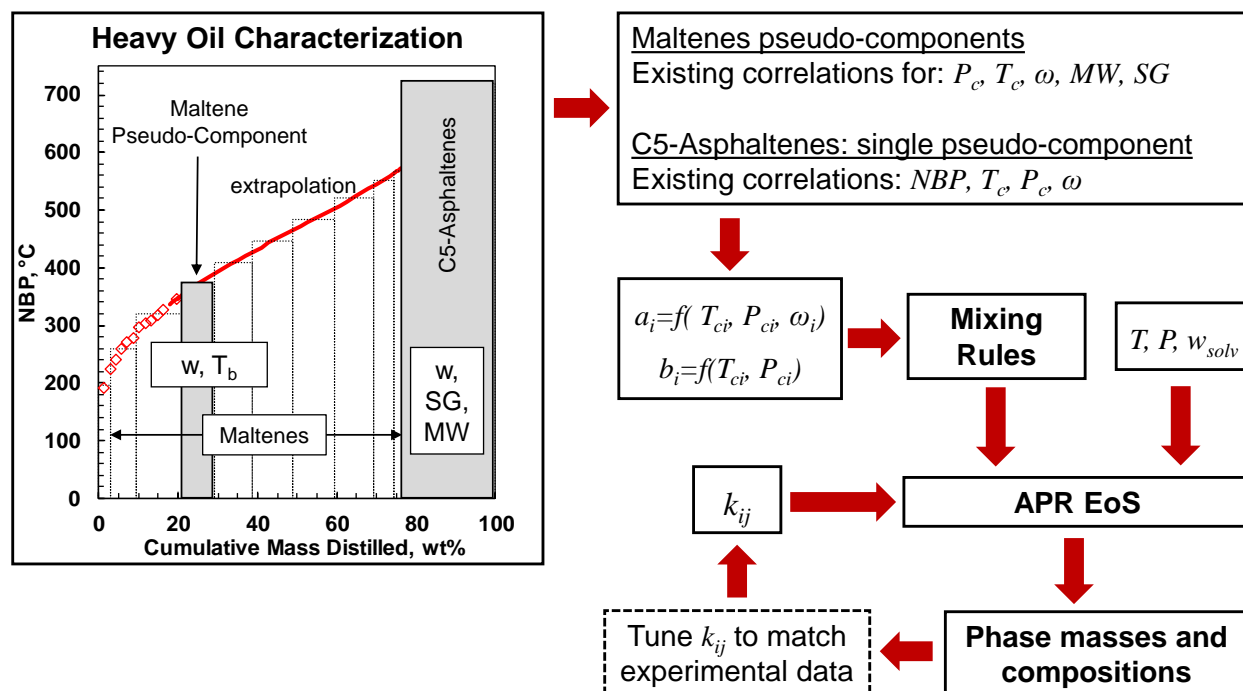
Figure 4.1 Schematic of characterization and tuning procedure for modeling bitumen/solvent phase behaviour using the APR EoS.

Maltene Characterization

Since only 19.5 wt% of the maltenes was distillable, a Gaussian extrapolation was performed to extend the distillation curve over the entire range of the maltene fraction, Figure 4.1. The distillation curve was divided into ten pseudo-components as follows: two in the light oil section (192.5-318.3°C), five in the medium oil section (318.3-507.9°C), and three in the heavy oil section (507.9-573.3°C). A distribution of pseudo-components is necessary to model phase boundaries (VL$_1$ and L$_1$/L$_1$L$_2$ boundary) and C5-asphaltene and pitch* yields (Agrawal *et al*., 2012; Castellanos-Diaz *et al*., 2011). Agrawal *et al*. (2012) found that two maltene pseudo-components were sufficient to match saturation pressures and yields; however, more pseudo-components are desirable if oil fractionation is to be considered. For this reason and for straightforward comparison with these previously published results, the 10 pseudo-components were retained in this thesis

The pseudo-components physical properties required as input for the Advanced Peng-Robinson equation of state (APR-EoS) are the critical temperature, critical pressure and acentric factor. These properties were calculated from the Lee-Kesler correlations (1975) using normal boiling point and specific gravity as inputs. The normal boiling point was taken directly from the distillation curve. The specific gravity of each pseudo-component was calculated from the Katz-Firoozabadi correlation (1978). The molecular weight of the pseudo-component, required to convert mass fraction to mole fraction, was calculated from the Lee-Kesler correlation using normal boiling point and specific gravity as inputs.

The initial specific gravities and molecular weights of the pseudo-components were tuned to match the density and the molecular weight of the whole maltene fraction, respectively, using constant common multipliers. The whole maltene specific gravity was calculated from those of the pseudo-components using a regular solution mixing rule (zero excess volume of mixing). The maltene molecular weight was calculated as the molar average. The experimental maltene specific gravity (1005 kg/m³) and molecular weight (450 g/mol), required for tuning, were previously measured and reported by Ramos-Pallares *et al*. (2016) and Sanchez-Lemus *et al*. (2016), respectively. Maltene pseudo-component physical and critical properties based on the normal boiling point (NBP) curve are presented in Table 3.2 and are summarized in Table 4.1.

Table 4.1 WC-B-B5 bitumen pseudo-component properties.

Species	Mole Fraction	Mass Fraction	MW g/mol	NBP °C	SG	P_c kPa	T_c °C	ω
Maltene 1	0.075	0.030	215	195	0.901	3130	408	0.40
Maltene 2	0.126	0.066	285	260	0.939	2611	475	0.51
Maltene 3	0.174	0.113	354	321	0.966	2192	532	0.63
Maltene 4	0.107	0.083	423	371	0.990	1918	579	0.72
Maltene 5	0.109	0.096	478	409	1.008	1740	614	0.80
Maltene 6	0.105	0.103	535	446	1.025	1579	648	0.88
Maltene 7	0.095	0.104	596	484	1.040	1426	680	0.96
Maltene 8	0.081	0.098	661	522	1.051	1273	711	1.05
Maltene 9	0.039	0.051	715	552	1.058	1161	735	1.13
Maltene 10	0.016	0.022	744	568	1.062	1103	748	1.17
C5-Asphaltene	0.071	0.235	1800	721	1.120	1057	906	1.27

C5-Asphaltene Characterization

The asphaltene fraction was characterized as a single pseudo-component. The critical temperature, the critical pressure, and acentric factor of the fraction are required as inputs for the APR-EoS. These properties were estimated from the Twu correlations (1984) using the normal boiling point and specific gravity as inputs. The boiling point was calculated from the Søreide correlation (1989) using the average molecular weight (1800 g/mol) and specific gravity (1120 kg/m³) reported by Barrera *et al*. (2013). The asphaltene pseudo-component properties are included in Table 4.1.

4.2 The Advanced Peng-Robinson Equation of State (APR-EoS)

The Advanced Peng-Robinson equation of state (APR-EoS) as used in VMGSim™ (VMG, 2011) is shown below:

$$P = \frac{RT}{v - b} - \frac{a\,\alpha(T_r, \omega)}{v(v + b) + b(v - b)} \tag{4.1}$$

where P is the absolute pressure, v is the molar volume, T is the absolute temperature, R is the universal gas constant, and, a and b are fluid-specific parameters that account for attractive and repulsive interactions respectively. They are related to its critical properties as follows:

$$a_i = 0.457235 R^2 T_{ci}^2 / P_{ci} \tag{4.2}$$

$$b_i = 0.0777969 R T_{ci} / P_{ci} \tag{4.3}$$

where T_c is the critical temperature, P_c is the critical pressure, and the subscript i denotes the component. The parameter α in Equation 4.1 is an empirical modification introduced to improve the prediction of saturation pressures for pure components:

$$\alpha(T_r, \omega) = \left[1 + m\left(1 - \sqrt{T_r}\right)\right]^2 \tag{4.4}$$

where T_r is the reduced temperature and m is given by:

$$\text{for } \omega \leq 0.49: \quad m = 0.37464 + 1.54226\omega - 0.26992\omega^2 \tag{4.5}$$

$$\text{for } \omega > 0.49: \quad m = 0.3796 + 1.485\omega - 0.1644\omega^2 + 0.01667\omega^3 \tag{4.6}$$

and ω is the acentric factor.

Mixing Rules

The APR-EoS treats a mixture as a single component fluid with parameters a_{mix} and b_{mix} which in this thesis were determined from the classical van der Waals mixing rules given by:

$$a_{mix} = \sum_i \sum_j x_i x_j \sqrt{a_i a_j}(1 - k_{ij}) \tag{4.7}$$

$$b_{mix} = \sum_i x_i b_i \tag{4.8}$$

where x_i and x_j are the mole fraction of components i and j, respectively, and k_{ij} is a binary interaction parameter. The binary interaction parameters were fitted to the experimental saturation pressure and yield data with the two alternative approaches as described below.

1. Temperature Dependent Binary Interaction Parameters (k_{ij})

Temperature dependent binary interaction parameters were proposed by Agrawal *et al.* (2012) in order to fit the APR-EoS to measured saturation pressures and onsets of asphaltene precipitation. These binary interaction parameters are a function of the absolute temperature (in K) and are given by:

- maltenes with each other or with solvent:

$$k_{ij} = k_{ij}^0 \left(1 + \frac{k_{ij}^1}{T} + k_{ij}^2 ln(T) \right) \tag{4.9}$$

- C5-asphaltenes with maltenes or solvent:

$$k_{ij} = k_{ij}^0 (1 + a_A T + b_A T^2) \tag{4.10}$$

where k_{ij}^0 is a reference interaction parameter given by (Gao *et al.*, 1992):

$$k_{ij}^0 = 1 - \left[\frac{2\sqrt{T_{ci} T_{cj}}}{T_{ci} + T_{cj}} \right]^n \tag{4.11}$$

where T_{ci}, T_{cj} are the critical temperatures of paired component i and j, respectively. The exponent n is an adjustable parameter set to the default value of 0.27, as recommended by Agrawal *et al.* (2012). The parameters k_{ij}^1 and k_{ij}^2, in Equation 4.9 were determined by fitting the APR-EoS to experimental saturation pressures at temperatures from 50 to 230°C and *n*-butane amounts from 3 to 48 wt%. Parameters a_A and b_A in Equation 4.10 were determined by fitting the equation of state to the onset of asphaltene precipitation at temperatures from 50 to 180°C and pressures from 5 to 10 MPa. The parameters used to fit the data in this thesis are summarized in Table 4.2.

Table 4.2 Tuned parameters for the temperature dependent parameter correlations.

Pseudo-Component Pair	$k_{ij}{}^1$	$k_{ij}{}^2$	a_A	b_A
	K		K^{-1}	K^{-2}
Maltenes	443.50	0.00809	-	-
C5-Asphaltene	-	-	-0.00747	0.0000262

2. Composition Dependent Binary Interaction Parameters (k_{ij}*)

The temperature dependent binary interaction parameters were used as described above except for the binary interaction parameters between *n*-butane and the heaviest oil pseudo-components (Maltene 8, Maltene 9, Maltene 10, and C5-Asphaltene, Table 4.1). These pseudo-components were chosen to match the mass of the pitch* yield. The composition-dependent binary interaction parameters were calculated as follows (Mancilla-Polanco *et al.*, 2018):

$$k_{ij}^* = a + b(1 - e^{-6.5(w_{solv} - w_{LL})}) \tag{4.12}$$

$$a = a_1 NBP + a_2 \tag{4.13}$$

$$b = b_1 NBP + b_2 \tag{4.14}$$

with the following constraints:

$$\text{If } k_{ij}^* > 0, k_{ij} = k_{ij}^*$$

$$\text{If } k_{ij}^* \leq 0, k_{ij} = 0$$

where NBP is the pseudo-component normal boiling point in °C and w_{solv} is the solvent mass fraction in the feed. The parameter w_{LL} is set equal to the measured mass fraction of solvent at the onset of asphaltene precipitation. The parameters a_1, a_2, b_1, and b_2 are constants and were tuned to fit the measured C5-asphaltene and pitch* yield data using a least squares regression. The fitted parameters are provided in Table 4.3.

Table 4.3 Tuned parameters for the composition dependent parameter correlations.

Parameter	Value
w_{LL}	0.41
a_1	0.000077029 °C^{-1}
a_2	0.00001011
b_1	0.00010358 °C^{-1}
b_2	0

4.3 Calculation Procedure in VMG

In this study, VMGSim^{TM} (VMG, 2011) was used to calculate the vapour pressures (VL$_1$ boundary), asphaltene onset (L$_1$/L$_1$L$_2$ boundary), lower boundary of the L$_1$L$_2$ region (L$_1$L$_2$/V L$_1$L$_2$ boundary), C5-asphaltene and pitch* yield, and phase compositions using the APR-EoS, Figure 4.1. The inputs were the heavy oil pseudo-component mass fractions and properties as defined in Section 4.1, the solvent content in the feed, the temperature or compositional dependent interaction parameter matrix as defined in Section 4.2, the temperature, and the pressure. Flash calculations were performed using VMGSim^{TM} (VMG, 2011), which combines the material balance equations of the Rachford-Rice algorithm (1952) with a stability analysis to minimize the Gibbs free energy (Michelsen, 1982).

Chapter 5: Results and Discussion

This chapter presents the experimental phase behaviour data and modeling results for mixtures of n-butane and WC-B-B5 bitumen. Pressure-composition (P-X) phase diagrams, including saturation pressures (L_1/VL_1 boundaries) and onsets (L_1/L_1L_2 boundaries), are presented at different temperatures and pressures. The morphology of the pitch (L_2) phase in the L_1L_2 phase region is also presented. The C5-asphaltene and pitch* yields are reported where C5-asphaltenes are the n-pentane insoluble components and pitch* refers to the C5-asphaltenes plus maltenes in the pitch phase (*i.e.* n-butane-free pitch). The L_1 and L_2 phase compositions are presented in ternary diagrams. Equilibrium ratios (K) are determined from the ternary diagrams and correlated to the feed n-butane content. The equilibrium ratios are used to calculate yields and phase compositions at any feed n-butane content in order to check the consistency of the data. Then, the APR EoS with composition dependent binary interaction parameter is tuned to match the data. Finally, the experimental and modeling results for n-butane diluted bitumen are compared with previous results for propane and n-pentane diluted bitumen.

5.1 Phase Behaviour Measurements

5.1.1 Phase Boundaries

Saturation pressures (VL_1 boundary) at temperatures of 50, 90, 130, 180, and 230°C are shown in Table 5.1. Onsets (L_1/L_1L_2 boundary) at 50, 90, 130, and 180°C and two pressures 5 and 10 MPa are reported in Table 5.2. The uncertainty of the measurements is detailed in Appendix A.

Table 5.1 Measured saturation pressure for mixtures of *n*-butane and WC-B-B5 bitumen. The uncertainty in the *n*-butane content is ± 0.1 wt%. The uncertainty in the saturation pressure is ± 0.14 MPa.

Temperature °C	*n*-Butane Content wt%	Pressure MPaa
50	4.0	0.22
50	8.7	0.45
50	20.0	0.49
50	33.9	0.60
50	48.2	0.63
90	4.0	0.34
90	8.7	0.87
90	20.0	1.14
90	33.9	1.24
90	48.2	1.30
130	4.0	0.56
130	8.7	1.37
130	20.0	2.20
130	33.9	2.38
130	48.2	2.52
180	4.0	0.97
180	8.7	2.25
180	20.0	4.17
180	33.9	4.58
230	4.0	1.26
230	8.7	3.04
230	20.0	6.18
230	33.9	7.20

Table 5.2 Measured onsets of the heavy pitch phase in mixtures of *n*-butane and bitumen. The uncertainty in the onset is ± 1.6 wt% *n*-butane.

Temperature °C	Pressure MPa	*n*-Butane Content wt%
50	5	39.2
90	5	41.0
130	5	38.7
50	10	38.5
90	10	41.0
130	10	39.6
180	10	40.5

The data from Tables 5.1 and 5.2 were used to generate pressure-composition (P-X) diagrams, Figure 5.1. At approximately 40 wt% *n*-butane in the feed, the mixtures formed a vapour and a liquid phase (VL_1 region) below the saturation pressure and a single liquid phase (L_1) above the saturation pressure. Above this *n*-butane content, the mixtures still formed a (VL_1) region below a certain pressure (the $L_1L_2/V\ L_1L_2$ boundary) but divided into two liquid phases (L_1L_2 region) above this pressure.

The saturation pressure (L_1/VL_1 boundary) increased with temperature as expected. The onset (L_1/L_1L_2 boundary) was insensitive to temperature and only slightly sensitive to pressure (a vertical line on the P-X diagram). The average onset was 39.8 wt% *n*-butane. This value is consistent with the trends for mixtures of bitumen with different carbon number *n*-alkanes. For example, the onsets for bitumen mixed with propane and *n*-pentane are approximately 30 wt% (Mancilla-Polanco *et al*., 2018) and 50 wt% (Johnston *et al*., 2017b), respectively. The L_1L_2/VL_1L_2 boundary was approximately equal to the vapour pressure of *n*-butane (a horizontal line on the P-X diagram). However, the L_1L_2/VL_1L_2 boundary disappeared at temperatures higher than the critical temperature of *n*-butane (152°C) and above 48 wt% *n*-butane, Figure 5.1d and 5.1e. At these conditions, the L_1 phase appeared to be a supercritical fluid.
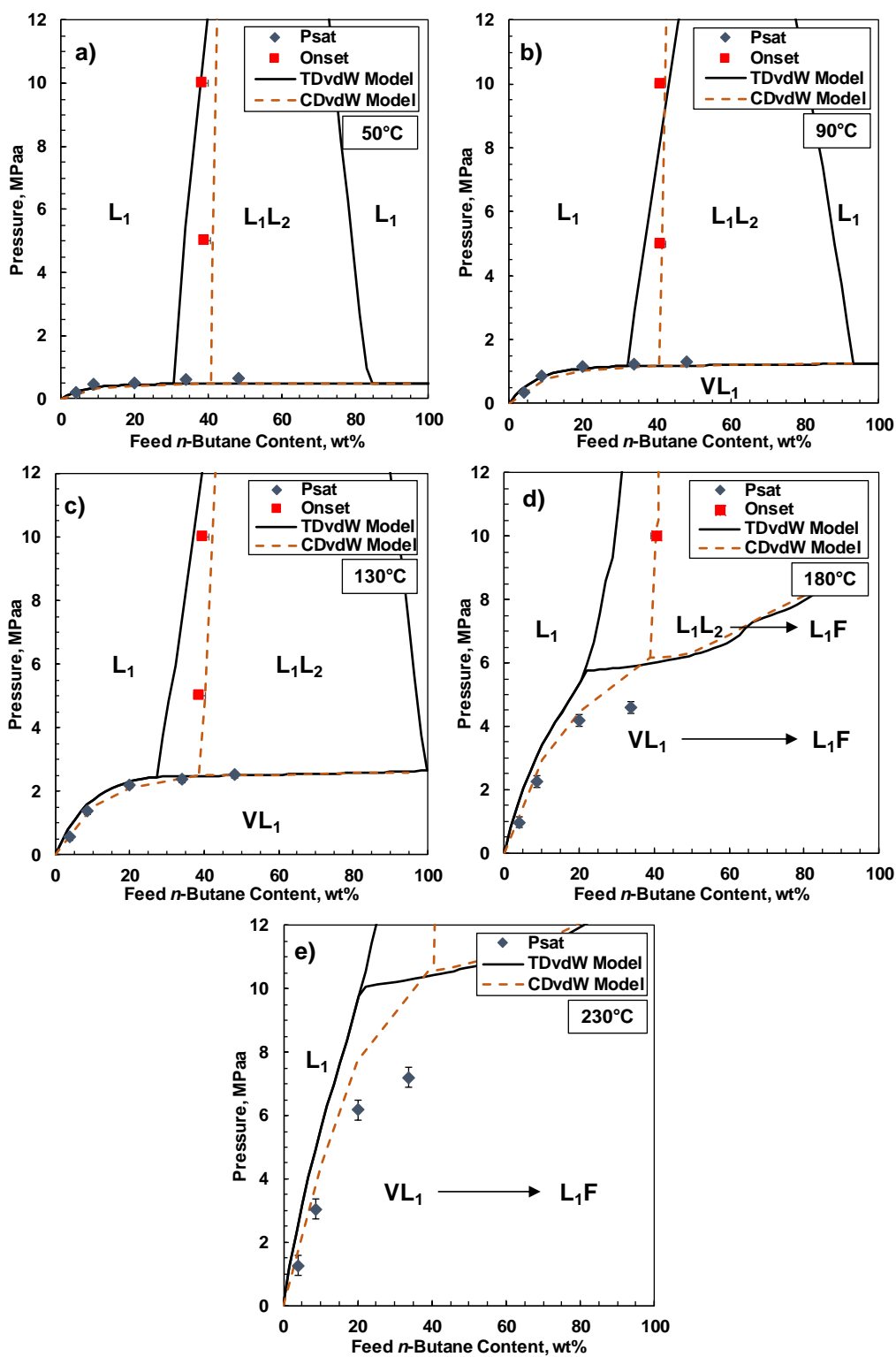
Figure 5.1 Measured and modeled (TDvdW and CDvdW approaches) P-X diagrams for mixtures of *n*-butane and WC-B-B5 bitumen at: a) 50°C; b) 90°C; 130°C; d) 180°C; e) 230°C. *F* is a supercritical fluid phase.

5.1.2 Pitch Phase Morphology

The pitch (L_2) phase was opaque and the *n*-butane-rich (L_1) phase was translucent in the high pressure microscope at all of the temperatures, pressures, and feed compositions of this study. The pitch phase appeared as small particles or droplets just above the onset as shown in Figures 5.2a and 5.2c. At 50 and 90°C, as the feed *n*-butane content increased, the pitch phase became more liquid-like (or possibly was in a glass transition state) and the particles/droplets aggregated, Figure 5.2b. At 130°C, the pitch phase was a liquid and, with an increased *n*-butane content in the feed, it coalesced and settled into a distinct layer, Figure 5.2d.
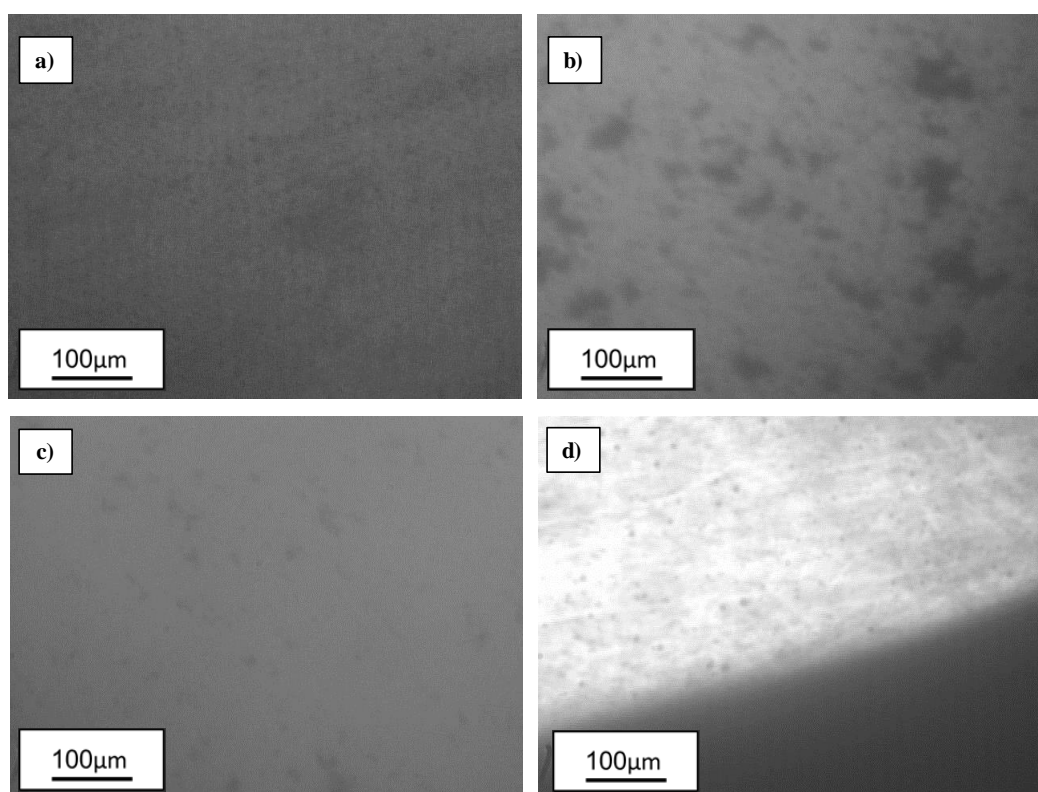
Figure 5.2 HPM micrographs of the L_1L_2 region in mixtures of *n*-butane and WC-B-B5 bitumen at: a) 50°C, 5 MPa, 41.9 wt% *n*-butane; b) 50°C, 10 MPa, 42.3 wt% *n*-butane; c) 130°C, 5 MPa, 40.2 wt% *n*-butane; d) 130°C, 10 MPa, 52.8 wt% *n*-butane. The *n*-butane-rich (L_1) phase is light and the pitch (L_2) phase is dark.

5.1.3 Heavy Phase Yields

The heavy phase yields for mixtures of *n*-butane and WC-B-B5 bitumen from the blind cell experiments are presented in Table 5.3. The pitch* and C5-asphaltene yields are shown in Figure 5.3. The pitch phase contained 40 to 50 wt% of the bitumen just above the onset. The bitumen fraction decreased to near the C5-asphaltene content of the bitumen as the feed *n*-butane content increased. The pitch* and C5-asphaltene yields were insensitive to temperature and pressure for all the cases except at 20°C and 2 MPa where higher yields were observed. The yield data demonstrate that the L_1L_2 region extends to a feed *n*-butane content of at least 90 wt%. A repeat run was performed at 50°C, 10 MPa and five different *n*-butane feed contents, and the repeatability of the measured C5-asphaltene and pitch* yields were ±0.5 and ±2.1 wt%, respectively, as shown in Figure 5.3b. The propagated error in the yield calculation are higher (±0.6 and ±4.1 wt%, respectively) and are taken as the uncertainty of the yield measurements.

Table 5.3 Measured yields for mixtures of *n*-butane and WC-B-B5 bitumen. On average, the uncertainty of C5-asphaltene and pitch* yields were ±0.6 and ±4.1 wt%, respectively.

Temperature °C	Pressure MPa	Feed C4 Content wt%	C5-Asph Yield wt%	Pitch* Yield wt%
20	2	41.6	21.9	57.9
20	2	50.4	22.7	53.3
20	2	60.4	23.3	48.0
20	2	76.1	23.5	47.4
20	2	90.0	23.5	44.2
20	5	43.3	18.8	43.6
20	5	51.4	20.6	41.4
20	5	61.2	22.2	39.0
20	5	76.1	23.1	40.6
90	5	45.2	18.0	38.7
90	5	55.2	21.6	32.9
90	5	65.3	23.0	31.4
90	5	75.1	24.3	32.1
90	5	89.9	23.5	23.3
130	5	44.8	21.5	41.4
130	5	55.4	20.2	43.2
130	5	64.6	21.2	35.6

130	5	76.0	17.1	28.8
50	10	44.2	20.7	35.3
50	10	55.9	23.1	36.9
50	10	64.6	22.9	35.9
50	10	74.7	23.4	33.7
50	10	90.0	23.4	33.0
50	10	45.4	13.9	45.3
50	10	55.2	21.7	38.2
50	10	59.7	22.3	34.1
50	10	65.0	20.2	33.1
50	10	79.0	23.4	32.7
90	10	46.0	19.2	40.0
90	10	53.9	21.5	40.2
90	10	65.1	23.2	35.7
90	10	75.1	23.5	32.9
90	10	90.1	23.5	31.0
130	10	46.5	21.1	49.0
130	10	55.5	22.0	38.2
130	10	64.3	23.1	35.8
130	10	75.3	23.5	32.7
130	10	90.0	23.5	27.4
180	10	44.3	15.8	35.5
180	10	54.6	20.5	29.8
180	10	65.9	21.0	31.0
180	10	76.7	25.1	34.0
180	10	90.6	23.5	-
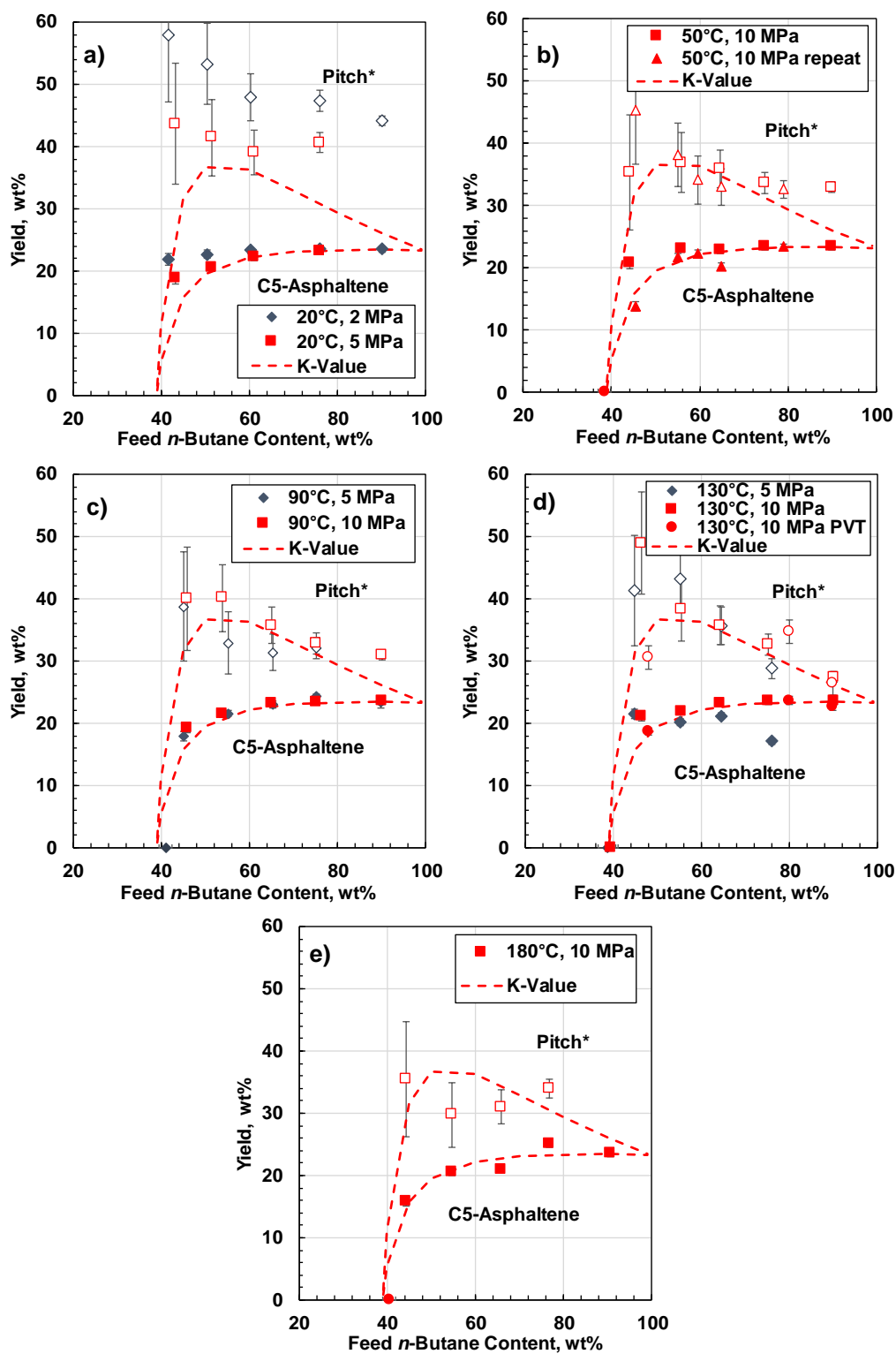
Figure 5.3 Measured and modeled (*K*-value approach) C5-asphaltene and pitch* yields for mixtures of *n*-butane and WC-B-B5 bitumen at: a) 20°C; b) 50°C; c) 90°C; d) 130°C; e) 180°C. Open and solid symbols represent pitch* and C5-asphaltene measurements, respectively.

5.1.4 Phase Compositions

Phase compositions from the PVT cell experiments were determined for the L_1L_2 region at 130°C, 10 MPa, and feed n-butane contents of 48.0, 80.0, and 89.7 wt%. The C5-asphaltene and pitch* yields and the phase densities from these experiments are presented in Table 5.4. The yields are also shown in Figure 5.3d. The phase compositions in terms of the n-butane, maltene, and C5-asphaltene content are tabulated for the three feed n-butane contents in Tables 5.5, 5.6, and 5.7, respectively, and shown in Figure 5.4. Almost all of the asphaltenes were rejected from the n-butane-rich phase even near the onset. The n-butane content in the pitch phase was approximately 20 wt% near the onset and decreased monotonically towards near zero at high dilution. The phase compositions were also used to generate a ternary diagram at 130°C and 10 MPa as shown in Figure 5.5.

The repeatability of the light phase compositions was ±0.3 wt% and is based on a 90% confidence interval for the set of paired samples collected in each experiment. The repeatability of the n-butane content in the heavy phase composition was ±1.0 wt%. The uncertainty of the asphaltene and maltene content of the heavy phase was higher (±4.1 wt%) because an accurate separation of the asphaltenes and maltenes was experimentally challenging. Recall that a modified procedure was implemented for the heavy phase analysis, as described in Section 3.5.

Table 5.4 Measured yields and phase densities of mixtures of n-butane and WC-B-B5 bitumen at 130°C and 10 MPa. The uncertainties of the feed composition, C5-asphaltene yield, pitch* yield, L_2/F ratio and the densities were ±0.1 wt%, ±1.6 wt%, ±1.9 wt%, 0.01, and ±5 kg/m³, respectively.

Feed C4 Content wt%	C5-Asph. Yield wt%	Pitch* Yield wt%	L_2/F Ratio w/w	L_1 Phase Density kg/m³	L_2 Phase Density kg/m³
48.0	18.7	30.5	0.20	665	-
80.0	23.7	34.7	0.08	515	782
89.7	22.7	26.4	0.03	486	877

Table 5.5 Measured phase composition of mixtures of *n*-butane and WC-B-B5 bitumen at 130°C, 10 MPa, and 48 wt% *n*-butane. The uncertainties of the feed composition, light phase compositions, *n*-butane content in heavy phase, and C5-asphaltene and maltene content in the heavy phase were ±0.1 wt%, ±0.3 wt%, ±1.0 wt%, and ±4.1 wt%, respectively.

Component	Feed wt%	Light Phase wt%	Heavy Phase wt%	MB Error %
n-Butane	48.0	55.3	21.1	1.0
Maltenes	39.8	41.3	30.6	1.7
C5-Asphaltenes	12.2	3.4	48.3	1.6

Table 5.6 Measured phase composition of mixtures of *n*-butane and WC-B-B5 bitumen at 130°C, 10 MPa, and 80 wt% *n*-butane. The uncertainties are the same as reported in Table 5.5.

Component	Feed wt%	Light Phase wt%	Heavy Phase wt%	MB Error %
n-Butane	80.0	85.2	10.1	0.7
Maltenes	15.3	14.8	28.5	3.7
C5-Asphaltenes	4.7	0.0	61.4	0.7

Table 5.7 Measured phase composition of mixtures of *n*-butane and WC-B-B5 bitumen at 130°C, 10 MPa, and 90 wt% *n*-butane. The uncertainties are the same as reported in Table 5.5.

Component	Feed wt%	Light Phase wt%	Heavy Phase wt%	MB Error %
n-Butane	89.7	91.7	7.9	7.7
Maltenes	7.8	8.3	13.0	0.1
C5-Asphaltenes	2.4	0.0	79.1	3.5
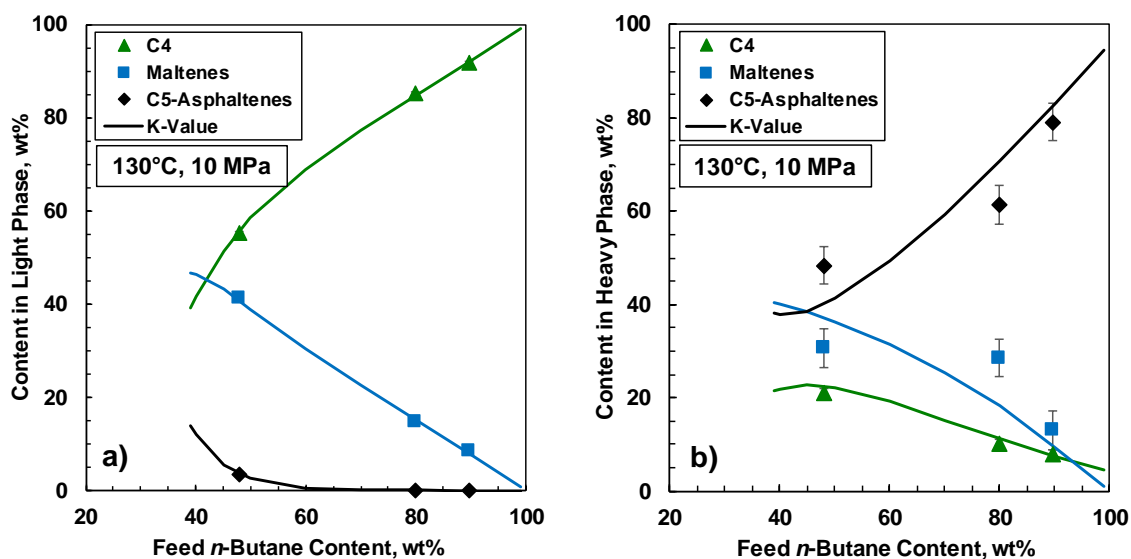
Figure 5.4 Measured and modeled (*K*-value approach) phase compositions at 130°C and 10 MPa for: a) n-butane-rich (L_1) phase; b) pitch (L_2) phase.
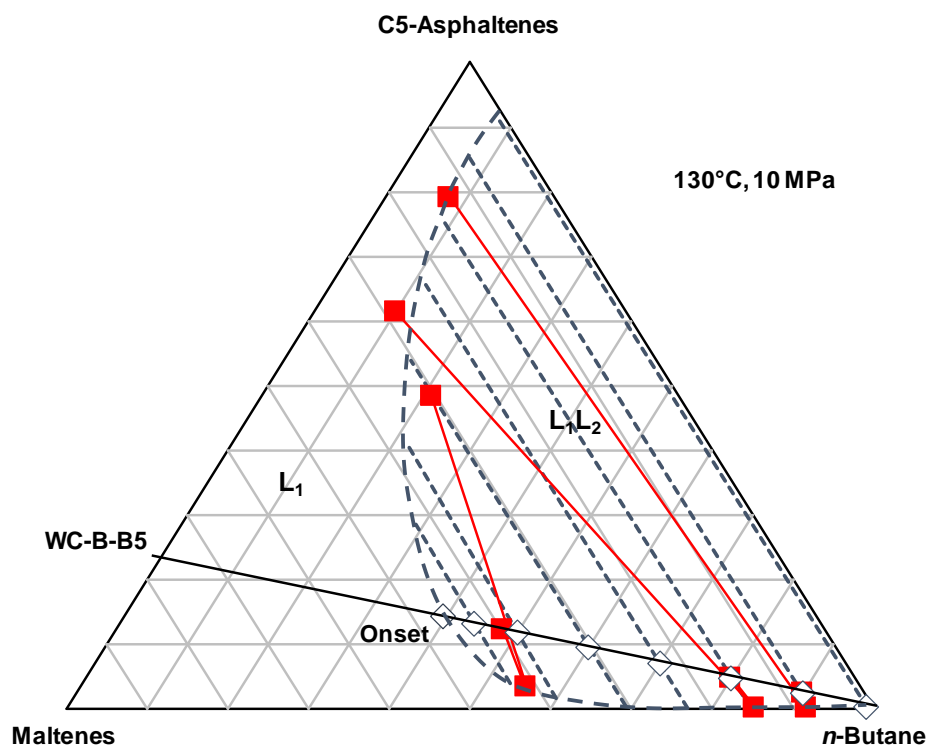
Figure 5.5 Ternary phase diagram for mixtures of *n*-butane and WC-B-B5 bitumen at 130°C and 10 MPa. Symbols are experimental data, the dashed line is the estimated boundary of the L_1L_2 region; and the dotted lines are tie-lines.

5.2 *K*-Values for Mixtures of *n*-Butane, Maltenes, and C5-Asphaltenes

The equilibrium constant, or *K*-value, of a component is defined as follows:

$$K_i = \frac{x_i^{L2}}{x_i^{L1}}$$ (5.1)

where x_i is the mole fraction of component *i*. and superscripts L_1 and L_2 indicate the phase. *K*-values can be used to determine the phase composition and yields at any feed composition using a straightforward equilibrium flash calculation.

A set of *K*-values for the pseudo-ternary mixtures of *n*-butane, maltenes, and C5-asphaltenes at 130°C and 10 MPa were determined directly from the end points of the tie-lines from their ternary diagram, Figure 5.5, and are listed in Table 5.8. While ternary diagrams were not available at other temperatures and pressures, the onset composition was the same at all temperatures and pressures considered in this study. Hence, the ternary diagrams are likely to be similar at all conditions, and the *K*-values determined at 130°C and 10 MPa can be used to check the consistency of the data collected at other conditions.

Table 5.8 *K*-values of *n*-butane, maltenes, and C5-asphaltenes at 130°C and 10 MPa determined from the ternary diagram shown in Figure 5.5.

Feed *n*-Butane Content, wt%	*n*-Butane	Maltenes	C5-Asphaltenes
44	0.889	1.60	11.8
50	0.815	2.13	56.2
60	0.722	3.14	479
70	0.643	4.20	3500
80	0.573	5.60	23300
90	0.501	6.78	152000
99	0.541	7.28	644000

The K-values from Table 5.8 were correlated to the feed n-butane content as follows:

$$K_{C_4} = a_{1,C4} + a_{2,C4} \left(1 - \frac{1}{\left(1 - \frac{w_s^F}{a_{3,C4}}\right)} \right) \tag{5.2}$$

$$K_M = a_{1,M} \, exp(a_{2,M} * w_s^F) \tag{5.3}$$

$$K_A = a_{1,A} \, exp(a_{2,A} * w_s^F) \tag{5.4}$$

where, w_s^F is the mass fraction of n-butane in the feed, a_1, a_2, and a_3 are fitting parameters, and subscripts C_4, M, and A indicate n-butane, maltenes, and C5-asphaltenes, respectively. The fitted parameters are provided in Table 5.9. The correlations fit the estimated K-values to within 23.7%. The correlations are independent of temperature and pressure since the measured data were insensitive to these conditions.

Table 5.9 Fitted parameter for the K-value correlations.

Component	a_1	a_2	a_3
n-butane	0.98	0.35	1.6
Maltenes	0.35	3.5	-
C5-Asphaltenes	0.00284	18.8	-

The pitch* and C5-asphaltene yields were calculated and are compared with the measured data in Figure 5.3. Except at 20°C, the calculated yields are within the experimental error of the measurements, confirming the consistency of the yield measurements at different conditions. It is not known if the deviation at 20°C is from a change in phase behaviour or a result of poor mixing and equilibration when the bitumen viscosity is high. Phase compositions for both the n-butane-rich and pitch phase were also calculated and are compared with the measured values in Figure 5.4. The K-value approach fit the experimental data for the n-butane-rich phase compositions to within experimental error of ±0.3 wt%, Figure 5.4a. This approach matched the trends for the pitch phase compositions but larger deviations were observed for the maltenes and C5-asphaltene content in the pitch phase, Figure 5.4b. These deviations are attributed mainly to the uncertainty

in the measured heavy phase composition. Finally, Figure 5.6 shows that the calculated H/F ratios are within the error of the measurements at high dilution and slightly exceed the measured value near the onset. The measured compositions and H/F ratios are least reliable near the onset and therefore the measurements, the derived *K*-values, and the *K*-value based calculations are also all less accurate near the onset.
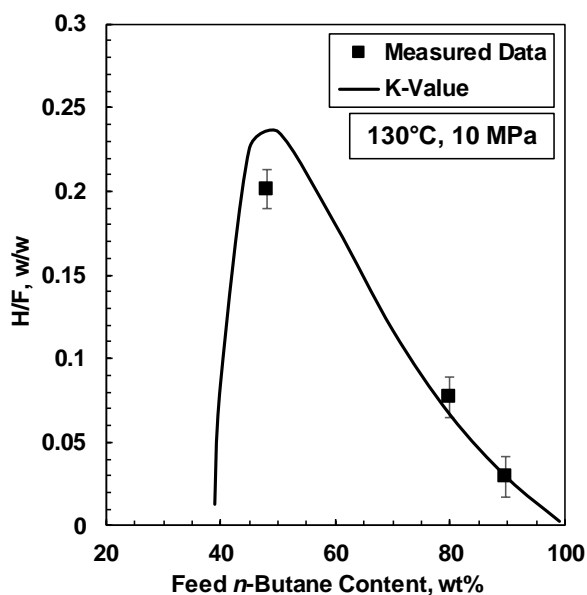
Figure 5.6 Measured and modeled (*K*-value approach) H/F ratio for *n*-butane WC-B-B5 diluted bitumen at 130°C and 10 MPa.

5.3 EoS Modeling

The first approach was to model the data using the APR EoS with temperature dependent interaction parameters (TDvdW). Figure 5.1 shows that, below the critical temperature of *n*-butane (152°C), this approach fit the saturation pressures and onsets at high pressures with AAD of ±0.12 MPa and 3.7 wt%, respectively, almost within the respective experimental errors of ±0.14 MPa and 1.6 wt%. The model became less accurate above the *n*-butane critical temperature. At 130°C, it predicted a non-existent L_1L_2/L_1 boundary above 90 wt% *n*-butane content and significantly under-predicted the C5-asphaltene and maltene contents in the pitch phase, Figure 5.7. The TDvdW approach also severely under-predicted the pitch* yields (not shown here) and predicted that the asphaltenes become soluble at high solvent dilutions, while experimental data showed that

the asphaltenes remain insoluble. Cubic EoS are well suited for vapour-liquid equilibria but not for liquid-liquid equilibria (LLE). They must be tuned extensively to match LLE and, in this case, temperature dependent parameters were insufficient to match the data.

Therefore, the APR EoS with composition dependent binary interaction parameters (CDvdW) was used instead. This model allows the binary interaction parameters to be tuned to different phase compositions and hence provides more parameters with which to match the measured data. Below the critical temperature of n-butane, this approach matched the measured saturation pressure and onsets (Figure 5.1) and the yields (Figure 5.9) generally to within the experimental error. The model became less accurate above the n-butane critical temperature but still predicted an L_1L_2 region at 90 wt% n-butane in the feed. This approach also fit the measured n-butane-rich (L_1) phase compositions to within the experimental error of ± 0.3 wt%, Figure 5.4. It predicted the correct trends for the pitch (L_2) phase compositions but under-predicted the n-butane content in the pitch phase by approximately 6.4 wt%, Figure 5.7. Some flash calculation instabilities occurred at temperatures higher than the critical temperature of the n-butane (152°C). The instabilities created discontinuities in the in the separation pressure trend versus temperature.
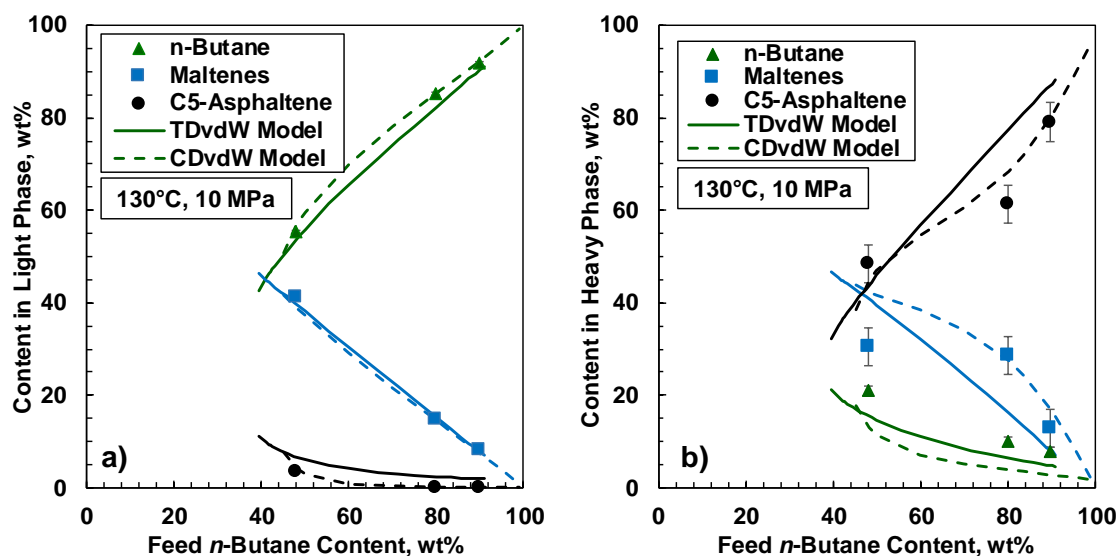
Figure 5.7 Measured and modeled (TDvdW and CDvdW approaches) phase compositions at 130°C and 10 MPa for: a) n-butane-rich (L_1) phase; b) pitch (L_2) phase.
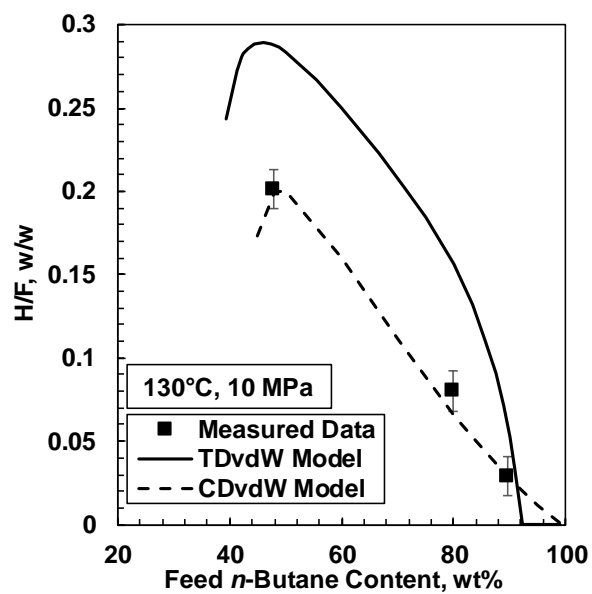
Figure 5.8 Measured and modeled (TDvdW and CDvdW approaches) H/F ratio for *n*-butane WC-B-B5 diluted bitumen at 130°C and 10 MPa.
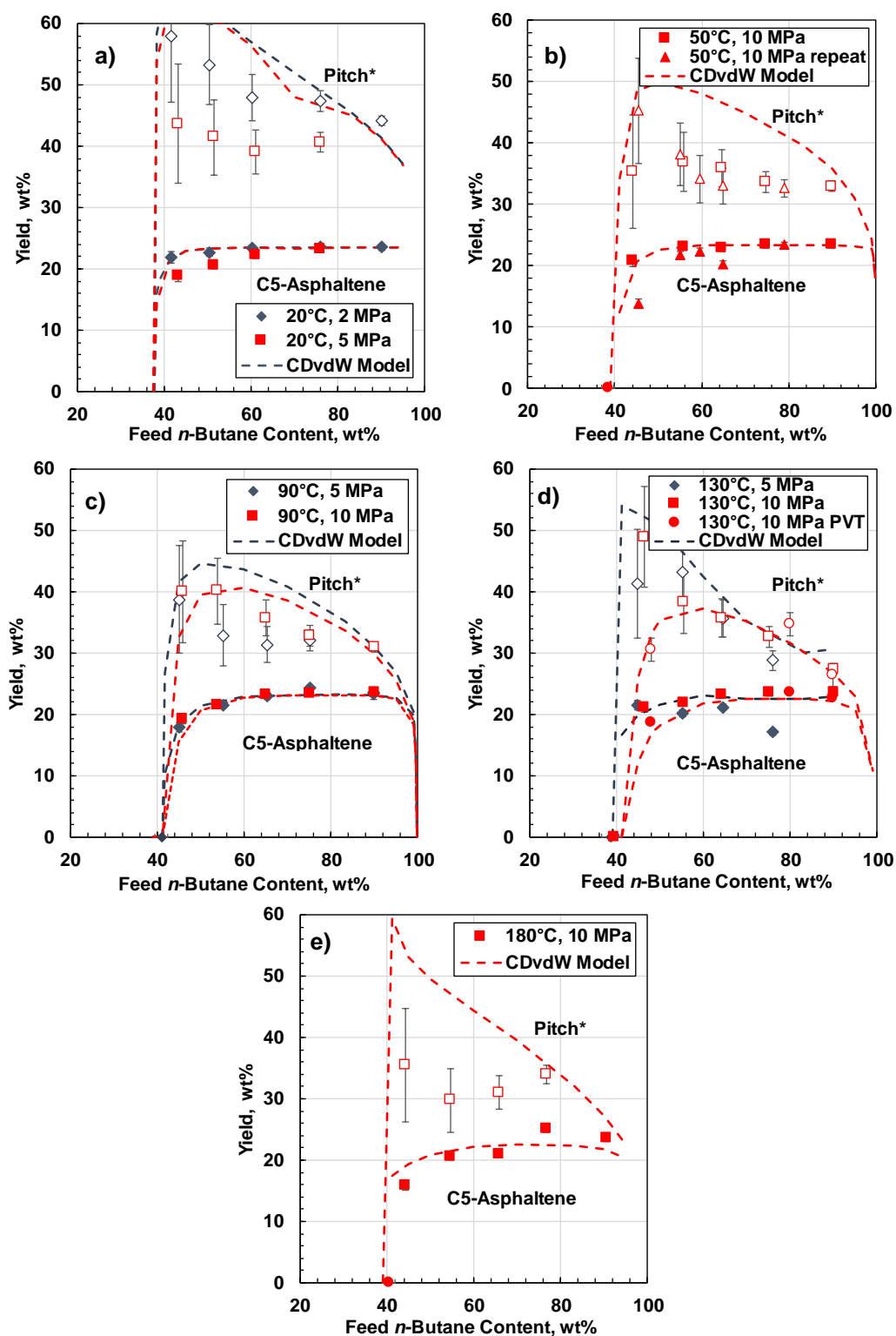
Figure 5.9 Measured and modeled (CDvdW approach) C5-asphaltene and pitch* yields for mixtures of *n*-butane and WC-B-B5 bitumen at: a) 20°C; b) 50°C; c) 90°C; d) 130°C; e) 180°C. Open and solid symbols represent pitch* and C5-asphaltene measurements, respectively.

5.4 Comparison with Mixtures of Bitumen with Propane and *n*-Pentane

Phase behaviour for *n*-butane diluted bitumen was compared with literature data for mixtures of propane and bitumen (Mancilla-Polanco *et al*., 2018) and *n*-pentane and bitumen (Johnston *et al*., 2017a, 2017b). The differences in the phase boundaries, yields, and ternary diagrams are discussed below. The application of the CDvdW approach to the three *n*-alkanes is also discussed.

P-X Diagram

Figure 5.10 shows the pressure-composition (P-X) diagram at 90°C for propane, *n*-butane and *n*-pentane diluted bitumen. As expected, the phase boundaries for mixtures of *n*-butane and bitumen fall between those of propane and *n*-pentane with bitumen. The saturation pressures decreases with increasing *n*-alkane carbon number because the volatility of the *n*-alkane decreases. Similarly, all saturation pressures increase with temperature as the volatility of the components increased.

The onsets increase with increasing *n*-alkane carbon number (approximately 30, 40 and 50 wt% with propane, *n*-butane and *n*-pentane, respectively) indicating that asphaltenes are more soluble in higher carbon number *n*-alkanes. While not shown here, the onsets are sensitive to pressure for propane but almost insensitive to pressure for *n*-butane and *n*-pentane diluted bitumen systems. The onsets are insensitive to temperature with propane and *n*-butane and slightly sensitive to temperature with *n*-pentane.
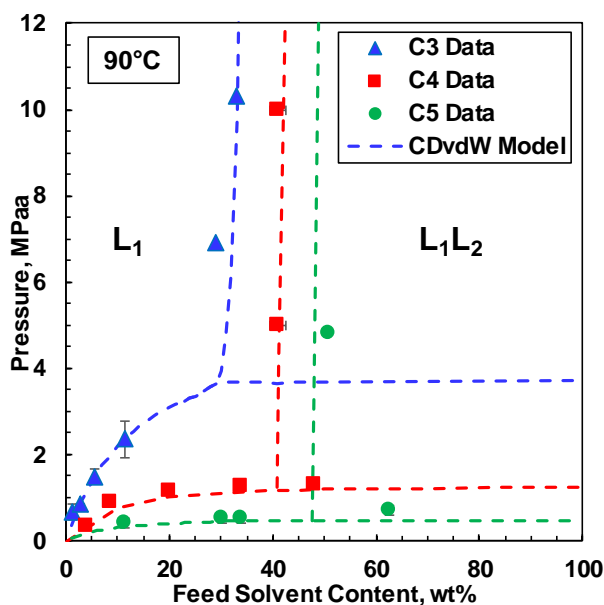
Figure 5.10 Measured and modeled (CDvdW approach) pressure-composition diagram for mixtures of bitumen with propane, *n*-butane, and *n*-pentane at 90°C. Propane data from Mancilla-Polanco *et al*. (2018) and *n*-pentane data from Johnston *et al*. (2017a).

Yields

Figure 5.11 shows that the pitch yields from mixtures of *n*-butane and bitumen also fall between those of propane and bitumen (Mancilla-Polanco *et al*., 2018) and *n*-pentane and bitumen (Johnston *et al*., 2017a). The yields decrease with increasing carbon number because the asphaltenes are more soluble in higher carbon number *n*-alkanes. In propane, approximately half the bitumen partitions to each phase while in *n*-pentane mainly asphaltenes are rejected as the pitch phase. While not shown here, the yields tend to decrease slightly with increasing pressure and have a similar sensitivity to temperature as the onsets.
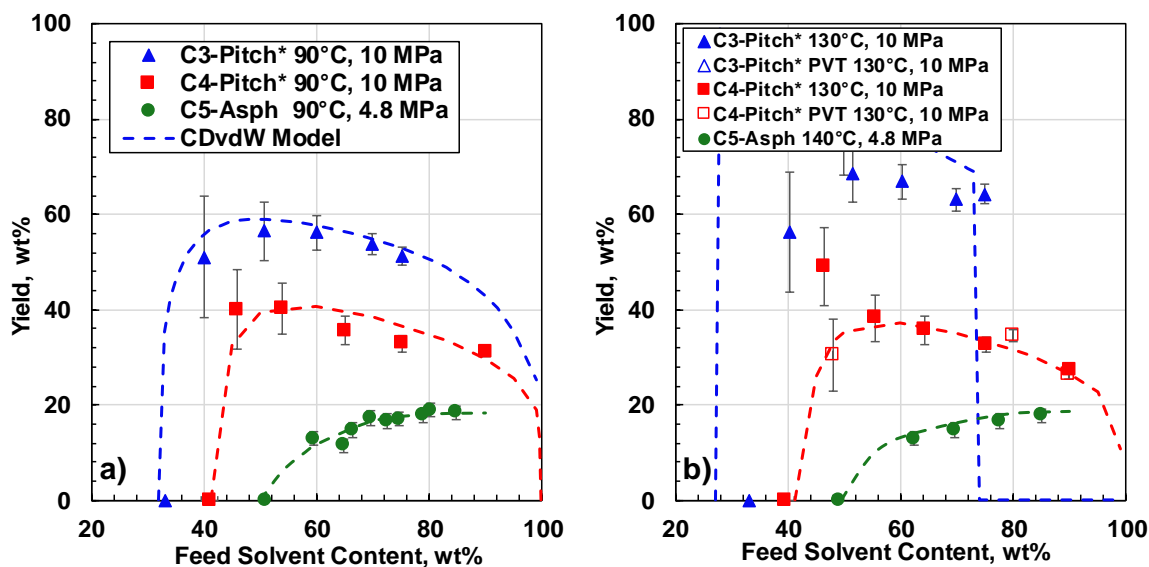
Figure 5.11 Measured and modeled (CDvdW approach) C5-asphaltene and pitch* yield curves for mixtures of bitumen with propane, *n*-butane, and *n*-pentane at: a) 90°C; b) 130°C. Propane data is from Mancilla-Polanco *et al*. (2018) and *n*-pentane data is from Johnston *et al*. (2017a).

Ternary Diagram

Figure 5.12 compares ternary diagrams for mixtures of propane and bitumen (Mancilla-Polanco *et al*., 2018), *n*-butane and bitumen (this thesis), and *n*-pentane and bitumen (Johnston *et al*., 2017b). The size of the L_1L_2 region increases as the carbon number of the *n*-alkane decreases and the solubility of the asphaltenes decreases (lowest solubility and largest L_1L_2 region in propane). While not shown here, in propane, the size of the L_1L_2 region is sensitive to pressure. In *n*-butane, the L_1L_2 region is nearly insensitive to temperature and pressure. There are not enough data to comment on the behaviour with *n*-pentane but based on the onset and yield data, the L_1L_2 region is expected to be only slightly sensitive to temperature and pressure.
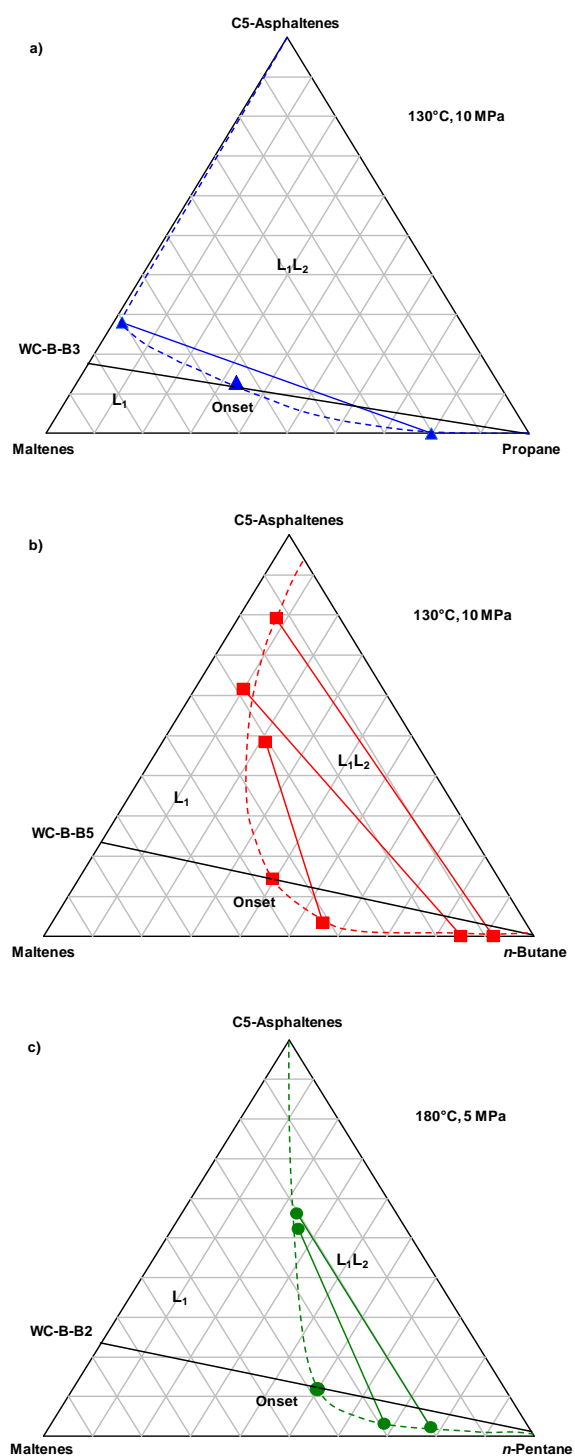
Figure 5.12 Ternary diagrams for mixtures of: a) propane and bitumen at 130°C, 10 MPa (Mancilla-Polanco *et al*., 2018); *n*-butane and bitumen at 130°C and 10 MPa (this thesis); *n*-pentane and bitumen at 180°C and 5 MPa (Johnston *et al*., 2017b). Symbols are experimental data and dashed lines are the estimated phase boundaries.

TDvdW Model Approach

The TDvdW approach was primarily used to match all of phase boundaries below the critical temperature of the solvent. In all cases, the model deviated above the solvent critical temperature (not shown here). However, this approach under-predicted the yield data for the three solvents and predicted an unobserved L_1L_2/L_1 boundary above 90 wt% feed *n*-butane content.

The coefficients of the fitted binary interaction parameters for each *n*-alkane are provided in Table 5.10. The parameters k_{ij}^1 and b_A increased monotonically with increasing carbon number of the *n*-alkane increases while the parameter k_{ij}^2 decreased monotonically. The a_A parameter was set to zero for propane and *n*-pentane but had a non-zero value for *n*-butane. It was necessary in order to match the onset boundary. Except for *aA*, all of the parameters for *n*-butane diluted bitumen are consistent with the values for propane and *n*-pentane diluted bitumen. It is possible that the parameters for all three *n*-alkanes could be retuned for more consistency but that work is beyond the scope of this thesis.

Table 5.10 Tuned coefficients for the temperature dependent (TDvdW) binary interaction parameters with propane (Mancilla-Polanco *et al*., 2018), *n*-butane (this thesis), and *n*-pentane (Johnston *et al*., 2017b) diluted bitumen.

n-Alkane	Pseudo-Component Pair	k_{ij}^1 K	k_{ij}^2	a_A K^{-1}	b_A K^{-2}
C3	Maltenes	-350	0.014	-	-
	C5-Asphaltene	-	-	0	6.44×10^{-6}
C4	Maltenes	443.50	0.00809	-	-
	C5-Asphaltene	-	-	-0.00747	0.000026
C5	Maltenes	2550	-1.5	-	
	C5-Asphaltene	-	-	0	0.0000127

CDvdW Model Approach

The CDvdW model results from this thesis and the literature (Mancilla-Polanco *et al*., 2018; Johnston *et al*., 2017a) are shown in Figures 5.10 and 5.11. This approach was able to match all of phase boundaries below the critical temperature of the solvent. In all cases, the model deviates above the solvent critical temperature (not shown here). This approach was also able to match all of the yield data except for that of propane above its critical temperature at high dilution (> 75 wt% propane in the feed). While the approach is suitable for single component solvents, the correlation of the binary interaction parameters to the solvent content in the feed means that a new methodology would be required to predict the binary interaction parameters for the components within a mixed solvent.

The correlation for the composition dependent *n*-butane binary interaction parameters had the same form as the correlation for the propane parameters from Mancilla-Polanco *et al*. (2018). The coefficients of the two correlations are compared in Table 5.11. A different correlation was proposed for the binary interaction parameter between the *n*-pentane and the asphaltenes pseudo-components (Johnston *et al*., 2017a) and is given by:

$$k_{ij}^* = a_{C5}T + b_{C5}(e^{(c_{C5}T + d_{C5})w_{solv}})$$

(5.5)

where T is temperature in °C and parameters a_{C5}, b_{C5}, c_{C5} and d_{C5} are constants. The constants were tuned to fit the measured C5-asphaltene yield data and are provided in Table 5.12.

Table 5.11 Tuned coefficients for the composition dependent parameter correlations with propane (Mancilla-Polanco *et al.*, 2018) and *n*-butane (this thesis).

Parameter	Value C3	Value C4
w_{LL}	0.3	0.41
a_1	0.0001474 °C^{-1}	0.000077029 °C^{-1}
a_2	-0.05536	0.00001011
b_1	0.0002374°C^{-1}	0.00010358 °C^{-1}
b_2	-0.05661	0

Table 5.12 Tuned parameters for the composition dependent parameter correlations with *n*-pentane (Johnston *et al.*, 2017a).

Parameter	Value C5
a_{C5}	0.00001 °C^{-1}
b_{C5}	0.0345
c_{C5}	0.0059 °C^{-1}
d_{C5}	0.9125

The binary interaction parameters for the solvent/asphaltene pairs are compared in Figure 5.13.The binary interaction parameters for propane/asphaltenes and for *n*-butane/asphaltenes follow a similar trend since both were obtained from the same mathematical expression. The parameters for *n*-pentane were obtained from a different expression and follow a different trend. In the example shown in Figure 5.13 at 20°C, the *n*-pentane parameters are higher than those of both propane and *n*-butane below 40 wt% solvent but are lower at higher solvent contents. In other words, the parameters do not trend consistently with the carbon number of the *n*-alkane. It is possible that the parameters for all three *n*-alkanes could be retuned for more consistency but it is more likely that the inconsistency indicates the limitations of the compositional dependent approach. It is challenging to match propane and *n*-butane diluted bitumen with the same form of

binary interaction parameters as *n*-pentane diluted bitumen because the former *n*-alkanes cause so much more of the oil to enter the bitumen-rich L_2 phase.
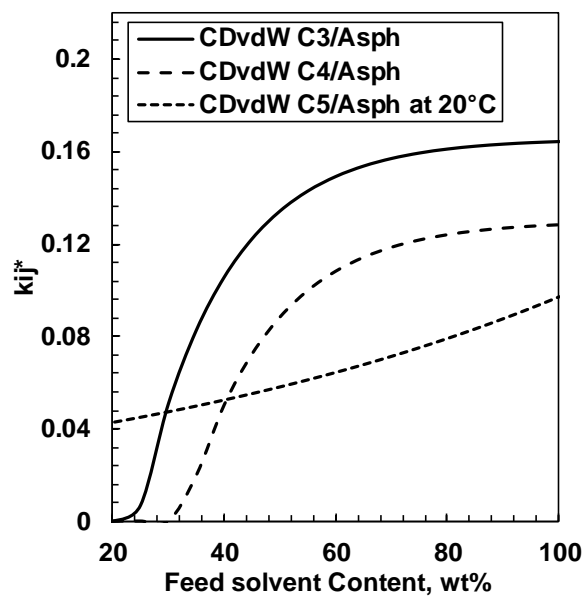

Figure 5.13 Binary interaction correlation for propane/asphaltene (Mancilla-Polanco *et al*., 2018) *n*-butane/asphaltene (this thesis), and *n*-pentane/asphaltene (Johnston *et al*., 2017a) using the CDvdW approach.

Chapter 6: Conclusions and Recommendations

This thesis aimed to: 1) collect phase behaviour data for mixtures of n-butane diluted bitumen at different temperatures, pressures, and feed solvent contents; 2) tune the APR EoS with composition dependent binary interaction parameters to match the data. The data and model are intended to support the design of *in situ* heavy oil recovery or deasphalting processes. The main conclusions and recommendations are summarized below.

6.1 Conclusions

6.1.1 Experimental Methodology

The methodologies developed by previous authors (Johnston *et al*., 2017b; Mancilla-Polanco *et al*., 2018) to measure phase boundaries (L_1/VL_1 and L_1/L_1L_2), yields, and phase compositions were successfully applied to mixtures of n-butane and WC-B-B5 bitumen. A modification was made to the procedure for yield measurements in the blind cells. It was found that convective mixing occurred at the interface between the L_1 and L_2 phases when the oven door was opened to collect the n-butane-rich (L_1) phase sample. Therefore, the blind cell was wrapped with thermal insulation and a longer re-equilibration time was used before collecting the pitch (L_2) phase sample.

In the PVT cell experiments, the interface between the L_1 and L_2 phases could only be distinguished at n-butane contents of 75 wt% or greater. At lower n-butane contents, the L_1 and L_2 phase samples were collected following the blind cell procedure.

6.1.2 Experimental Data

The phase behaviour for mixtures between n-butane and WC-B-B5 bitumen were examined at temperatures from 20 to 230°C and pressures up to 10 MPa. Liquid (L_1), vapour-liquid (VL_1) and liquid-liquid (L_1L_2) phase regions were observed. As expected, the saturation pressure (L_1/VL_1 boundary) increased with temperature and n-butane content. The onset of the second liquid phase (L_1/L_1L_2 boundary) was insensitive to temperature and slightly sensitive to pressure. On average, the second phase appeared at n-butane contents 39.8 ±1.6 wt%. The L_1L_2/VL_1L_2 boundary corresponded approximately to the vapour pressure of n-butane.

The pitch phase morphology was examined at temperatures from 50 to 180°C and pressures up to 10 MPa. The pitch phase appeared as small particles or droplets just above the onset. At 130°C, the pitch phase was a liquid and, at increased *n*-butane content in the feed, it coalesced and settled into a distinct layer.

The C5-asphaltene and pitch* (*n*-butane-free) yield from the pitch phase were measured at temperatures from 20 to 180°C and pressures up to 10 MPa. Immediately above the onset, the pitch phase contained 40 to 50 wt% bitumen. The bitumen fraction decreased to near the C5-asphaltene content of the bitumen as the feed *n*-butane content increased. The pitch* and C5-asphaltene yields were insensitive to temperature and pressure for all the cases except at 20°C and 2 MPa where higher yields were observed. The yield data demonstrate that the L_1L_2 region extends to a feed *n*-butane content of at least 90 wt%

The phase compositions were analyzed in terms of the *n*-butane, maltene, and C5-asphaltene content. Almost all of the asphaltenes were rejected from the *n*-butane-rich phase even near the onset. The *n*-butane content in the pitch phase was approximately 20 wt% near the onset and decreased monotonically towards near zero at high dilution.

6.1.3 Consistency of Experimental Data

The equilibrium constant, or *K*-value was used as a thermodynamic tool to check the data consistency of the phase composition data. *K*-values were determined from a ternary diagram based on the phase composition data collected at 130°C and 10 MPa. Phase compositions and yields were then calculated at any given temperature, pressure, and *n*-butane content in the feed. The calculated yields were within the experimental error measurements (except at 20°C), confirming the consistency of the yield measurements at different conditions. Higher values were observed at 20°C and 2 MPa but it is not known or not determined if the deviation is caused by a change in phase behaviour or poor mixing when the bitumen is very viscous. The calculated phase compositions were consistent with the measured values. The calculated H/F ratios were within the error of the measurements at high dilution and slightly exceeded the measured value near the onset.

The measured compositions and H/F ratios are least reliable near the onset and therefore the measurements, the derived K-values, and the K-value based calculations are all less accurate near the onset.

The phase boundaries for mixtures of n-butane and bitumen fall between those of propane and n-pentane with bitumen. The saturation pressures decreased with increasing n-alkane carbon number because the volatility of the n-alkane decreases. The onsets (L_1L_2 boundary) increased with increasing n-alkane carbon number (approximately 30, 40 and 50 wt% with propane, n-butane and n-pentane, respectively) indicating that asphaltenes are more soluble in higher carbon number n-alkanes.

The pitch* yields from mixtures of n-butane and bitumen also fall between those of propane and bitumen (Mancilla-Polanco *et al*., 2018) and n-pentane and bitumen (Johnston *et al*., 2017b). The yields decreased with increasing carbon number because the asphaltenes are more soluble in higher carbon number n-alkanes. In propane, approximately half the bitumen partitions to each phase while in n-pentane mainly asphaltenes are rejected as the pitch phase.

Ternary diagrams for mixtures of propane and bitumen (Mancilla-Polanco *et al*., 2018), n-butane and bitumen (this thesis), and n-pentane and bitumen (Johnston *et al*., 2017b). The size of the L_1L_2 region increased as the carbon number of the n-alkane decreased and the solubility of the asphaltenes decreased (lowest solubility and largest L_1L_2 region in propane).

6.1.4 Modeling

The APR EoS was implemented to model the phase boundaries, yields, and phase compositions for mixtures of n-butane and WC-B-B5 bitumen Temperature and composition dependent binary interaction parameters were tested. The APR EoS with temperature dependent binary interaction parameters fit both the vapour-liquid and liquid-liquid boundaries to within the uncertainty of the measurements at temperatures below the critical temperature of n-butane (152°C). However, larger deviation were found at temperatures above the n-butane critical temperature. The temperature dependent approach significantly under-predicted the pitch* yields.

The APR EoS with composition dependent interaction parameters fit not only the phase boundaries but also the yields and compositions to within the experimental error at temperatures below the *n*-butane critical temperature. However, larger deviations were found at temperatures above the *n*-butane critical temperature.

6.2 Recommendations

It is recommended that measurements of the phase behaviour for bitumen with other solvents that are relevant for in situ heavy oil recovery. These might include cyclohexane, condensates, and mixed solvents.

The APR CEoS was tuned to match the experimental data using composition dependent interaction parameters. This approach is useful or interpolating rather than predicting results. In addition, composition dependent parameters introduce thermodynamic inconsistencies into the CEoS and are challenging to implement with mixed solvents. It is recommended that other modeling approaches should be tested:

- EoS that have already shown promising results in modeling the phase behaviour of heavy oil/*n*-alkane systems; for example, the Cubic Plus Association EoS and the PC-SAFT EoS (Tavakkoli *et al*., 2014; Fouad *et al*., 2018; Zhang, *et al*.,2019).
- the regular solution approach for modeling yield data (Alboudwarej *et al*., 2003; Akbarzadeh *et al*., 2005; Tharanivasan *et al*., 2009).
- the equilibrium constant (*K*-value) approach with *K*-values correlated to the *n*-alkane carbon number.

Appendix A: Error Analysis

A.1 Saturation Pressure Data

Uncertainties in the measurements for saturation pressure were determined from the deviations of each data point from a modified Henry's law model (Badamchi-Zadeh *et al.*, 2009) fitted to all of the data. The modified Henry's law model was defined as follows:

$$P_{sat} = x_{c4}H_{c4} + x_{bit}\gamma_{bit}P_{v,bit} \qquad \text{A.1}$$

where,

$$H_{C4} = \exp\left(A_{C4} + \frac{B_{C4}}{T} + \frac{C_{C4}P_{sat}}{RT}\right) \qquad \text{A.2}$$

$$P_{v,bit} = \exp\left(A_{bit} - \frac{B_{bit}}{T}\right) \qquad \text{A.3}$$

and where P_{sat} is the predicted saturation pressure, x is the mole fraction, H is the Henry's law constant, γ is the activity coefficient, P_v is the vapour pressure, A, B, and C are fitted constants, and subscripts *C4* and *bit* represent *n*-butane and bitumen, respectively.

The mole fractions of *n*-butane and bitumen were determined from their mass fractions measured from experiments and their respective molecular weight. The vapour pressure of bitumen was estimated based on a measurement of 380 kPa at 180°C and an assumption of 90 kPa at 60°C (the barometric pressure at the temperature of the dewatering procedure). The activity coefficient of the bitumen was assumed to be unity for lack of data and because the contribution of the bitumen to the saturation pressure was small. The Henry's law constants were fitted to the experimental saturation pressure dataset by minimizing the sum of the absolute deviation between the measured and the predicted values. The fitted constants are provided in Table A.**1**1. The uncertainties in the saturation pressures for the experiments at 50, 90, 130, 180 and 230°C were 0.07, 0.06, 0.08, 0.18, and ±0.31 MPa, respectively, based on 90% interval confidence. On average, the uncertainty of saturation pressure was ±0.14 MPa. Note, the modified Henry model is not intended to be a rigorous phase behaviour model and is only used to fit the data to assess the uncertainty of the measurements.

Table A.1 Fitted Henry's law model constants for Equation A.3 and Equation A.2 using a WC-B-B5 bitumen. Pressure is in MPa and temperature is in K.

Constants	Value
A_{bit}	9.99
B_{bit}, K	1836.85
A_{C4}	11.216
B_{C4}, K	-14.739
C_{C4}, L/mol	0.5203

A.2 HPM Onset Data

The main source of uncertainty in measuring the n-butane content at which second phase appears is the mass of solvent (n-butane) injected at each injection step (typically at increments of 2 wt%). The mass of solvent injected at each step was estimated using the cathetometer readings and the solvent density at experimental conditions. The pump readings were used as verification, as described in Section 3.3. The uncertainty of n-butane content was estimated based on the uncertainties in the volume of n-butane injected at each step ($\pm$ 0.01 cm³ based on cathetometer readings) multiplied by the number of steps. The uncertainty of the solvent density ($\pm$0.001 g/cm³) was also accounted for. Based on all of the HPM data collected to date, the uncertainty in the composition was determined to be $\pm$0.5 wt%. This uncertainty is added to the precision of the measurement (half of the solvent increment $\pm$1.1 wt%) to obtain a total uncertainty of $\pm$1.6 wt%.

A.3 Blind Cell Phase Composition and Yield Data

Phase Sample Composition: Two samples of each phase were collected and analyzed using the mass evaporation technique to determine the phase compositions, as described in Section 3.4. The reported phase compositions are the average of the two measured values. The repeatability of the light phase compositions was $\pm$0.3 wt% based on a 90% confidence interval for the set of the paired samples collected in each experiment.

Yield Data: The uncertainty of the yields were determined as the sum of the uncertainty of a yield measurement plus the uncertainty in the yield calculation based on the assumed solvent content in

the heavy phase. The uncertainty of the yield measurement was determined as the 90% confidence interval of the deviations of the yield around a best fit yield curve. The uncertainty of the yield from the assumed solvent content was determined as the difference in yield at solvent contents of 0 and 30 wt%. The combined uncertainties were plotted versus the solvent content in the feed and fitted with the following relationship:

$$Uncertainty = \left(1 - A\left(1 - e^{(-B(w_{solv}-C))}\right)\right)100 \qquad \text{A.4}$$

where *A, B,* and *C* are the tuned constants, and w_{solv} is the solvent mass fraction. The fitted constants are shown in Table A2 for both the pitch* and C5-asphaltene yields. On average, the uncertainty of C5-asphaltene and pitch* yields were 0.6 and ±4.1 wt%, respectively. Note that the uncertainty in the pitch* yield increased significantly near the onset (approximately ±15 wt% at <40 wt% *n*-butane in the feed). A repeat run was performed at 50°C, 10 MPa and five different *n*-butane feed contents, and the repeatability of the measured C5-asphaltene and pitch* yields were ±0.5 and ±2.1 wt%, respectively.

Table A2. Tuned exponential correlation parameters to fit pitch* and C5-asph error curves.

Constants	Pitch* error	C5-asph error
A	0.9990	0.9952
B	5.64	12.92
C	0.0180	-0.0051

A.4 PVT Cell Phase Composition and Yield Data

The major sources of error in the phase composition and yield calculations are as follows:

1. Mass of Bitumen and Solvent in Feed: The mass of bitumen and solvent injected at the experimental conditions was calculated in two ways, using the injected volume recorded from either the PVT cell (cathetometer) or the pump, as described in Section 3.5. The reported mass of solvent was taken as the average of these two values. The uncertainty of

the mass measurement was determined as the 90% confidence interval from the deviations between the two measurements for all of the data collected to date. The uncertainty of the mass of bitumen and solvent injected were 0.3 and ±0.15 g, respectively. Solvent refers to *n*-butane.

2. Phase Sample Composition: Two samples of each phase were collected and analyzed using the mass evaporation technique to determine the phase compositions, as described in Section 3.5. The reported phase compositions are the average of the two measured values. The uncertainty was calculated from the deviations of the two values for all of the data collected to date using a 90% confidence interval. The repeatability of the light phase compositions was ±0.3 wt% based on a 90% confidence interval for the set of the paired samples collected in each experiment. The repeatability of the *n*-butane content in the heavy phase composition was ±1.0 wt%. The uncertainty of the asphaltene and maltene content of the heavy phase was higher (±4.1 wt%) because an accurate separation of the asphaltenes and maltenes was experimentally challenging.

3. Mass of light Phase: After equilibrium, the volume of the light phase was measured using the cathetometer with a precision of ±0.01 cm³. Both phases were collected through blind cells and the masses were measured with a precision of ±0.01 g. The mass of fluid in the transfer line was also measured with a precision of ±0.02 g. The propagated uncertainty of the light phase mass was ±0.05 g.

4. Mass of heavy phase: The mass of the heavy phase was determined as described for the light phase. The dead volume of the PVT cell is also required and is an additional source of error. The mass of the fluid in the dead volume of the PVT cell was determined from the dead volume and solvent density with an uncertainty of ±0.22 g. The propagated uncertainty of the heavy phase mass was ±0.25 g.

The uncertainty in the yield calculations includes all three contributions and was determined from the propagation of error. The final uncertainty of the C5-asphaltene and pitch* yields were 1.6 and ±1.9 wt%.

References

Adachi, Y., and Sugie, H. (1986). A new mixing rule—modified conventional mixing rule. Fluid Phase Equilibria, 28(2), 103-118.

Agrawal, P., Schoeggl, F. F., Satyro, M. A., Taylor, S. D., and Yarranton, H. W. (2012). Measurement and modeling of the phase behavior of solvent diluted bitumens. Fluid Phase Equilibria, 334, 51-64.

Akbarzadeh, K., Alboudwarej, H., Svrcek, W. Y., and Yarranton, H. W. (2005). A generalized regular solution model for asphaltene precipitation from n-alkane diluted heavy oils and bitumens. Fluid Phase Equilibria, 232(1-2), 159-170.

Alberta Energy Regulator. (2018). ST98, 2018. Alberta's Energy Reserves and Supply/Demand Outlook. Government of Alberta.

Alboudwarej, H., Akbarzadeh, K., Beck, J., Svrcek, W. Y., and Yarranton, H. W. (2003). Regular solution model for asphaltene precipitation from bitumens and solvents. AIChE Journal, 49(11), 2948-2956.

Ali, Syed Mohammad Farouq . (2015). *Practical heavy oil recovery*. Book Draft, 1-1.

Altgelt, K. H. (2016). Composition and analysis of heavy petroleum fractions. CRC Press.

Altgelt, K. H., and Boduszynski, M. M. (1994). Composition and analysis of heavy petroleum fractions. New York: Marcel Deckker, Inc.

Andersen, S. I., and Birdi, K. S. (1991). Aggregation of asphaltenes as determined by calorimetry. Journal of Colloid and Interface Science, 142(2), 497-502.

Andersen, S. I., and Stenby, E. I. (1996). Thermodynamics of asphaltene precipitation and dissolution investigation of temperature and solvent effects. *Fuel Science and Technology International*, *14*(1-2), 261-287.

Andersen, S. I., Lindeloff, N., and Stenby, E. H. (1998). Investigation of asphaltene precipitation at elevated temperature. Petroleum science and technology, 16(3-4), 323-334.

Arya, A., Liang, X., von Solms, N., and Kontogeorgis, G. M. (2017). Modeling of Asphaltene Precipitation from Crude Oil with the Cubic Plus Association Equation of State. Energy & Fuels, 31(2), 2063-2075.

ASTM D1160. (2018). Standard Test Method for Distillation of Petroleum Products at Reduced Pressure. Annual Book of Standards.

ASTM D2887. (2015). Standard Test Method for Boiling Range Distribution of Petroleum Fractions by Gas Chromatography. Annual Book of Standards.

ASTM D2892. (2018). Standard Test Method for Distillation of Crude Petroleum. Annual Book of Standards.

ASTM D4626. (2015). Standard Practice for Calculation of Gas Chromatographic Response Factors. Annual Book of Standards.

ASTM D5236. (2018). Standard Test Method for Distillation of Heavy Hydrocarbon Mixtures (Vacuum Potstill Method). Annual Book of Standards.

ASTM D5307. (2007). Standard Test Method for Determination of Boiling Rabge Distribution of Crude Petroleum by Gas Chromatography. Annual Book of Standards.

ASTM D6352. (2015). Standard Test Method for Boiling Range Distribution of Petroleum Distillates in Boiling Range from 174 °C to 700 °C by Gas Chromatography. Annual Book of Standards.

ASTM D7169. (2018). Standard Test Method for Boiling Point Distribution of Samples with Residues Such as Crude Oils and Atmospheric and Vacuum Residues by High Temperature Gas Chromatography. Annual Book of Standards.

ASTM D86. (2018). Standard Test Method for Distillation of Petroleum Products and Liquid Fuels at Atmospheric Pressure. Annual Book of Standards.

Badamchi-Zadeh, A., Yarranton, H. W., Maini, B. B., and Satyro, M. A. (2009). Phase Behaviour and Physical Property Measurements for VAPEX Solvents: Part II. Propane, Carbon Dioxide and Athabasca Bitumen. Petroleum Society of Canada.

Badamchi-Zadeh, A., Yarranton, H. W., Svrcek, W. Y., and Maini, B. B. (2009). Phase Behaviour and Physical Property Measurements for VAPEX Solvents: Part I. Propane and Athabasca Bitumen. Petroleum Society of Canada.

Barker, J. A., and Henderson, D. (1967). Perturbation theory and equation of state for fluids. II. A successful theory of liquids. The Journal of chemical physics, 47(11), 4714-4721.

Barrera, D. M., Ortiz, D. P., and Yarranton, H. W. (2013). Molecular weight and density distributions of asphaltenes from crude oils. *Energy and fuels*, *27*(5), 2474-2487.

Bayestehparvin, B., Farouq Ali, S. M., and Abedi, J. (2018). Solvent-Based and Solvent-Assisted Recovery Processes: State of the Art. *SPE Reservoir Evaluation & Engineering*.

Boduszynski, M. M. (1987). Composition of heavy petroleums. 1. Molecular weight, hydrogen deficiency, and heteroatom concentration as a function of atmospheric equivalent boiling point up to 1400. degree. F (760. degree. C). Energy & Fuels, 1(1), 2-11.

BP. (2018). Statistical Review of World Energy. 67th edition.

Butler, R. M., McNab, G. S., and Lo, H. Y. (1981). Theoretical studies on the gravity drainage of heavy oil during in-situ steam heating. *The Canadian journal of chemical engineering*, *59*(4), 455-460.

Castellanos Díaz, O., Modaresghazani, J., Satyro, M. A., and Yarranton, H. W. (2011). Modeling the phase behavior of heavy oil and solvent mixtures. Fluid Phase Equilibria, 304(1-2), 74-85.

Castellanos Díaz, O., Sanchez-Lemus, M. C., Schoeggl, F. F., Satyro, M. A., Taylor, S. D., and Yarranton, H. W. (2014). Deep-vacuum fractionation of heavy oil and bitumen, part I: Apparatus and standardized procedure. Energy & Fuels, 28(5), 2857-2865.

Chang, J., Ivory, J. J., Forshner, K., and Feng, Y. (2013). Impact of solvent loss during solvent injection processes. In *SPE Heavy Oil Conference-Canada*. Society of Petroleum Engineers.

Chapman, W. G., Gubbins, K. E., Jackson, G., and Radosz, M. (1989). SAFT: Equation-of-state solution model for associating fluids. Fluid Phase Equilibria, 52, 31-38.

Christian, S. D. (1971). Regular and Related Solutions: The Solubility of Gases, Liquids, and Solids (Hildebrand, Joel H; Prausnitz, John M.).

Chueh, P. L., and Prausnitz, J. (1968). Calculation of high-pressure vapor-liquid equilibria. Industrial and Engineering Chemistry, 60(3), 34-52.

CMG User Guide. (2016). Computer Modeling Group Ltd, Calgary, Canada CMG.

Dickie, J. P., and Yen, T. F. (1967). Macrostructures of the asphaltic fractions by various instrumental methods. Analytical chemistry, 39(14), 1847-1852.

Dini, Y., Becerra, M., and Shaw, J. M. (2016). Phase Behavior and Thermophysical Properties of Peace River Bitumen+ Propane Mixtures from 303 K to 393 K. Journal of Chemical and Engineering Data, 61(8), 2659-2668.

Eclipse User's Manual. (2016). Schulmberger Information Systems.

Flory, P. J. (1942). Thermodynamics of high polymer solutions. *The Journal of chemical physics*, *10*(1), 51-61.

Flory, P. J. (1953). Principles of polymer chemistry. Cornell University Press.

Fouad, W. A., Abutaqiya, M. I., Mogensen, K., Yap, Y. F., Goharzadeh, A., Vargas, F. M., and Vega, L. F. (2018). Predictive Model for Pressure–Volume–Temperature Properties and Asphaltene Instability of Crude Oils under Gas Injection. Energy and fuels, 32(8), 8318-8328.

Gao, G., Daridon, J. L., Saint-Guirons, H., Xans, P., and Montel, F. (1992). A simple correlation to evaluate binary interaction parameters of the Peng-Robinson equation of state: binary light hydrocarbon systems. Fluid phase equilibria, 74, 85-93.

Gao, J., Okuno, R., and Li, H. A. (2017). An Experimental Study of Multiphase Behavior for n-Butane/Bitumen/Water Mixtures. Society of Petroleum Engineers.

Gilgenast, E., Boczkaj, G., Przyjazny, A., and Kamiński, M. (2011). Sample preparation procedure for the determination of polycyclic aromatic hydrocarbons in petroleum vacuum residue and bitumen. Analytical and bioanalytical chemistry, 401(3), 1059-1069.

Gonzalez, D. L., Hirasaki, G. J., Creek, J., and Chapman, W. G. (2007). Modeling of asphaltene precipitation due to changes in composition using the perturbed chain statistical associating fluid theory equation of state. Energy and fuels, 21(3), 1231-1242.

Gonzalez, D. L., Ting, P. D., Hirasaki, G. J., and Chapman, W. G. (2005). Prediction of asphaltene instability under gas injection with the PC-SAFT equation of state. Energy and fuels, 19(4), 1230-1234.

Gray, M. R., Assenheimer, G., Boddez, L., and McCaffrey, W. C. (2004). Melting and fluid behavior of asphaltene films at 200− 500 C. Energy and fuels, 18(5), 1419-1423.

Gray, R. M. (1994). *Upgrading petroleum residues and heavy oils*. CRC press.

Gross, J., and Sadowski, G. (2001). Perturbed-chain SAFT: An equation of state based on a perturbation theory for chain molecules. Industrial and engineering chemistry research, 40(4), 1244-1260.

Hirschberg, A., DeJong, L. N. J., Schipper, B. A., and Meijer, J. G. (1984). Influence of temperature and pressure on asphaltene flocculation. Society of Petroleum Engineers Journal, 24(03), 283-293.

Huggins, M. L. (1941). Solutions of long chain compounds. The Journal of chemical physics, 9(5), 440-440.

Jamaluddin, A. K. M., Kalogerakis, N. E., and Chakma, A. (1991). Predictions of CO2 solubility and CO2 saturated liquid density of heavy oils and bitumens using a cubic equation of state. Fluid phase equilibria, 64, 33-48.

Jhaveri, B. S., and Youngren, G. K. (1988). Three-parameter modification of the Peng-Robinson equation of state to improve volumetric predictions. SPE reservoir engineering, 3(03), 1-033.

Johnston, K. A., Satyro, M. A., Taylor, S. D., and Yarranton, H. W. (2017a). Can a Cubic Equation of State Model Bitumen–Solvent Phase Behavior?. Energy and Fuels, 31(8), 7967-7981.

Johnston, K. A., Schoeggl, F. F., Satyro, M. A., Taylor, S. D., and Yarranton, H. W. (2017b). Phase behavior of bitumen and n-pentane. Fluid Phase Equilibria, 442, 1-19.

Katz, D. L., and Firoozabadi, A. (1978). Predicting phase behavior of condensate/crude-oil systems using methane interaction coefficients. Journal of Petroleum Technology, 30(11), 1-649.

Kesler, M. G. (1976). Improve prediction of enthalpy of fractions. Hydrocarbon processing, 153.

Kontogeorgis, G. M., Michelsen, M. L., Folas, G. K., Derawi, S., von Solms, N., and Stenby, E. H. (2006). Ten years with the CPA (Cubic-Plus-Association) equation of state. Part 1. Pure compounds and self-associating systems. Industrial and engineering chemistry research, 45(14), 4855-4868.

Kontogeorgis, G. M., Voutsas, E. C., Yakoumis, I. V., and Tassios, D. P. (1996). An equation of state for associating fluids. Industrial and engineering chemistry research, 35(11), 4310-4318.

Lee, B. I., and Kesler, M. G. (1975). A generalized thermodynamic correlation based on three-parameter corresponding states. AIChE Journal, 21(3), 510-527.

Li, Z., and Firoozabadi, A. (2010). Modeling asphaltene precipitation by n-alkanes from heavy oils and bitumens using cubic-plus-association equation of state. Energy & fuels, 24(2), 1106-1113.

Mancilla Polanco, A. A. (2017). The Phase Behavior of Heavy Oil and Propane Mixtures. M.Sc Thesis, University of Calgary. Calgary, Canada.

Mancilla-Polanco, A., Johnston, K., Richardson, W. D. L., Schoeggl, F. F., Zhang, Y. G., Yarranton, H. W., and Taylor, S. D. (2018). Phase Behavior of Heavy-Oil/Propane Mixtures. Society of Petroleum Engineers.

Mancilla-Polanco, A., Schoeggl, F.F., Johnston, K., Richardson, W.D., Yarranton, H.W. and Taylor, S.D. 2017.The Phase Behavior of Heavy Oil and Propane Mixtures. Paper SPE-presented at the SPE Canada Heavy Oil Technical Conference held in Calgary, Alberta, Canada, 15-16 February 2017.

Mansoori, G. A., Carnahan, N. F., Starling, K. E., and Leland Jr, T. W. (1971). Equilibrium thermodynamic properties of the mixture of hard spheres. The Journal of Chemical Physics, 54(4), 1523-1525.

Mathias, P. M., Naheiri, T., and Oh, E. M. (1989). A density correction for the Peng—Robinson equation of state. Fluid Phase Equilibria, 47(1), 77-87.

Maxwell, J. B., and Bonnell, L. S. (1957). Derivation and precision of a new vapor pressure correlation for petroleum hydrocarbons. Industrial and Engineering Chemistry, 49(7), 1187-1196.

McKenna, A. M., Purcell, J. M., Rodgers, R. P., and Marshall, A. G. (2010). Heavy petroleum composition. 1. Exhaustive compositional analysis of Athabasca bitumen HVGO distillates by Fourier transform ion cyclotron resonance mass spectrometry: A definitive test of the Boduszynski model. Energy & Fuels, 24(5), 2929-2938.

Mehrotra, A. K., and Svrcek, W. Y. (1988). Characterization of Athabasca bitumen for gas solubility calculations. Journal of Canadian Petroleum Technology, 27(6), 107-110.

Mehrotra, A. K., and Svrcek, W. Y. (1988). Properties of Cold Lake bitumen saturated with pure gases and gas mixtures. The Canadian Journal of Chemical Engineering, 66(4), 656-665.

Mehrotra, A. K., and Svrcek, W. Y. (1985). Viscosity, density and gas solubility data for oil sand bitumens. Part I: Athabasca bitumen saturated with CO and C2H6. AOSTRA J. Res, 1(4), 263-268.

Mehrotra, A. K., Eastick, R. R., and Svrcek, W. Y. (1989). Viscosity of Cold Lake bitumen and its fractions. The Canadian journal of chemical engineering, 67(6), 1004-1009.

Michelsen, M. L. (1982). The isothermal flash problem. Part I. Stability. Fluid phase equilibria, 9(1), 1-19.

Michelsen, M. L., and Hendriks, E. M. (2001). Physical properties from association models. Fluid phase equilibria, 180(1-2), 165-174.

Miller, K. A., Carlson, J. E., Morgan, R. J., Thornton, R. W., and Willis, K. (2003). Preliminary results from a solvent gas injection field test in a depleted heavy oil reservoir. *Journal of Canadian Petroleum Technology*, *42*(02).

Mullins, O. C. (2007). Petroleomics and structure–function relations of crude oils and asphaltenes. In *Asphaltenes, heavy oils, and petroleomics* (pp. 1-16). Springer, New York, NY.

Nielsen, B. B., Svrcek, W. Y., and Mehrotra, A. K. (1994). Effects of temperature and pressure on asphaltene particle size distributions in crude oils diluted with n-pentane. Industrial and engineering chemistry research, 33(5), 1324-1330.

Nishiumi, H., Arai, T., and Takeuchi, K. (1988). Generalization of the binary interaction parameter of the Peng-Robinson equation of state by component family. *Fluid Phase Equilibria*, *42*, 43-62.

Panagiotopoulos, A. Z., and Reid, R. C. (1986). New mixing rule for cubic equations of state for highly polar, asymmetric systems.

Panuganti, S. R., Vargas, F. M., Gonzalez, D. L., Kurup, A. S., and Chapman, W. G. (2012). PC-SAFT characterization of crude oils and modeling of asphaltene phase behavior. Fuel, 93, 658-669.

Pedersen, K. S., Christensen, P. L., Shaikh, J. A., and Christensen, P. L. (2006). Phase behavior of petroleum reservoir fluids. CRC press.

Péneloux, A., Rauzy, E., and Fréze, R. (1982). A consistent correction for Redlich-Kwong-Soave volumes. Fluid phase equilibria, 8(1), 7-23.

Peng, D. Y., and Robinson, D. B. (1976). A new two-constant equation of state. Industrial and Engineering Chemistry Fundamentals, 15(1), 59-64.

Peramanu, S., Singh, C., Agrawala, M., and Yarranton, H. W. (2001). Investigation on the reversibility of asphaltene precipitation. Energy and Fuels, 15(4), 910-917.

Pfeiffer, J. P., and Saal, R. N. J. (1940). Asphaltic bitumen as colloid system. The Journal of Physical Chemistry, 44(2), 139-149.

Powers, D. P., Sadeghi, H., Yarranton, H. W., and Van Den Berg, F. G. A. (2016). Regular solution based approach to modeling asphaltene precipitation from native and reacted oils: Part 1, molecular weight, density, and solubility parameter distributions of asphaltenes. Fuel, 178, 218-233.

Prausnitz, J. M., Lichtenthaler, R. N., and de Azevedo, E. G. (1998). Molecular thermodynamics of fluid-phase equilibria. Pearson Education.

Rachford Jr, H. H., and Rice, J. D. (1952). Procedure for use of electronic digital computers in calculating flash vaporization hydrocarbon equilibrium. Journal of Petroleum Technology, 4(10), 19-3.

Ramos-Pallares, F., Schoeggl, F. F., Taylor, S. D., Satyro, M. A., and Yarranton, H. W. (2015). Predicting the viscosity of hydrocarbon mixtures and diluted heavy oils using the expanded fluid model. Energy & Fuels, 30(5), 3575-3595.

Ramos-Pallares, F., Taylor, S. D., Satyro, M. A., Marriott, R. A., and Yarranton, H. W. (2016). Prediction of viscosity for characterized oils and their fractions using the expanded fluid model. Energy and Fuels, 30(9), 7134-7157.

Rastegari, K., Svrcek, W. Y., and Yarranton, H. W. (2004). Kinetics of asphaltene flocculation. Industrial and Engineering Chemistry Research, 43(21), 6861-6870.

Riazi, M. R. (2005). *Characterization and properties of petroleum fractions* (Vol. 50). West Conshohocken, PA: ASTM international.

Saber, N., Zhang, X., Zou, X. Y., and Shaw, J. M. (2012). Simulation of the phase behaviour of Athabasca vacuum residue+ n-alkane mixtures. Fluid Phase Equilibria, 313, 25-31.

Sánchez-Lemus, M. C., Schoeggl, F., Taylor, S. D., and Yarranton, H. W. (2016). Physical properties of heavy oil distillation cuts. Fuel, 180, 457-472.

Sánchez-Lemus, M. C., Schoeggl, F., Taylor, S. D., Růžička, K., Fulem, M., and Yarranton, H. W. (2014). Deep-vacuum fractionation of heavy oil and bitumen, Part II: interconversion method. Energy & Fuels, 28(5), 2866-2873.

Sedghi, M., and Goual, L. (2009). Role of resins on asphaltene stability. Energy and Fuels, 24(4), 2275-2280.

Sirota, E. B. (2005). Physical structure of asphaltenes. Energy and fuels, 19(4), 1290-1296.

Soave, G. (1972). Equilibrium constants from a modified Redlich-Kwong equation of state. Chemical engineering science, 27(6), 1197-1203.

Soreide, I. (1989). Improved phase behavior predictions of petroleum reservoir fluids from a cubic equation of state. Dr. Ing. dissertation, Norwegian Inst. of Technology, Trondheim, Norway.

Speight, J. G. (2007). *The Chemistry and Technology of Petroleum* (4 Ed.). Boca Raton, FL, USA: CRC Press.

Subramanian, S., Simon, S., and Sjöblom, J. (2016). Asphaltene precipitation models: a review. Journal of Dispersion Science and Technology, 37(7), 1027-1049.

Svrcek, W. Y., and Mehrotra, A. K. (1986). Measurement and Correlation of the Viscosity, Density and Gas Solubility of Alberta Bitumens. University of Calgary.

Tavakkoli, M., Chen, A., and Vargas, F. M. (2016). Rethinking the modeling approach for asphaltene precipitation using the PC-SAFT Equation of State. Fluid Phase Equilibria, 416, 120-129.

Tavakkoli, M., Panuganti, S. R., Taghikhani, V., Pishvaie, M. R., and Chapman, W. G. (2014). Understanding the polydisperse behavior of asphaltenes during precipitation. Fuel, 117, 206-217.

Tavakkoli, M., Panuganti, S. R., Taghikhani, V., Pishvaie, M. R., and Chapman, W. G. (2013). Precipitated asphaltene amount at high-pressure and high-temperature conditions. Energy and Fuels, 28(3), 1596-1610.

Tharanivasan, A. K., Svrcek, W. Y., Yarranton, H. W., Taylor, S. D., Merino-Garcia, D., and Rahimi, P. M. (2009). Measurement and modeling of asphaltene precipitation from crude oil blends. Energy and Fuels, 23(8), 3971-3980.

Tharanivasan, A. K., Yarranton, H. W., and Taylor, S. D. (2010). Application of a regular solution-based model to asphaltene precipitation from live oils. Energy & Fuels, 25(2), 528-538.

Ting, P. D., Gonzalez, D. L., Hirasaki, G. J., and Chapman, W. G. (2007). Application of the PC-SAFT equation of state to asphaltene phase behavior. In Asphaltenes, heavy oils, and petroleomics (pp. 301-327). Springer, New York, NY.

Ting, P. D., Joyce, P. C., Jog, P. K., Chapman, W. G., and Thies, M. C. (2003). Phase equilibrium modeling of mixtures of long-chain and short-chain alkanes using Peng–Robinson and SAFT. Fluid phase equilibria, 206(1-2), 267-286.

Turek, E. A., Metcalfe, R. S., and Fishback, R. E. (1988). Phase Behavior of Several CO2/West Texas-Reservoir-Oil Systems. SPE reservoir engineering, 3(02), 505-516.

Twu, C. H. (1984). An internally consistent correlation for predicting the critical properties and molecular weights of petroleum and coal-tar liquids. Fluid phase equilibria, 16(2), 137-150.

van der Waals, J. D. (1873). On the continuity of the gaseous and liquid states Doctoral Dissertation Leiden University. Leiden, The Netherlands.

Van Konynenburg, P. H., and Scott, R. L. (1980). Critical lines and phase equilibria in binary van der Waals mixtures. Phil. Trans. R. Soc. Lond. A, 298(1442), 495-540.

Verdier, S., Carrier, H., Andersen, S. I., and Daridon, J. L. (2006). Study of pressure and temperature effects on asphaltene stability in presence of CO2. Energy and fuels, 20(4), 1584-1590.

Vickers, A. K. (2002). Higher-Temperature Simulated Distillation with DB-HT Sim Dis Columns. Applications. Agilent Technologies Inc.

VMG User's Manual. (2011). Virtual Materials Group Inc, Calgary, Canada.

Wang, J. X., and Buckley, J. S. (2001). A two-component solubility model of the onset of asphaltene flocculation in crude oils. Energy & Fuels, 15(5), 1004-1012.

Wertheim, M. S. (1986). Fluids with highly directional attractive forces. III. Multiple attraction sites. Journal of statistical physics, 42(3-4), 459-476.

Whitson, C. H. (1983). Characterizing hydrocarbon plus fractions. Society of Petroleum Engineers Journal, 23(04), 683-694.

Whitson, C. H., and Brulé, M. R. (2000). Phase behavior. Richardson, TX: Henry L. Doherty Memorial Fund of AIME, Society of Petroleum Engineers.

Wiehe, I. A., Yarranton, H. W., Akbarzadeh, K., Rahimi, P. M., and Teclemariam, A. (2005). The paradox of asphaltene precipitation with normal paraffins. Energy and Fuels, 19(4), 1261-1267.

Yarranton, H. W., Alboudwarej, H., and Jakher, R. (2000). Investigation of asphaltene association with vapor pressure osmometry and interfacial tension measurements. *Industrial and engineering chemistry research*, *39*(8), 2916-2924.

Yarranton, H. W., and Masliyah, J. H. (1996). Molar mass distribution and solubility modeling of asphaltenes. AIChE Journal, 42(12), 3533-3543.

Yarranton, H. W., Fox, W. A., and Svrcek, W. Y. (2007). Effect of Resins on Asphaltene Self-Association and Solubility. *The Canadian Journal of Chemical Engineering*, *85*(5), 635-642.

Yarranton, H. W., Ortiz, D. P., Barrera, D. M., Baydak, E. N., Barré, L., Frot, D., ... and Becerra, M. (2013). On the size distribution of self-associated asphaltenes. *Energy and Fuels*, *27*(9), 5083-5106.

Yarranton, H. W., Powers, D. P., Okafor, J. C., and van den Berg, F. G. A. (2018). Regular solution based approach to modeling asphaltene precipitation from native and reacted oils: Part 2, molecular weight, density, and solubility parameter of saturates, aromatics, and resins. Fuel, 215, 766-777.

Yazdani, A., and Maini, B. B. (2007). Measurements and Modelling of Phase Behaviour and Viscosity of a Heavy Oil-Butane System. In Canadian International Petroleum Conference. Petroleum Society of Canada.

Zhang, Y., Arya, A., Kontogeorgis, G., and Yarranton, H. (2019). Modeling the phase behaviour of bitumen/n-alkane systems with the cubic plus association (CPA) equation of state. Fluid Phase Equilibria, 486, 119-138.

Zhang, Y., Takanohashi, T., Sato, S., Saito, I., and Tanaka, R. (2004). Observation of glass transition in asphaltenes. Energy and Fuels, 18(1), 283-284.

Zou, X. Y., Zhang, X., and Shaw, J. A. (2007). Phase Behavior of Athabasca Vacuum Bottoms + N-alkane Mixtures. SPE Prod and Oper 22 (2): 265–272. SPE-97661-PA.